

UC San Diego

UC San Diego Electronic Theses and Dissertations

Title

Tropical Pacific nutrient dynamics in the modern and pleistocene ocean : insights from the nitrogen isotope system

Permalink

<https://escholarship.org/uc/item/2df3m2v1>

Author

Rafter, Patrick Anthony

Publication Date

2009

Peer reviewed|Thesis/dissertation

UNIVERSITY OF CALIFORNIA, SAN DIEGO

Tropical Pacific Nutrient Dynamics in the Modern and Pleistocene Ocean:
Insights from the Nitrogen Isotope System

A dissertation submitted in partial satisfaction
of the requirements for the degree Doctor of Philosophy

in

Oceanography

by

Patrick Anthony Rafter

Committee in charge:

Christopher D. Charles, Chair
Lihini I. Aluwihare
Ralph F. Keeling
Richard D. Norris
Margaret J. Schoeninger

2009

Copyright
Patrick Anthony Rafter, 2009
All rights reserved

The Dissertation of Patrick Anthony Rafter is approved, and it is accepted in quality
and form for publication on microfilm and electronically:

Chair

University of California, San Diego

2009

iii

DEDICATION

This dissertation is dedicated to the dedicated.

EPIGRAPH

Whenever I find myself growing grim about the mouth; whenever it is a damp, drizzly November in my soul; whenever I find myself involuntarily pausing before coffin warehouses, and bringing up the rear of every funeral I meet; and especially whenever my hypos get such an upper hand of me, that it requires a strong moral principle to prevent me from deliberately stepping into the street, and methodically knocking people's hats off--then, I account it high time to get to sea as soon as I can.

—H. Melville

Don't Try – Tombstone message from *H. C. Bukowski*

TABLE OF CONTENTS

Signature Page iii

Dedication iv

Epigraph v

Table of Contents vi

List of Tables viii

List of Figures ix

Acknowledgements xi

Vita xiv

Abstract xv

Introduction 1

 References 4

I. Subsurface tropical Pacific nitrogen isotope measurements of nitrate:
a tracer for denitrification, N₂ fixation, and subsurface circulation

 1.0 Introduction 5

 1.1 Background—tropical Pacific circulation..... 7

 1.2 Materials and Methods..... 9

 1.3 Results 11

 1.4 Discussion 14

 1.5 Conclusions 22

 1.6 Acknowledgements..... 23

 1.7 Figures 24

1.8	References	31
II.	Tropical Pacific nutrient dynamics of the past 1200kyr: an eastern equatorial Pacific record of surface nitrate uptake using sediment N isotopes	
2.0	Introduction	37
2.1	Background	38
2.2	Materials and Methods	41
2.3	Results	42
2.4	Discussion	49
2.5	Conclusions	54
2.6	Figures	56
2.7	References	67
III.	The composition and evolution of deep-sea sediment nitrogen	
3.0	Introduction	69
3.1	Materials and Methods	70
3.2	Results	73
3.3	Discussion	78
3.4	Conclusions	88
3.5	Figures and Tables	90
3.6	References	101
Appendix A	Supplementary Material for Chapter 1	107
Appendix B	Supplementary Material for Chapter 2	113

LIST OF TABLES

Table 3.1	Information for sediment cores discussed in Chapter 3	100
Table A1	Hydrocast station information for Chapter 1.....	111

LIST OF FIGURES

Figure 1.1	Pacific Ocean dissolved oxygen concentrations at 400m and along 95°W.....	24
Figure 1.2	Pacific Ocean nitrate deficit (N*) at 400m.....	25
Figure 1.3	Tropical Pacific mean annual subsurface zonal circulation	26
Figure 1.4	Tropical Pacific mean annual nitrate concentrations and hydrological station locations.....	27
Figure 1.5	Measurements of $\delta^{15}\text{N-NO}_3^-$ versus depth.....	28
Figure 1.6	Measurements of NO_3^- versus depth.....	29
Figure 1.7	Measurements of $\delta^{15}\text{N-NO}_3^-$ and zonal subsurface circulation	30
Figure 2.1	Pacific Ocean mean annual nitrate concentrations and sediment core site locations.....	56
Figure 2.2	Measurements of $\delta^{15}\text{N-NO}_3^-$ and expected $\delta^{15}\text{N}$ export to sediment.....	57
Figure 2.3	Sediment age model synchronization using the $\delta^{18}\text{O}$ of benthic foraminifera	58
Figure 2.4	Schematic for calculating $\Delta\delta^{15}\text{N}$: isolating the nitrate utilization signal	59
Figure 2.5	Sediment $\delta^{15}\text{N}$ for the western and eastern equatorial Pacific, California Margin, and $\Delta\delta^{15}\text{N}$ (nitrate utilization record).....	60
Figure 2.6	Comparison of $\Delta\delta^{15}\text{N}$ with global icesheet volume, EEP SST, and EEP %Opal.....	61
Figure 2.7	Comparison of $\Delta\delta^{15}\text{N}$ with modeled eastern equatorial Pacific SST anomaly.....	62
Figure 2.8	Comparison of $\Delta\delta^{15}\text{N}$ with global icesheet volume and atmospheric dust concentrations.....	63
Figure 2.9	Blackman-Tukey spectral analysis of $\Delta\delta^{15}\text{N}$ over three time periods of the past 1200kyr.....	64
Figure 2.10	Blackman-Tukey spectral analysis of icesheet volume over three time periods of the past 1200kyr.....	65
Figure 2.11	Comparison of $\Delta\delta^{15}\text{N}$ with calculated equatorial Pacific SST gradient.....	66
Figure 3.1	Pacific Ocean mean annual nitrate concentrations and sediment core site locations.....	90
Figure 3.2	Sediment age model synchronization using the $\delta^{18}\text{O}$ of benthic foraminifera	91
Figure 3.3	Sediment $\delta^{15}\text{N}$ records from the equatorial Pacific.....	92

Figure 3.4	Published deep-sea sediment $\delta^{15}\text{N}$ records.....	93
Figure 3.5	The difference between WEP and CA Margin sediment $\delta^{15}\text{N}$ ($\Delta\delta^{15}\text{N}$)	94
Figure 3.6	Comparison between $\Delta\delta^{15}\text{N}$, sedimentary component percent nitrogen and $\delta^{15}\text{N}$	95
Figure 3.7	Comparison between $\Delta\delta^{15}\text{N}$ and deep-sea sediment composition including WEP fragmentation index.....	96
Figure 3.8	Diatom-bound $\delta^{15}\text{N}$ compared with whole sediment $\delta^{15}\text{N}$	97
Figure 3.9	Predicted versus actual coretop $\delta^{15}\text{N}$ from relatively shallow sediment sites.....	98
Figure 3.10	Synthesis of factors determining long-term trends in deep-sea sediment $\delta^{15}\text{N}$	99
Figure A1	Concentrations of nitrate and $\delta^{15}\text{N}$ of nitrate for samples at all sampling sites.....	108
Figure A2	Dissolved oxygen measurements for hydrocast stations on the 110°W transect for October/November 2003.....	109
Figure A3	Nitrate to silicic acid ratio versus depth along the 0° and 1°N in the tropical Pacific.....	110
Figure A4	Nitrate deficit [Nitrate – phosphate*16] and zonal velocity for waters along 110°W.....	110
Figure B1	Calculations of $\delta^{15}\text{N}$ exported to sediments versus nitrate consumed.....	115
Figure B2	Sediment %N measurements for equatorial Pacific sediment.....	116
Figure B3	Frequency versus phase angle for sediment %N at equatorial Pacific sites.....	117

ACKNOWLEDGEMENTS

It is with some sadness that I am writing the acknowledgments section of my Ph.D. dissertation because the years I have spent at Scripps Institution of Oceanography have been among the best years of my life (so far). After starting at Scripps, friends would ask about all the “student loans” I must be acquiring for graduate school, only to hear my reply, “they pay *me!*” Of course, “they” did not pay very much... but I feel very lucky to have been able to advance my scientific training without having to take out a single loan.

Now, in standard Acknowledgments language, I would like to thank my advisor Christopher Charles for his considerable contributions to my scientific training. Lihini Aluwihare was a huge resource to me and I would like to thank her for providing the yang to Chris’ yin. Ralph Keeling has provided me with excellent advice and I always enjoy talking with him. It was very fun to discuss my work with Margaret Schoeninger and to discuss the anthropological application of nitrogen isotopes—very interesting! I would also like to give an extra big thanks to committee member Richard “Dick” Norris, who played a key role in my development here at Scripps.

This dissertation would be a pale version of itself without the help of Daniel Sigman at Princeton University who provided me with the resources to produce a major survey of nitrate in the tropical Pacific and I look forward to our future collaborations. In addition to Danny, during my many visits to Princeton, NJ, there were several excellent humans that took care of me, especially Eric Galbraith, Julie

Granger, Masha Prokopenko, John DiGenni, Tom and Lorraine Serwatka, and the entire Pellini family (Jim, Joan, Brian, Matty, and Alicia) who alternately volunteered advice, their cars, car rides, and a place to rest during several of my visits to Princeton.

Furthermore, my work at Princeton would have been severely limited without the approval of my water-sampling program through the National Oceanographic and Atmospheric Administration's Pacific Marine Environmental Laboratory. I especially want to thank the Tropical Atmosphere Array (TAO) Program Director Mike McPhaden, then-TAO Operations Manager Brian Lake, several CTD technicians (too many to list), and the entire crews of the RVs *Ka'imimoana* and *Ronald Brown*. In the case of the former, they were excellent hosts for many days out to sea, even if I ended up with a really bad haircut. Sediment samples were provided by the Lamont Doherty Earth Observatory's Deep Sea Sample Repository, the Ocean Drilling Program, and SIO's own Geological Collections with special thanks to Warren Smith for helping and for providing me with vintage geology textbooks!

I also need to thank the SIO Analytical Facilities and especially Bruce Deck for all their help, for allowing me to be the first to run my own samples and for their patience while I tested new techniques for preparing my samples. Financial support came from a variety of sources including a California Space Institute grant, several Whole Earth Society grants, and a fellowship from the Joint Oceanographic Institutions.

Of my SIO peers, there were many that provided invaluable help and solace—first office-mate Daniel Deeds, JJ Becker, Jenna Munson, Drew Lucas,

second office-mate Lydia Roach, the one-of-a-kind Evan Solomon for being just as excited about science as I am, and relative new comer Danny Richter for being “that guy”.

Finally, I thank my wife for marrying me. Remember Asbury Park?

VITA

- 2002-2009 Ph.D. Oceanography
Scripps Institution of Oceanography, La Jolla, CA, USA
- 2006-2007 Joint Oceanographic Institutions, Ocean Drilling Program
Schlanger Fellow
- 2000 B.S. Environmental Science
Florida Institute of Technology, Melbourne, FL, USA
- 2000 B.S. Marine Environmental Studies
Florida Institute of Technology, Melbourne, FL, USA

ABSTRACT OF THE DISSERTATION

Tropical Pacific Nutrient Dynamics in the Modern and Pleistocene Ocean:
Insights from the Nitrogen Isotope System

by

Patrick Anthony Rafter

Doctor of Philosophy in Oceanography

University of California, San Diego, 2009

Professor Christopher D. Charles, Chair

The tropical Pacific is a region where nutrient delivery, upper ocean dynamics, and global climate variability are tightly coupled. For example, the depth of the eastern equatorial Pacific (EEP) thermocline, for the most part, determines the delivery of the essential nutrient nitrate, but it is also a key aspect of an ocean-atmosphere feedback system responsible for global climate variability—the El Niño Southern Oscillation (ENSO). To provide a unique view of the upper ocean processes

directly responsible for nutrient and climate dynamics in this region, I apply a single tracer—the ratio of ^{15}N to ^{14}N (hereafter “ $\delta^{15}\text{N}$ ”)—in modern seawater and sediment throughout the tropical Pacific. I find that the $\delta^{15}\text{N}$ of nitrate is homogenous throughout the tropical Pacific and is elevated by 2‰ relative to the Southern and Atlantic Oceans by mixing with the denitrified waters of the eastern tropical Pacific. The results of this modern ocean survey are used to devise a new application of $\delta^{15}\text{N}$ in eastern and western equatorial Pacific (WEP) sediments that provides a record of EEP nitrate consumption over the past 1,200,000 years. This record strongly suggests that the depth of the EEP thermocline—and therefore the upper ocean conditions driving the tropical climate system—has little to no response to high-latitude processes such as icesheet dynamics. Instead, as has been suggested by coupled ocean-atmosphere models, the east/west thermocline tilt responded primarily to changes in local seasonal insolation over thousands of years (a product of planetary axial precession). Some of the long-term changes in these deep-sea sediment $\delta^{15}\text{N}$ records would seem to suggest an alteration of the original surface ocean signal, but additional $\delta^{15}\text{N}$ measurements of sedimentary size fractions and components support the fidelity of bulk sedimentary $\delta^{15}\text{N}$ as an archive of surface ocean nutrient cycling.

Introduction

This dissertation exploits nitrogen (N) isotopic measurements (referred to here as “ $\delta^{15}\text{N}$ ” in units of ‰) performed on modern seawater and sediment throughout the tropical Pacific. While this isotopic tool has been primarily used to identify links in the cycling of biologically available (“fixed”) nitrogen—an essential nutrient to all life—in this study I show that measurements of $\delta^{15}\text{N}$ can also provide insight to water mass history and upper ocean dynamics. However, this additional information can only be obtained when the spatial distribution and geographic location of $\delta^{15}\text{N}$ measurements have been taken into consideration.

One example of this approach is highlighted by a survey of the N isotopic composition of nitrate (represented as $\delta^{15}\text{N}\text{-NO}_3^-$) throughout the modern tropical Pacific (Chapter 1), which not only finds an extensive region of relatively high $\delta^{15}\text{N}\text{-NO}_3^-$ (~7‰), but also a distinct volume of relatively low $\delta^{15}\text{N}\text{-NO}_3^-$ water. Coupling these measurements with in-situ and historical observations of circulation patterns, I find that eastern tropical Pacific nitrate, isotopically enriched by denitrification, is mixed throughout the tropics via large scale zonal subsurface mixing known as the “deep tropical gyres” [Rowe *et al.*, 2000]. Furthermore, my measurements of isotopically depleted nitrate are closely associated with a subsurface “jet” that most likely originates from extra-tropical source waters where lower $\delta^{15}\text{N}\text{-NO}_3^-$ is produced through N_2 fixation. The results provided by these measurements of modern seawater demonstrate the application of $\delta^{15}\text{N}\text{-NO}_3^-$ as a unique water mass tracer. Future

investigations using this tracer will certainly further constrain the sources and pathways of subsurface waters throughout the Pacific basin.

Identifying the source of the $\delta^{15}\text{N-NO}_3^-$ variability in the modern tropical Pacific is crucial to reconstructing a history of tropical Pacific nutrient dynamics (Chapter 2) using the N isotope composition of sediment (“sediment $\delta^{15}\text{N}$ ”). Sediment $\delta^{15}\text{N}$ is primarily derived from the exported products of surface ocean photosynthesis, which respond to changes in the $\delta^{15}\text{N-NO}_3^-$ delivered to surface waters and changes in the relative consumption of surface NO_3^- . Where these competing influences on sediment $\delta^{15}\text{N}$ are not constrained, it is difficult to obtain a valuable interpretation, but in this study I demonstrate that by using a distribution of sediment $\delta^{15}\text{N}$ records, each of these competing isotopic signals can be isolated. For example, sediment $\delta^{15}\text{N}$ in the western equatorial Pacific (WEP) only records the secular variability of $\delta^{15}\text{N-NO}_3^-$ because nitrate is completely consumed above this core site. Assuming homogeneity in tropical Pacific $\delta^{15}\text{N-NO}_3^-$ as we see in the modern ocean, WEP sediment $\delta^{15}\text{N}$ can then be used to disentangle the record of incomplete nitrate consumption from eastern equatorial Pacific (EEP) sediment. In effect, the WEP sediment $\delta^{15}\text{N}$ can be used as a baseline value for complete nitrate consumption in other cores. Therefore, the difference between WEP and EEP sediment $\delta^{15}\text{N}$ provide an estimate of EEP relative nitrate consumption, which is driven by the depth of the EEP thermocline [*Turk et al.*, 2001]. Because this aspect of equatorial Pacific nutrient dynamics is closely tied to the upper ocean processes involved with global climate variability in the modern ocean—processes that are likely to be relevant on long-timescales—the history of EEP

nitrate consumption can be used to illustrate long-term variability of this important component of the tropical climate system. This record of EEP upwelling strongly suggests that high-latitude processes (such as changes in the volume of the continental ice sheets) do not influence this aspect of the tropical Pacific climate system; it is primarily influenced by changes in local seasonal insolation as suggested by *Clement et al.*, [1999]. Of particular interest with regards to future work is the extension of this EEP upwelling record into the Pliocene, which through the use of sediment-based sea surface temperature proxies is thought to be an extended period of reduced eastern upwelling in the eastern tropical Pacific [*Dekens et al.*, 2007].

The fidelity of deep-sea sediment $\delta^{15}\text{N}$ records as a proxy for surface ocean processes is discussed in the final section of this dissertation. Specifically, the source of long-term trends—trends that at first glance might be considered to be a post-depositional alteration of the $\delta^{15}\text{N}$ signal—is closely examined with new $\delta^{15}\text{N}$ measurements of principal sedimentary components. I find that changes in $\delta^{15}\text{N}$ during decomposition (so-called diagenetic fractionation) are not likely and that selective preservation or selective export, cannot explain the long-term trends in sediment $\delta^{15}\text{N}$. The simplest explanation that is consistent with a variety of deep-sea sediment $\delta^{15}\text{N}$ records is that the long-term trends in sediment $\delta^{15}\text{N}$ are representative of a long-term increase in eastern tropical south Pacific (ETSP) denitrification. While I cannot confirm these results for all deep-sea sediment $\delta^{15}\text{N}$ sites, resolving the uncertainty surrounding these measurements would be an important development in the application of this paleoceanographic tool.

References

Clement, A.C., R. Seager, and M.A. Cane (1999), Orbital controls on the El Niño/Southern Oscillation and the tropical climate, *Paleoceanography*, *14*, 441-456.

Dekens, P.S., A.C. Ravelo, and M.D. McCarthy (2007), Warm upwelling regions in the Pliocene warm period, *Paleoceanography*, *22*, PA3211, doi:10.1029/2006PA001394.

Rowe, G.D., Firing, E., and G.C. Johnson (2000), Pacific equatorial subsurface countercurrent velocity, transport, and potential vorticity, *Journal of Physical Oceanography*, *30*, 1172–1187.

Turk, D., M. J. McPhaden, A. J. Busalacchi, M. R. Lewis (2001), Remotely sensed biological production in the equatorial Pacific, *Science*, *293*, 471-474.

I. Subsurface tropical Pacific nitrogen isotope measurements of nitrate: a tracer for denitrification, N₂ fixation, and subsurface circulation

1.0 Introduction

The tropical Pacific is of primary importance for global nutrient cycling because of the confluence of both fixed nitrogen (N) sources (*Dupouy et al.*, 1988 and others) and sinks (see *Deutsch et al.*, 2001 and *Brandes et al.*, 2002 for review)—processes that regulate the ocean-wide concentration of the limiting nutrient, nitrate.

The major source of marine nitrate (NO₃⁻) is the “fixation” of gaseous N₂ into organic matter via a variety of single- and multi-cellular photosynthetic organisms in surface waters (see *Mahaffey et al.*, [2005] for a recent review). In the Pacific Ocean, these processes are thought to be confined to warm, NO₃⁻ limited, well-stratified surface waters such as the north and south Pacific gyres [*Karl et al.*, 1992; *Raimbault and Garcia*, 2008] as well as the southwestern tropical / subtropical Pacific [*Dupouy et al.*, 1988; *Campbell et al.*, 2005; *Masotti et al.*, 2007; *Garcia et al.*, 2007; *Biegala et al.*, 2008]. There have also been less direct inferences of N₂ fixation in the eastern tropical Pacific [*Brandes et al.*, 1998; *Sigman et al.*, 2005; *Deutsch et al.*, 2007].

The tropical Pacific Ocean also contains some of the primary sinks of NO₃⁻. Poor ventilation and high oxygen demand from the remineralization of sinking organic matter combine to create the so-called Oxygen Deficient Zones (ODZs) (Figure 1.1). Where dissolved oxygen (here referred to simply as “oxygen”) concentrations are very low (less than 2μM), nitrate and nitrite become energetically favorable electron acceptors during organic matter remineralization—a microbially mediated process

known as denitrification. Denitrification in the water column of the Eastern Tropical North Pacific (ETNP) and Eastern Tropical South Pacific (ETSP) is estimated to account for up to 2/3 of the global loss of NO_3^- [Codispoti and Christensen, 1985; Codispoti and Packard, 1980; Codispoti and Richards, 1976; Deutsch et al., 2001]. While denitrification is constrained to very low oxygen waters, the effects on NO_3^- can be seen far from the ODZs. One indication of this far-field influence is the distribution of N^* , a parameter that measures the deviation of NO_3^- from its Redfield 16:1 ratio with phosphate [Gruber and Sarmiento, 1987]; maps of N^* in the Pacific Ocean show the influence of denitrification on NO_3^- (negative N^* signaling a NO_3^- deficit) for waters throughout the Pacific (Figure 1.2). The addition of NO_3^- through N_2 fixation would be seen as positive N^* .

Each of these processes— N_2 fixation and denitrification—also leaves an imprint on the ratio of $^{15}\text{N}/^{14}\text{N}$ in nitrate (“ $\delta^{15}\text{N}\text{-NO}_3^-$ ” where $\delta^{15}\text{N}$ is measured versus atmospheric N_2 and equals $[(^{15}\text{N}/^{14}\text{N})_{\text{sample}}/(^{15}\text{N}/^{14}\text{N})_{\text{atmosphere}}]-1$). The remineralization of organic matter produced through N_2 fixation results in a $\delta^{15}\text{N}\text{-NO}_3^-$ value of ~ -2 to 0‰ [Carpenter et al., 1997; Delwiche et al., 1979; Hoering and Ford, 1960]. Fractionation of nitrogen isotopes upon denitrification also imparts a strong isotopic enrichment of the remaining NO_3^- pool [Cline and Kaplan, 1975; Liu and Kaplan, 1989; Brandes et al., 1998; Voss et al., 2001; Sigman et al., 2005; Casciotti and McIlvin, 2007]. In addition to this, enrichment of the remaining nitrate pool occurs if the available nitrate is not completely consumed by phytoplankton, who preferentially select for $^{14}\text{N}\text{-NO}_3^-$. Thus, this isotopic tracer represents a valuable tool

for understanding diverse aspects of the global ocean, such as nitrogen budgets and cycling.

However, a complete survey of marine $\delta^{15}\text{N-NO}_3^-$ has not been performed even though identifying the baseline value of $\delta^{15}\text{N-NO}_3^-$ is crucial for investigations in a variety of disciplines, such as ecology [Graham *et al.*, 2007; Newsome *et al.*, 2006] and paleoceanography [Altabet and Francois, 1994]. In this study, I provide a synoptic view of the spatial distribution of tropical Pacific $\delta^{15}\text{N-NO}_3^-$ with measurements throughout the equatorial and eastern tropical Pacific—transects spanning 110,000 km and 2000 km respectively. These measurements provide the answers to several general, but fundamental questions: What processes can explain the spatial variability in $\delta^{15}\text{N-NO}_3^-$? And what does the $\delta^{15}\text{N-NO}_3^-$ distribution demonstrate about subsurface circulation and nutrient cycling processes in the tropical Pacific Ocean?

1.1 Background—Tropical Pacific Circulation

Though the processes of fixation, denitrification and uptake are responsible for the basic fractionation of nitrogen isotopes, the ultimate pattern of $\delta^{15}\text{N-NO}_3^-$ in the Pacific must be understood within the context of the generalized upper ocean circulation. Near the surface, the trade wind driven westward South and North Equatorial Currents (SEC and NEC respectively) and the Northern Equatorial Counter Current (Figure 1.3) account for the principal gradients in nutrient properties. The SEC and NEC are the equatorward limbs of the subtropical gyres and extend as deep as ~300m. At thermocline depths, the east to west sea surface height gradient and

subsurface pressure gradient help to drive the fast-moving Equatorial Under Current (EUC) (Figure 1.3). The EUC has been observed as far west as 142°E [*Gouriou and Toole, 1993*] and its source water appears to be the New Guinea Coastal Undercurrent [*Tsuchiya et al., 1989*]. Wind-forced Ekman pumping leads to upwelling of the cool, higher-nutrient EUC (and possibly Equatorial Intermediate Current water [*Sloyan et al., 2003*]) into the relatively productive surface waters. The EUC travels eastward through an increasingly homogenized water mass, previously named the “13°C Water” [*Tsuchiya, 1981*] but more commonly known as the equatorial thermostat (volume of water with constant temperature). The increased temperature homogeneity most likely results from the eastern EUC slowing and mixing with westward currents such as the SEC and Equatorial Intermediate Current [*Wyrski, 1967; Wyrski, 1981; Lukas, 1986*].

Less well studied are the easterly subsurface countercurrents—the Southern Subsurface Counter Current (SSCC) and the Northern Subsurface Counter Current (NSCC), together referred to as the “Tsuchiya Jets”. Contrary to the EUC, the TJs are slightly slower, lie somewhat deeper, and diverge from the equator towards the east (Figure 1.3) with clearly defined potential vorticity barriers on their poleward sides [*Johnson and Moore, 1997*]. In the east, some NSCC and SSCC waters recirculate equatorward, adding to the westward flowing North and South Equatorial Currents as well as the Equatorial Intermediate Current [*Gouriou and Toole, 1993; Johnson and Moore, 1997; and Rowe et al., 2000; Sloyan et al., 2003*]. This circulatory pattern—termed the “Deep Tropical Gyres” by *Rowe et al., [2000]*—results in

significant mixing and homogenization of water between the Tsuchiya Jets and may contribute to the eastward increase in the thermostad and pycnostad (volume of similar density) between the Tsuchiya Jets [Lukas, 1986].

1.2 Materials and Methods

Tropical Pacific water samples were acquired during the National Oceanic and Atmospheric Administration's (NOAA) routine maintenance of the Tropical-Atmosphere-Ocean (TAO) array of moored buoys that are strategically placed throughout the tropical Pacific to observe changing ocean and atmospheric conditions. I capitalized on these buoy-tending operations to create a wide distribution of sampling sites with negligible additional ship operating costs. Standard hydrocast methods include a rosette of water sampling bottles surrounding a Conductivity-Temperature-Depth and (periodically) a dissolved oxygen sensor package. Each ship has a hull-mounted Acoustic Doppler Current Profiler (ADCP), to identify direction and speed of circulatory features to a maximum depth of 400m.

All sampling and hydrocast locations can be seen in Figure 1.4 with further details in Appendix Table 1. Water sampling depths were pre-established by the TAO program with 12-13 sample bottles tripped per hydrocast, regardless of hydrocast depth. While the top 200m depths are consistent for every cast, the remaining sample bottles are closed at equal intervals over the entire sampling depth resulting in higher sampling resolution for the "shallow" casts of 1000m versus the "deep" casts to >3000m. In October and November of 2003, water samples were collected on board

the NOAA ship RV *Ronald H. Brown* for two meridional transects at 95°W and 110°W. The zonal transects are constructed from samples retrieved on the RVs *Ka'imimoana* and *Ronald H. Brown* at 0°N between 165°E and 125°W and at 1°N between 165°E and 95°W for fall 2004 and late summer/fall 2005 respectively. Differences between 0°N and 1°N are small for nutrient concentrations especially below the mixed layer, but the EUC may have slightly smaller volume at 1°N [Firing *et al.*, 1983; Johnson *et al.*, 2002].

All sample bottles (60 ml Nalgene HDPE) were acid-cleaned, rinsed three times with sample water, filled to a volume of ~50ml, kept frozen on site, and shipped overnight to laboratories at the Scripps Institution of Oceanography or Princeton University. The samples from 2003 and 2004 were analyzed for NO_3^- at Princeton University by reducing NO_3^- (and NO_2^- if present) to NO using a V-(III) reagent, followed by chemiluminescence measurement of NO [Braman and Hendrix, 1989]. For these samples, NO_2^- was not separately measured. The full suite of nutrient analyses (NO_3^- , NO_2^- , PO_4^{3-} , and SiOH) were performed on the fall 2005 water samples at the UCSB Marine Science Institute Analytical Lab and show very low to no NO_2^- below the mixed layer. The mixed layer depth is classically defined as the depth where temperature is ~0.5°C different than sea surface temperature, which typically occurs at ~20°C in the tropical Pacific.

All samples were analyzed for the $^{15}\text{N}/^{14}\text{N}$ of NO_3^- via the “Denitrifier Method” of Sigman *et al.*, [2001] and Casciotti *et al.*, [2002], with measurement error +/- 0.2%. The measurements of $\delta^{15}\text{N}-\text{NO}_3^-$ presented here were begun in 2003, and, as

result, span a progressive refinement of the Denitrifier Method [Sigman *et al.*, 2001; Casciotti *et al.*, 2002]. The main refinement involved the recognition and circumvention of NO_2^- effects: a recent study [Casciotti and McIlvin, 2007] shows the presence of NO_2^- can lead to a $\delta^{15}\text{N-NO}_3^-$ underestimation of 1–5‰ when using the original Denitrifier Method. For the sampling locations, previous data (WOCE line P18N) and my own data (not shown) find $\text{NO}_2^- > 0.1\mu\text{M}$ primarily at the base of the mixed layer and within ODZs. The limited volume of the remaining samples precludes us from re-analyzing all samples fitting this description, so discussion of mixed layer $\delta^{15}\text{N-NO}_3^-$ measurements has been removed. However, because $\delta^{15}\text{N-NO}_3^-$ measurements from low oxygen regions are important to this discussion, these measurements are included with the qualification that the high $\delta^{15}\text{N-NO}_3^-$ often found in ODZs may be a slight underestimate of “actual” $\delta^{15}\text{N-NO}_3^-$.

1.3 Results

Along the equatorial zonal transects (0°N and 1°N), all $\delta^{15}\text{N-NO}_3^-$ measurements range from 6.8–7.2‰ for samples between the base of the mixed layer and 600m, with the average being 7‰ (Figure 1.5). These equatorial measurements show maximum values at 400m (Figure 1.5 and Appendix Figure A1) and several “deep-casts” indicate that $\delta^{15}\text{N-NO}_3^-$ of 5‰ (the typical subthermocline value for the high-latitude Southern Ocean [Sigman *et al.*, 2000]) is not reached until 2000 to 3000m (Appendix Figure A1). The mixed layer has higher $\delta^{15}\text{N-NO}_3^-$ from

phytoplankton consumption and fractionation of NO_3^- and is not discussed here (Figure 1.5).

Along the meridional transects at 95° and 110°W , maximum $\delta^{15}\text{N-NO}_3^-$ and minimum oxygen values are found at 400m depth for the northern and southern extremes of these transects (Figures 1.1 and 1.5), which is the same depth of maximum $\delta^{15}\text{N-NO}_3^-$ seen along the equatorial Pacific. These depths also coincide with the most negative N^* (nitrate deficit) values for the tropical Pacific (Figure 1.2). The low oxygen, negative N^* , and high $\delta^{15}\text{N-NO}_3^-$ along the 95°W and 110°W transects are diagnostic of regions where denitrification is occurring. This is not surprising, since these sampling transects clearly straddle the ETNP and ETSP oxygen deficient zones, where active denitrification is expected [Deutsch *et al.*, 2001]. Furthermore, the depth range for the low oxygen / high $\delta^{15}\text{N-NO}_3^-$ waters of the northern and southern ends match the characteristics of the ETNP and ETSP zones of denitrification; active denitrification occurs over a much thinner depth range in the ETSP than for the ETNP [Deutsch *et al.*, 2001]. These results strongly suggest that off-equatorial denitrification has influenced much of the water along these meridional transects. In addition to this, the depth of maximum $\delta^{15}\text{N-NO}_3^-$ is shared for all samples, including the western equatorial Pacific, which implies that waters from the eastern tropical Pacific ODZs have some influence on the $\delta^{15}\text{N-NO}_3^-$ composition of much of the tropical Pacific. It should be noted, however, that because $[\text{NO}_2^-]$ of 1-3 μM may be found in these low oxygen to anoxic waters of the eastern tropical Pacific, these higher-than-average to very high $\delta^{15}\text{N-NO}_3^-$ measurements (up to

~16‰) may actually underestimate the true isotopic enrichment by more than 5‰ in the ODZ [*Casciotti and McIlvin, 2007*].

The large volume of elevated $\delta^{15}\text{N-NO}_3^-$ seen throughout the tropical Pacific is contrasted with $\delta^{15}\text{N-NO}_3^-$ of ~5.3‰ south of the equator; measurements that in other ocean basins would not be surprising, but are clearly anomalous in the tropical Pacific. Specifically, this depleted water is found centered on 5°S and 200m depth for both the 110°W and 95°W lines. Using the hull-mounted ADCP, it can be seen that these low $\delta^{15}\text{N-NO}_3^-$ measurements are almost entirely coincident with the eastward flowing SSCC (Figure 1.6). The $\delta^{15}\text{N-NO}_3^-$ for the other eastward subsurface jets such as the EUC and the NSCC are less distinct from surrounding waters (~7‰ and ~6.7‰ respectively). While the SSCC waters have distinct $\delta^{15}\text{N-NO}_3^-$, these waters appear to be no different than surrounding waters with regards to oxygen or nitrate (Figures 1.1 and 1.7).

The nitrate measurements show the classical nutrient profile with high concentrations (35-45 μM) at depth and lesser concentrations from photosynthetic uptake near the surface (Figure 1.7 and Appendix Figure A1). The distribution along the 110°W and 95°W transects shows a distinct bowl of lower $[\text{NO}_3^-]$ and higher oxygen water (Figures 1.1 and 1.7) centered on the equator above 200m and between 5°N and 5°S—an area that demarcates the water between the northern and southern Tsuchiya Jets. The shape of this bowl of lower $[\text{NO}_3^-]$ and higher oxygen water is better defined at 95°W than for the 110°W transect.

1.4 Discussion

This survey of the subsurface tropical Pacific finds that $\delta^{15}\text{N-NO}_3^-$ down to 600m averages $\sim 7\text{‰}$ (Figure 1.5 or Appendix Figure A1 for more detail)—an enrichment of 2‰ or more relative to $\delta^{15}\text{N-NO}_3^-$ at similar depths in the Southern and Atlantic Oceans [Sigman *et al.*, 2000; DiFiore *et al.*, 2005; Knapp *et al.*, 2005]. In fact, the tropical Pacific $\delta^{15}\text{N-NO}_3^-$ does not reach Atlantic or Southern ocean subthermocline values until between 2000 and 3000m. This large volume of elevated $\delta^{15}\text{N-NO}_3^-$ is in contrast to the anomalously low $\delta^{15}\text{N-NO}_3^-$ ($\sim 5.3\text{‰}$) associated with the waters of the SSCC subsurface jet (Figure 1.6). These new results are the first of their kind and here I discuss the possible mechanisms that brought about these anomalous conditions.

Addressing the elevated N isotopic composition of nitrate throughout the equatorial Pacific, nitrate consumption and denitrification are the only processes that leave the remaining nitrate pool enriched in $\delta^{15}\text{N-NO}_3^-$ and there are two possible regions where these processes could influence tropical Pacific nitrate: incomplete surface nitrate consumption in the high southern latitudes and denitrification in the eastern tropical Pacific. In Southern Ocean surface waters, nitrate delivered to surface waters is not completely consumed, resulting in higher $\delta^{15}\text{N-NO}_3^-$ of the remaining nitrate pool [Sigman *et al.*, 1999; DiFiore *et al.*, 2006]. To explain the higher tropical Pacific $\delta^{15}\text{N-NO}_3^-$, this subantarctic pool enriched in $\delta^{15}\text{N-NO}_3^-$ could be transported via subantarctic mode water (SAMW) to lower latitudes as suggested by several studies [McCartney, 1982; Toggweiler *et al.*, 1991; Sarmiento *et al.*, 2004]. These

subantarctic surface and mode waters have a distinctive imprint a nitrate / silicic acid molar ratio greater than 1, resulting from the uptake of silica by diatoms [Brzezinski *et al.*, 2003; Sarmiento *et al.*, 2004]. However, in the middle of the depth range where elevated $\delta^{15}\text{N-NO}_3^-$ is seen (~400m), nitrate is closely matched by silicic acid concentrations (See Appendix Figure A3). While it is possible that the high nitrate to silicic acid signal of SAMW is completely erased before the water mass reaches the tropics, this is not likely to occur without also disturbing the value of $\delta^{15}\text{N-NO}_3^-$. Therefore, the Southern Ocean surface waters are unlikely to be the ultimate source of subsurface tropical Pacific nitrate.

On the other hand, the influence of eastern tropical Pacific denitrification has been measured far from its source resulting from mixing with and advection from the oxygen deficient zones of the ETNP and ETSP [Codispoti and Richards, 1976; Liu and Kaplan, 1989; Castro *et al.*, 2001]. The measurements discussed here strongly suggest that the elevated $\delta^{15}\text{N-NO}_3^-$ seen throughout the tropical Pacific ultimately derive from mixing with the eastern ODZs and this is likely facilitated by the east to west circulation of the Deep Tropical Gyres [Rowe *et al.*, 2000]. This subsurface mixing process is accomplished when some of the off-equatorial jets (the NSCC and SSSC) slow east of 110°W [Kessler, 2006], turn equatorward, and join the westward flowing SEC and EIC [Gouriou and Toole, 1993; Johnson and Moore, 1997; and Rowe *et al.*, 2000; Sloyan *et al.*, 2003]. The equator-ward turn of these subsurface jets occurs on the equatorward edge of the ETNP and ETSP ODZs (Figures 1.2 and 1.3)

where they would necessarily mix and entrain water elevated in $\delta^{15}\text{N-NO}_3^-$ from denitrification, and advect this enriched nitrate throughout the tropical Pacific.

The relationship of nitrate to phosphate in the subsurface tropical Pacific (here as a simplified version of the *Gruber and Sarmiento*, [1997] “N*” in Figure 1.2) can provide additional insight to the tropical Pacific water mass history. For example, water with elevated $\delta^{15}\text{N-NO}_3^-$ by photosynthetic uptake should have a N:P ratio close to the Redfield 16:1 and therefore an N* value close to 0. However, during denitrification, $\delta^{15}\text{N-NO}_3^-$ increases, but N* decreases. The negative N* values found throughout the entire Pacific basin at 400m is diagnostic of mixing with the eastern tropical Pacific ODZs (Figure 1.2) and this depth coincides with the highest ETNP and ETSP denitrification [*Deutsch et al.*, 2001] and the depth of maximum eastern, central, and western equatorial Pacific $\delta^{15}\text{N-NO}_3^-$ (Figures 1.5 and Appendix Figure A1). This evidence strongly supports the enrichment of tropical Pacific $\delta^{15}\text{N-NO}_3^-$ via mixing with denitrified waters of the eastern tropical Pacific. The extent of the enrichment beyond the depths associated with eastern tropical Pacific denitrification (i.e. well below 1000m, see Appendix A), most likely results from the remineralization of organic matter produced from enriched $\delta^{15}\text{N-NO}_3^-$ (as seen off the Hawaiian islands and explained by *Sigman et al.*, [2009]).

In the context of the large and apparently basin-wide mixing of elevated $\delta^{15}\text{N-NO}_3^-$, the waters of the SSCC (5°S for 110°W and 95°W, centered at 200m depth) appear anomalously low with $\delta^{15}\text{N-NO}_3^-$ averaging $\sim 5.3\text{‰}$ (Figures 1.5 and 1.6). These low $\delta^{15}\text{N-NO}_3^-$ measurements cannot be explained as an analytical

underestimation of $\delta^{15}\text{N-NO}_3^-$ related to NO_2^- [e.g. *Casciotti and McIlvin, 2007*], because they are at least 50m below previously measured NO_2^- (based on World Ocean Circulation Experiment data available through <http://www.ewoce.org>) and are replicated between the two transects. One possibility is that mixing with the remineralized products of surface ocean local N_2 fixation (depleted in ^{15}N) produces this low $\delta^{15}\text{N-NO}_3^-$ water. N_2 fixation in the eastern tropical Pacific has been suggested from ocean color [*Westberry et al., 2006*] and the ratio of nutrient concentrations [*Deutsch et al., 2007*], but there are as yet no direct observations of active N_2 fixation in this region. The input of low $\delta^{15}\text{N-NO}_3^-$ from local N_2 fixation can be calculated using an isotopic mass balance and (assuming that N_2 fixation eventually produces $\delta^{15}\text{N-NO}_3^-$ of -2 to 0‰ [*Carpenter et al., 1997; Delwiche et al., 1979; Hoering and Ford, 1960*]) the $[\text{NO}_3^-]$ addition required to match the observations from this study is approximately 4 to $7\mu\text{M}$ (see Supplementary Text in Appendix A for more details of these calculations). Such an increase in $[\text{NO}_3^-]$ is not seen in SSCC waters or anywhere in the eastern tropical Pacific (Figure 1.7). Furthermore it is highly unlikely that the remineralized products of N_2 fixation would be organized at two distinct longitudes (95° and 110°W), coinciding only with the eastward SSCC flow, as is observed; if local N_2 fixation was the source, then this low $\delta^{15}\text{N-NO}_3^-$ should be evident in other eastern tropical Pacific water masses and at other depths as well.

Thus it is likely that this low $\delta^{15}\text{N-NO}_3^-$ water was advected by the SSCC water mass (Figure 1.6). An exact match between SSCC current location and $\delta^{15}\text{N-}$

NO_3^- in Figure 1.6 is not expected, because ADCP is only a “snapshot” and tropical instability waves may shift water masses meridionally. Furthermore, the distribution of tropical Pacific nutrients critically depends on the integrated physical conditions of the preceding month [Strutton *et al.*, 2008], conditions not likely to be consistent with the ADCP measurements. Additionally, because the Tsuchiya Jets recirculate into westward bound currents near and east of 110°W as part of the Deep Tropical Gyre [Rowe *et al.*, 2000 and others], mixing of lower $\delta^{15}\text{N-NO}_3^-$ values towards the equator is expected. This is in fact what is observed—a gradient of lower to higher $\delta^{15}\text{N-NO}_3^-$ immediately equatorward of the SSCC (Figure 1.6). There is no analogous gradient for the NSCC because the $\delta^{15}\text{N-NO}_3^-$ of that water mass is very similar to ambient $\delta^{15}\text{N-NO}_3^-$.

The structure of the SSCC provides some additional constraints on possible sources of this lower $\delta^{15}\text{N-NO}_3^-$. It is unlikely that the SSCC is altered en route from the western equatorial Pacific, because the Tsuchiya Jets are modified relatively little by lateral or vertical mixing over great distances [Johnson and Moore, 1997; Tsuchiya, 1981]. One major reason the Tsuchiya Jets retain their characteristics across the Pacific is the presence of poleward potential vorticity barriers that severely reduce mixing with the subtropical gyres. These constraints strongly suggest that the low $\delta^{15}\text{N-NO}_3^-$ associated with the eastern SSCC water must also be present in the source of the SSCC.

In determining the source of the SSCC, the classical geochemical tracers offer no definitive clues. For example, there is no significant difference between the SSCC

and other tropical waters for measurements of $[\text{NO}_3^-]$ (Figure 1.7), oxygen (Figure 1.1), N^* (Appendix Figure A4), or CFCs [Fine *et al.*, 2001]. On the basis of basin-wide distributions of nutrients, temperature, and salinity, Tsuchiya, [1981] argued that SSCC source waters begin in the North Tasman Sea, then move around the southern subtropical gyre, and through the Coral and Solomon Seas before forming the SSCC. In a more general sense, several studies argue that the subantarctic Pacific is a major supplier of subsurface water (especially nutrients) to the tropical Pacific [McCartney, 1982; Toggweiler *et al.*, 1991; Sarmiento *et al.*, 2004]. While I have previously dismissed the subantarctic surface waters as a source of tropical Pacific water, it is possible that deeper waters with lower $\delta^{15}\text{N}\text{-NO}_3^-$ (as are found for the high southern latitude subthermocline waters [Sigman *et al.*, 2000]) are the source of the depleted SSCC.

For each of these potential source water regions, the subsurface water mass is most likely created by an increased wintertime mixed layer (several hundreds of meters deep) followed by summertime stratification (after McCartney, [1982]). These deep-mixing processes could entrain low $\delta^{15}\text{N}\text{-NO}_3^-$ found in deep waters in the southern high latitudes and advect this signal towards the tropics, eventually forming the SSCC waters. One difficulty with this explanation is that low $\delta^{15}\text{N}\text{-NO}_3^-$ ($\sim 5\text{‰}$) water is only found near the surface (on the scale of 100s of meters) at latitudes greater than 60°S . In the more likely regions of mode water formation (the subantarctic), $\delta^{15}\text{N}\text{-NO}_3^-$ of $\sim 5\text{‰}$ is more than 1500m below the surface [Sigman *et al.*, 2000; DiFiore *et al.*, 2006; this study]. Following these constraints on SSCC

source water, it is not likely that the low $\delta^{15}\text{N-NO}_3^-$ of SSCC waters is derived from subthermocline waters of the higher latitudes.

If the lower $\delta^{15}\text{N-NO}_3^-$ signal in the SSCC is not derived from local N_2 fixation or subthermocline waters in the Southern Ocean, it is most likely that SSCC source waters mix with depleted $\delta^{15}\text{N-NO}_3^-$ produced from the remineralized products of N_2 fixation en route to the tropics. In fact, N_2 fixation is found occurring in the proposed source region of the North Tasman Sea [*Cliff Law Personal Communication*]. There is also abundant N_2 fixation in the Coral Sea [*Dupouy et al.*, 1988; *Campbell et al.*, 2005; *Masotti et al.*, 2007; *Garcia et al.*, 2007; *Biegala et al.*, 2008] and in the subtropical gyre [*Raimbault and Garcia*, 2008], which lie along the route proposed by *Tsuchiya*, [1981] for SSCC water. While further work is necessary to confirm this proposed source water region, such as $\delta^{15}\text{N-NO}_3^-$ measurements in the North Tasman and Coral Seas, the available evidence supports an SSCC source that is influenced by the products of N_2 fixation.

Tsuchiya Jet recirculation may also influence the characteristics of water to the poleward side of the subsurface jets. Previous $\delta^{15}\text{N-NO}_3^-$ studies in the eastern tropical Pacific ODZs have consistently found lower $\delta^{15}\text{N-NO}_3^-$ at shallower depths than the higher $\delta^{15}\text{N-NO}_3^-$ of the ODZ; a feature that has been described as the signature of N_2 fixation [*Brandes et al.*, 1998]. These same characteristics are found in the survey presented here (Figure 1.5). However, I propose an alternative model to explain this feature: mixing along isopycnal surfaces of ambient tropical Pacific $\delta^{15}\text{N-NO}_3^-$ above the ODZ. Previous studies have argued that while the Tsuchiya Jets certainly mix

towards the equator in the east, some of the Tsuchiya Jets also recirculate towards the poles in “the huge low-oxygen tongues at 10-15°N and 8-12°S” [Tsuchiya, 1981] and that the NSCC, “has a persistent northern component” in the east [Rowe *et al.* 2000]. Mixing between the NSCC and the top of the ODZ would predictably produce gradients of decreasing oxygen and increasing $\delta^{15}\text{N-NO}_3^-$, both of which are observed in this data (Figures 1.1 and 1.5) and which could be mistaken as resulting from N_2 fixation. This alternative explanation involving isopycnal mixing provides a physical explanation for this apparent depletion in $\delta^{15}\text{N-NO}_3^-$.

Finally, the equatorial thermostat—water of constant temperature sometimes described as “13°C water” [Tsuchiya, 1981]—is a well-known feature that is present throughout the equatorial Pacific. The thermostat is particularly well-defined in the east where its volume increases dramatically near the Galapagos Islands (~90°W) to a depth range of ~100 to 350m (data not shown); an expansion following the slowing of the EUC and increasing flow towards the west at this location [Lukas, 1986]. This expansion also coincides with the formation of a clearly defined bowl of homogenous nitrate and oxygen concentrations along the 95°W transect—a feature not found for 110°W (Figures 1.1, A1, and 1.7). The lower $[\text{NO}_3^-]$ (~20 μM) and higher oxygen of the 95°W thermostat is very similar to that measured in the EUC. This feature reflects the fact that EUC water “fills up” the thermostat with lower $[\text{NO}_3^-]$ and higher oxygen water as it slows and recirculates westward in the SEC, which was described originally using only temperature [Lukas, 1986]. These observations illustrate that the

processes responsible for strengthening the equatorial thermostat also generate a unique zone of relatively homogenous oxygen and nutrient concentrations.

1.5 Conclusions

Here we have provided and discussed the first synoptic view of tropical Pacific $\delta^{15}\text{N-NO}_3^-$. This almost basin-wide dataset illustrates that all $\delta^{15}\text{N-NO}_3^-$ in the tropical Pacific (throughout the top 600m, from 165°E to 95°W) has an average value of $\sim 7\text{‰}$ (Figure 1.5)—a value that is $\sim 2\text{‰}$ higher than subthermocline values in the Southern [Sigman *et al.*, 2000; DiFiore *et al.*, 2006] and Atlantic Oceans [Knapp *et al.*, 2005; Knapp *et al.*, 2008]. This paper argues that tropical Pacific $\delta^{15}\text{N-NO}_3^-$ is higher than in other regions from mixing with eastern Pacific ODZs—areas where denitrification causes an enrichment of the nitrate pool. Additional $\delta^{15}\text{N-NO}_3^-$ measurements from the eastern tropical Pacific show very high values ($>18\text{‰}$) in the heart of the northern ODZ and relatively low values ($\sim 5.3\text{‰}$) associated with the waters of the SSCC (Figures 1.5 and 1.6). It is likely that the depleted $\delta^{15}\text{N-NO}_3^-$ in the SSCC is derived through mixing with the remineralized products of N_2 fixation in the North Tasman Sea, Coral Sea, and / or the south Pacific gyre [Dupouy *et al.*, 1988; Campbell *et al.*, 2005; Masotti *et al.*, 2007; Garcia *et al.*, 2007; Biegala *et al.*, 2008; Cliff Law, Personal Communication; Raimbault and Garcia, 2008].

In summary, this study places special importance on subsurface mixing processes—between the eastward jets and westward currents—for the distribution of water mass properties throughout the tropical Pacific. Furthermore, these results

suggest larger circulatory patterns with a special role for the subtropics in providing source water to the SSCC.

1.6 Acknowledgements

This study would not have been possible without the help of Jan Kaiser (who sampled the 2003 95°W/110°W transects) and the support of the National Oceanic and Atmospheric Administration (NOAA), who were gracious in sampling on board their ships the *Ka'imimoana* and the *Ronald H. Brown*. Outstanding assistance was provided by Mike McPhaden, Brian Lake, Chris Beaverson, Jan Kaiser, Shawn Gendron, Tonya Watson, the crew of the aforementioned ships, and the Monterey Bay Aquarium Research Institute. Invaluable laboratory-based contributions were made by Greg Cane, Dennis Graham, and Yi Wang.

1.7 Figures

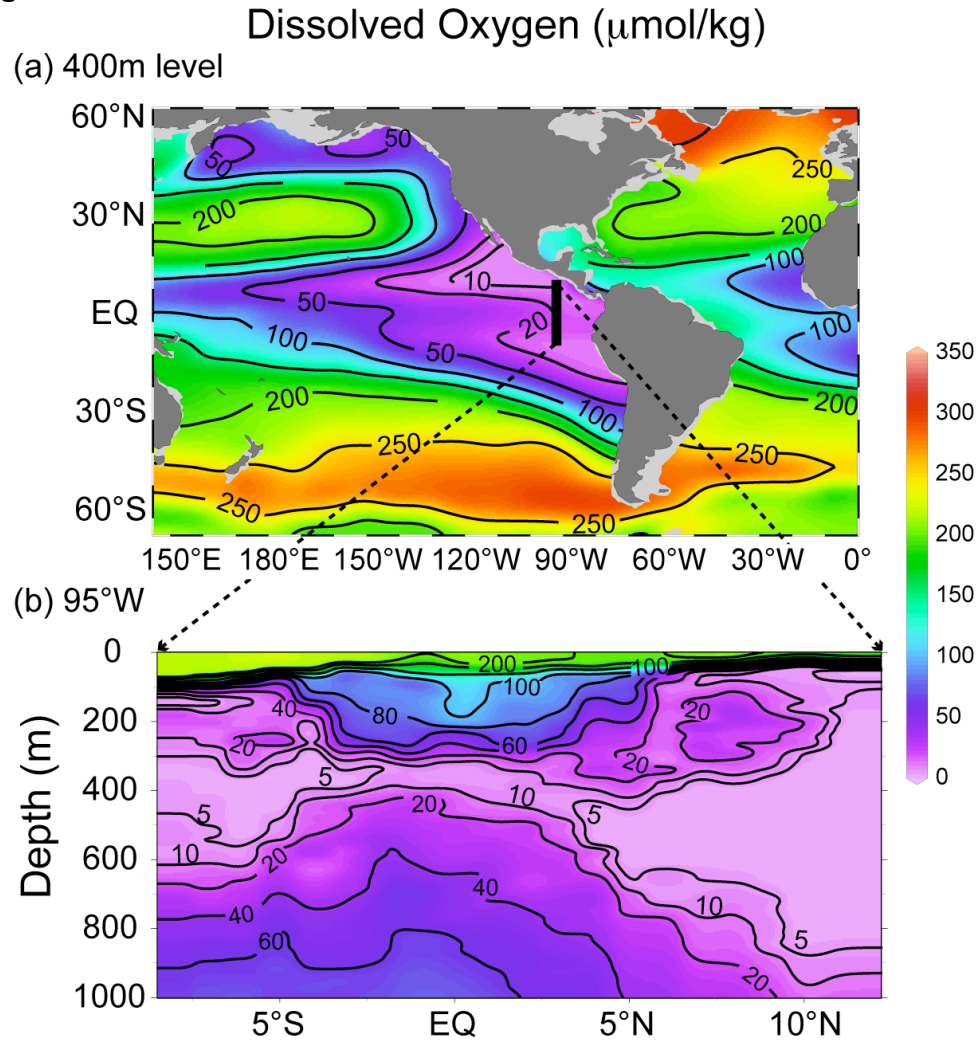


Figure 1.1: (a) Annual mean oxygen (“O₂” in $\mu\text{mol/kg}$) at 400m depth for Pacific Ocean (data from World Ocean Atlas [Garcia et al., 2006]). Tropical Pacific water at 400m is on approximately the same isopycnal (~26.7 sigma-theta). (b) Oxygen ($\mu\text{mol/kg}$) measured at hydrocast stations along the 95°W transect on the October/November 2003 *Ronald H. Brown* cruise (station locations represented by black bar in Figure 1.4). Data has been interpolated from a 1m depth interval with a 1° latitude resolution or better.

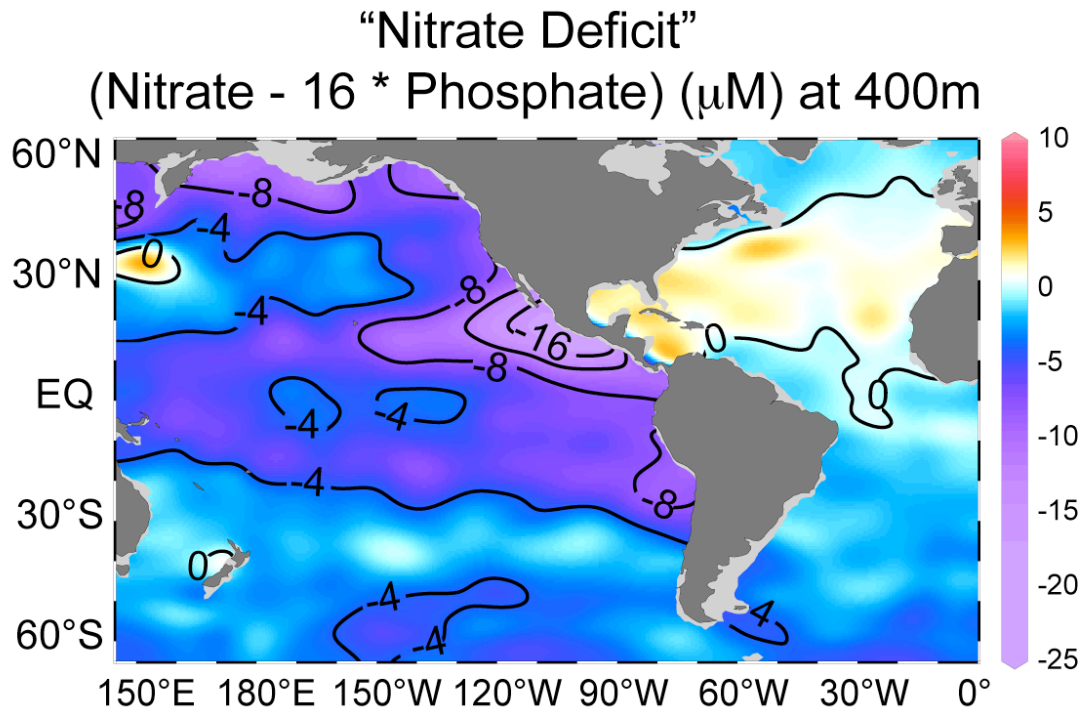


Figure 1.2: Deviation of nitrate: phosphate ratio based on Redfield ratio, “N Star” or “N*” [$N^* = \text{nitrate} - (16 * \text{phosphate})$] in units of $\mu\text{mol/liter}$ (μM) at 400m depth for Pacific Ocean (data from World Ocean Atlas 2005 [Garcia et al., 2006]).

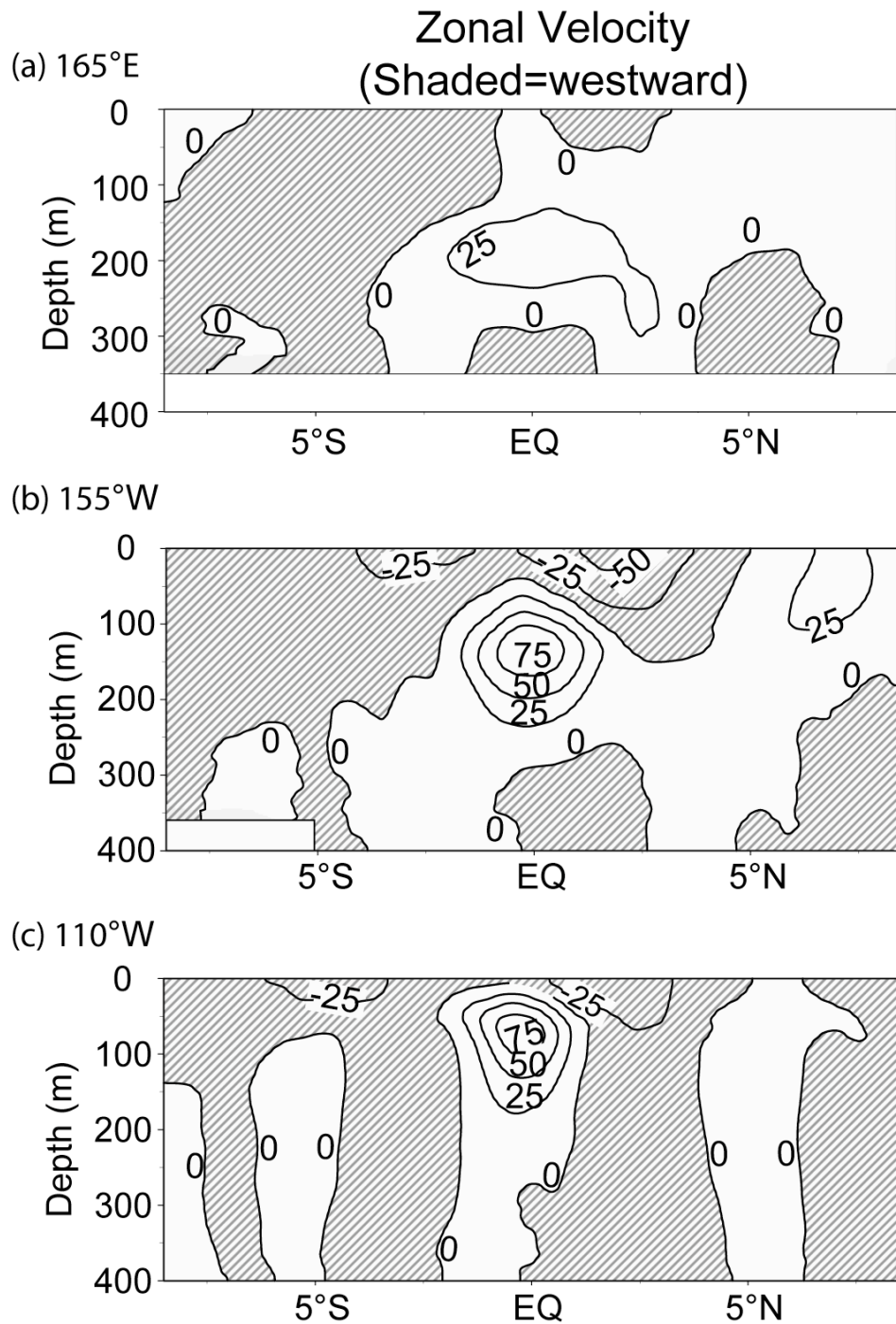


Figure 1.3: Tropical Pacific mean annual subsurface zonal circulation (cm/s) from *Johnson et al.*, [2002]. Shaded regions represent westward circulation. See text for detailed description of the interactions between each water mass.

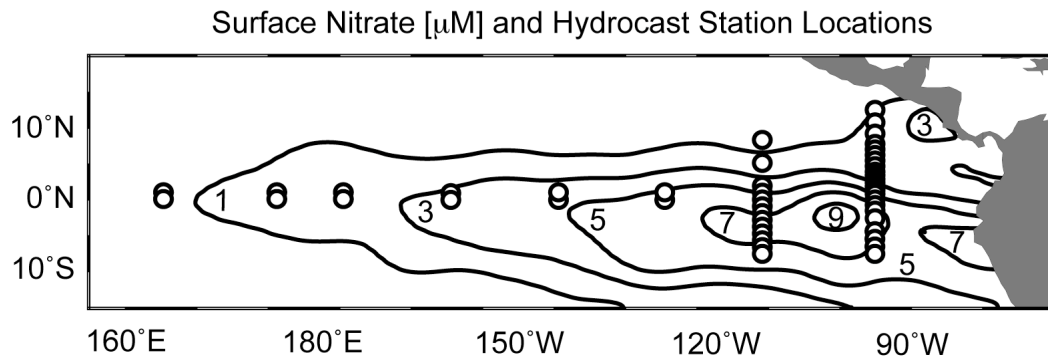


Figure 1.4: Tropical Pacific surface water mean annual nitrate concentrations (μM) with hydrocast station locations (circles) (see Appendix Table A1 for more information) (data from World Ocean Atlas 2005 [Garcia et al., 2006]).

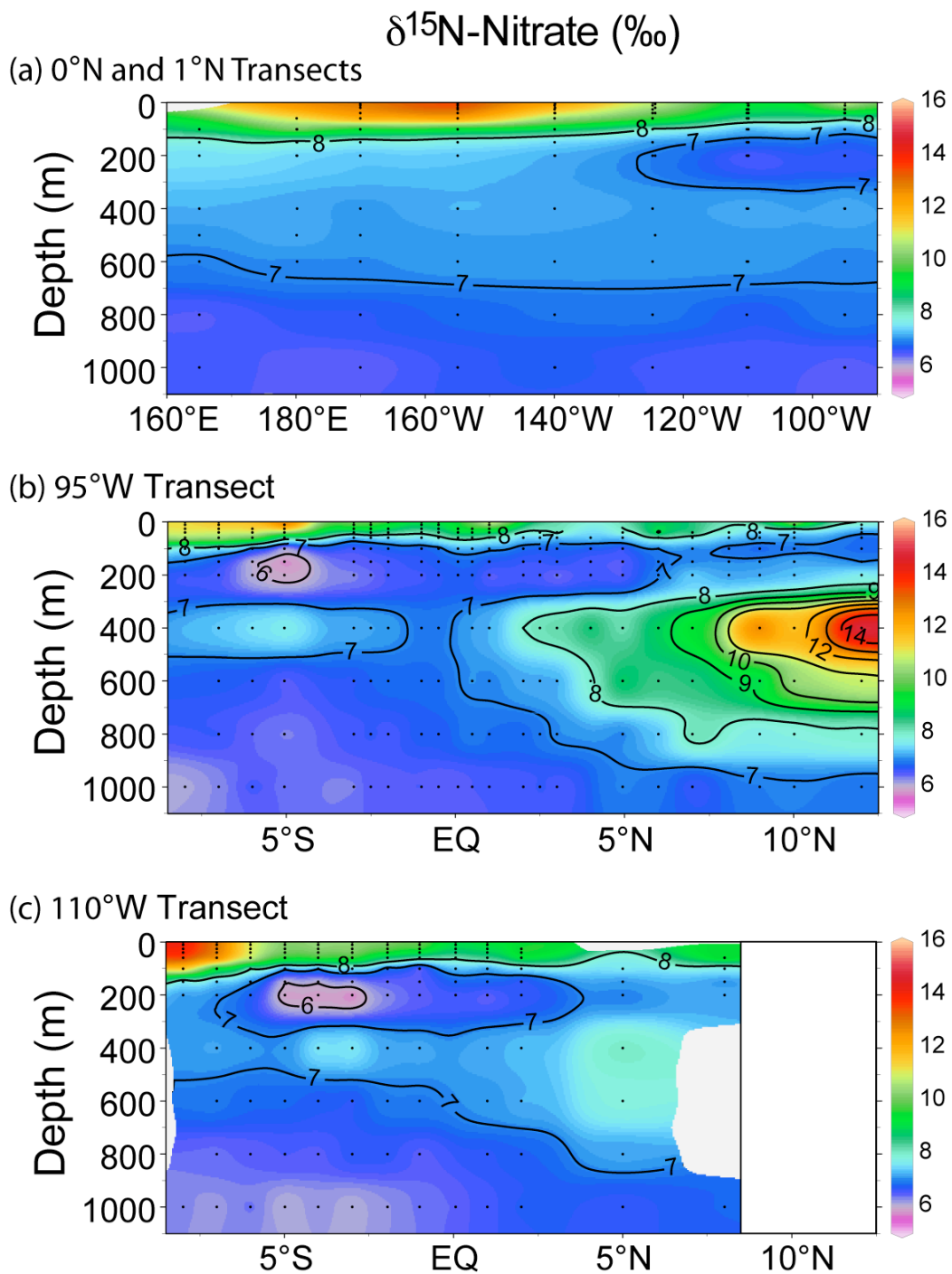
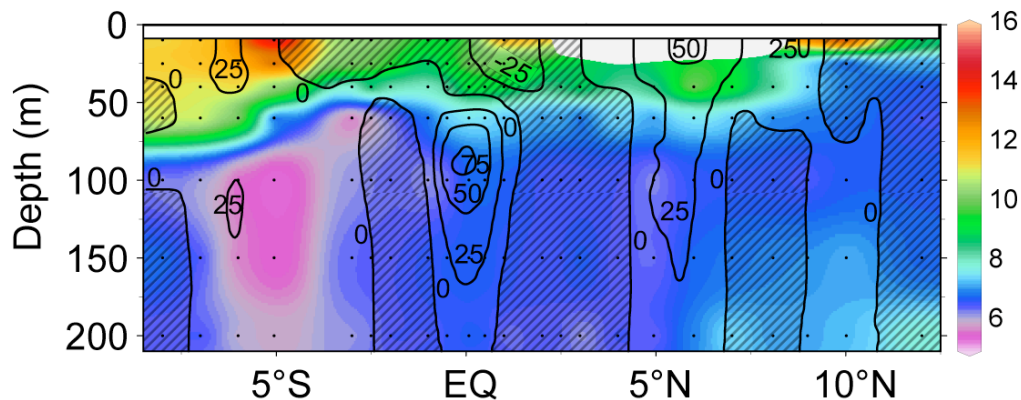


Figure 1.5: Measurements of $\delta^{15}\text{N-NO}_3^-$ (in ‰) for transects along (a) 0° and 1°N from the eastern to western equatorial Pacific, (b) 95°W , and (c) 110°W . See Figure 1.4 or Appendix Table A1 for more hydrocast station details.

$\delta^{15}\text{N-Nitrate}$ (‰) (color) and
Zonal Velocity (shaded=westward)

(a) 95°W Transect



(b) 110°W Transect

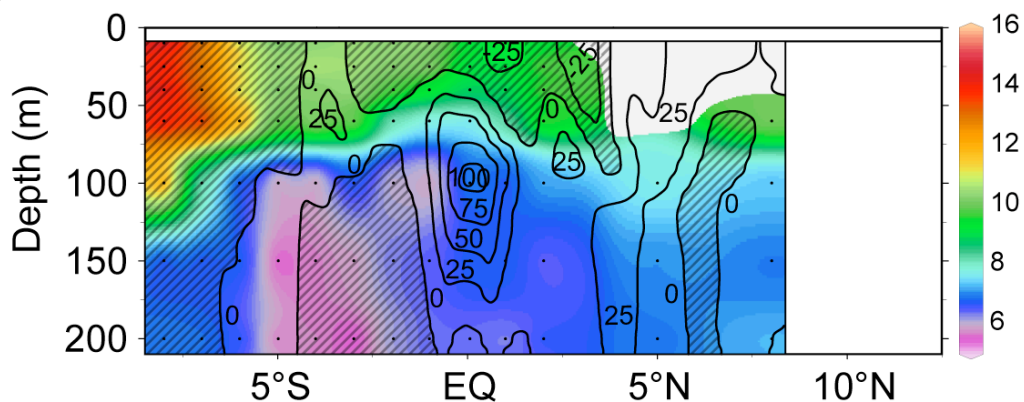


Figure 1.6: Measurements of $\delta^{15}\text{N-NO}_3^-$ (in ‰) for the (a) 95°W transect and (b) 110°W transect from Figure 1.5 (see color bar on right for values) and zonal current velocity from 40 to 210m from Acoustic Doppler Current Profiler (ADCP: black contour lines). Shaded contours represent westward circulation in cm/s. Note the lowest $\delta^{15}\text{N-NO}_3^-$ values are found for 100 and 150m depth at ~5°S.

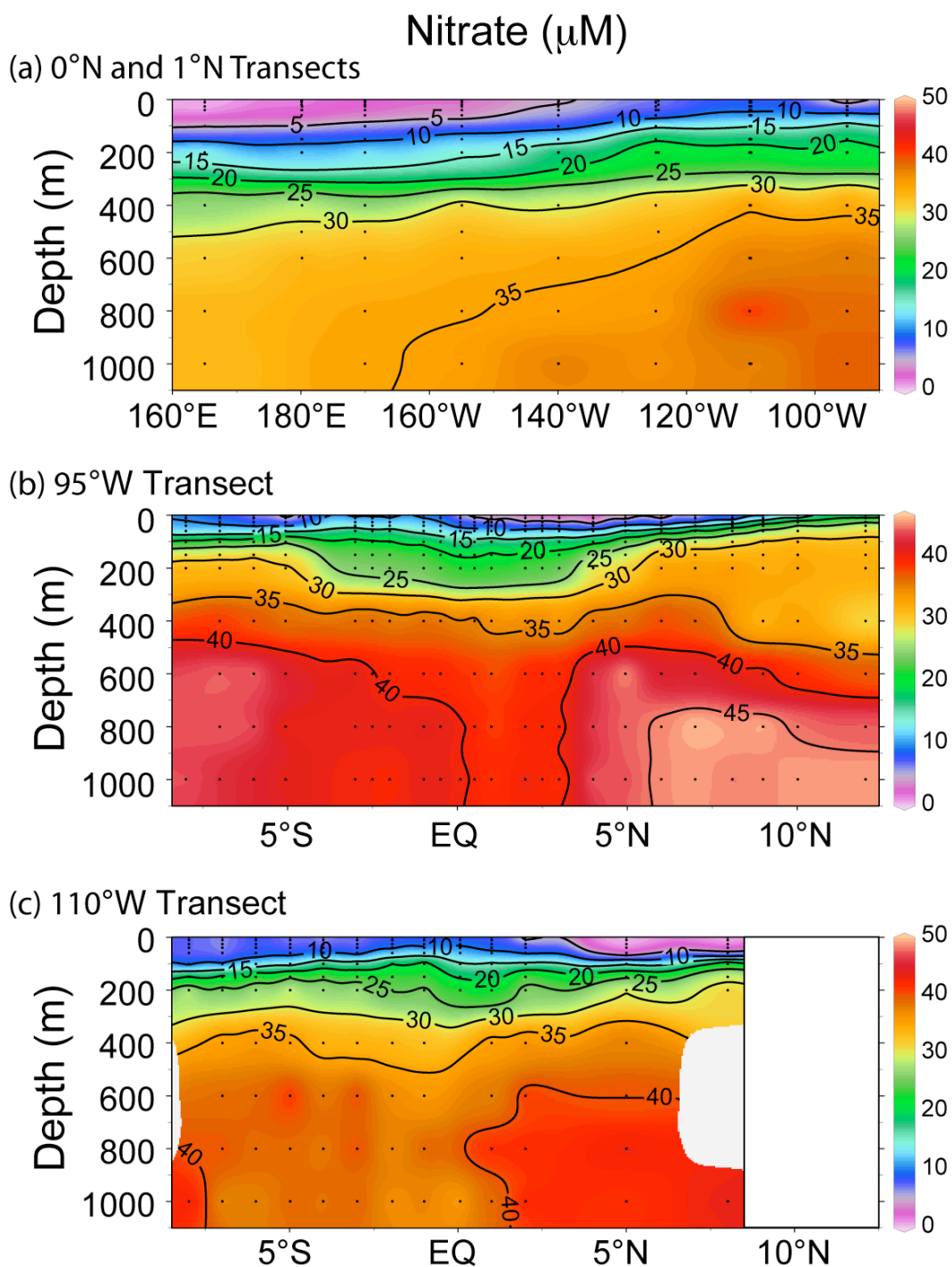


Figure 1.7: Measurements of NO_3^- (in μM) for transects along (a) 0° and 1°N from the eastern to western equatorial Pacific, (b) 95°W , and (c) 110°W . See Figure 1.4 or Appendix Table 1 for more hydrocast station details.

1.8 References

- Altabet, M.A. and R. Francois, (1994) Sedimentary nitrogen isotopic ratio as a recorder for surface ocean nitrate utilization, *Global Biogeochemical Cycles*, 8, 103-116.
- Biegala, I.C., and P. Raimbault (2008), High abundance of diazotrophic picocyanobacteria (< 3 μm) in a Southwest Pacific coral lagoon, *Aquatic Microbial Ecology*, 51, 45-53.
- Brandes, J.A., A.H. Devol, T. Yoshinari, A. Jayakumar, and S.W. A Naqvi, (1998), Isotopic composition of nitrate in the central Arabian Sea and eastern tropical North Pacific: A tracer for mixing and nitrogen cycles, *Limnology and Oceanography*, 43, 1680–1689.
- Brandes, J.A., and A.H. Devol (2002), A global marine fixed nitrogen isotopic budget: Implications for Holocene nitrogen cycling, *Global Biogeochemical Cycles*, 16, doi:10.1029/2001GB001856.
- Braman, R.S., and S.A. Hendrix (1989), Nanogram nitrite and nitrate determination in environmental and biological materials by V(III) reduction with chemiluminescence detection, *Anal. Chem.*, 61, 2715–2718.
- Brzezinski, M.A., M.L. Dickson, D.M. Nelson, and R. Sambrotto (2003), Ratios of Si, C and N uptake by microplankton in the Southern Ocean, *Deep-Sea Research II*, 50, 619–633.
- Butt, J. and E. Lindstrom (1994), Currents off the east-coast of New Ireland, Papua New Guinea and their relevance to regional undercurrents in the western equatorial Pacific Ocean, *Journal of Geophysical Research-Oceans*, 99, 12503-12514.
- Campbell L., E.J. Carpenter, J.P. Montoya, A.B. Kustka, and D.G. Capone (2006), Picoplankton community structure within and outside a *Trichodesmium* bloom in the southwestern Pacific Ocean, *Vie et Milieu*, 55, 185-195.
- Carpenter, E., H. Harvey, B. Fry, and D. Capone (1997), Biogeochemical tracers of the marine cyanobacterium *Trichodesmium*, *Deep Sea Research, Part I*, 44, 27– 38.
- Casciotti, K.L., and M.R. McIlvin (2007), Isotopic analyses of nitrate and nitrite from reference mixtures and application to Eastern Tropical North Pacific waters, *Marine Chemistry*, 107, 184-201.

- Casciotti, K.L., D.M. Sigman, M.G. Hastings, J.K. Bohlke, and A. Hilkert (2002), Measurement of the oxygen isotopic composition of nitrate in seawater and freshwater using the denitrifier method, *Anal. Chem.*, *74*, 4905–4912.
- Castro, C.G., F.P. Chavez, and C.A. Collins (2001), Role of the California Undercurrent in the export of denitrified waters from the eastern tropical North Pacific, *Global Biogeochemical Cycles*, *15*, 819-830.
- Cline, J.D., and I.R. Kaplan (1975), Isotopic fractionation of dissolved nitrate during denitrification in the eastern tropical North Pacific Ocean, *Mar. Chem.*, *3*, 271–299.
- Codispoti, L.A. and J.P. Christensen (1985), Nitrification, denitrification and nitrous oxide cycling in the eastern tropical South Pacific Ocean, *Mar. Chem.*, *16*, 277–300.
- Codispoti, L.A. and T.T. Packard (1980), Denitrification rates in the eastern tropical South Pacific, *J. Mar. Res.*, *38*, 453–477.
- Codispoti, L.A. and F.A. Richards (1976), An analysis of the horizontal regime of denitrification in the eastern tropical North Pacific, *Limnol. Oceanogr.*, *21*, 379–388.
- Delwiche, C.C., P.J. Zinke, C.M. Johnson, and R.A. Virginia (1979), Nitrogen isotope distribution as a presumptive indicator of nitrogen fixation, *Botanical Gazette*, *140*, 65–69.
- Deutsch, C., N. Gruber, R.M. Key, J.L. Sarmiento, and A. Ganaschaud (2001), Denitrification and N₂ fixation in the Pacific Ocean, *Global Biogeochem. Cycles*, *18*, GB4012, doi:10.1029/2003GB002189.
- Deutsch C., J.L. Sarmiento, D.M. Sigman, N. Gruber, J.P. Dunne (2007), Spatial coupling of nitrogen inputs and losses in the ocean, *Nature*, *445*, 163-167.
- DiFiore, P., D.M. Sigman, T.W. Trull, M.J. Lourey, K. Karsh, G. Cane, R. Ho (2006), Nitrogen isotope constraints on Subantarctic biogeochemistry. *Journal of Geophysical Research*, *111*, C08016, doi:10.1029/2005JC003216.
- Dupouy, C., M. Petit, and Y. Dandonneau (1988), Satellite detected cyanobacteria bloom in the southwestern tropical Pacific—Implication for oceanic nitrogen-fixation, *International Journal of Remote Sensing*, *9*, 389-396.
- Fine, R.A., K.A. Maillet, K.F. Sullivan, and D. Wiley (2001), Circulation and ventilation flux of the Pacific Ocean, *Journal of Geophysical Research—Oceans*, *106*, 22159-22178.

- Firing, E., R. Lukas, J. Sadler, and K. Wyrki (1983), Equatorial undercurrent disappears during the 1982–83 El Niño. *Science*, 222, 1121–1123.
- Garcia, H.E., R.A. Locarnini, T.P. Boyer, and J.I. Antonov, (2006) World Ocean Atlas 2005, Volume 4: Nutrients (phosphate, nitrate, silicate). S. Levitus, Ed. NOAA Atlas NESDIS 64, U.S. Government Printing Office, Washington, D.C., 396 pp.
- Garcia, N., P. Raimbault, V. Sandroni (2007), Seasonal nitrogen fixation and primary production in the Southwest Pacific: nanoplankton diazotrophy and transfer of nitrogen to picoplankton organisms, *Marine Ecology – Progress Series*, 343, 25-33.
- Gouriou, Y. and J. Toole (1993), Mean circulation of the upper layers of the western equatorial Pacific Ocean, *Journal of Geophysical Research*, 98, 22495–22520.
- Graham, B.S., D. Grubbs, K. Holland, and B.N. Popp (2007), A rapid ontogenetic shift in the diet of juvenile yellowfin tuna from Hawaii, *Marine Biology*, 150, 647-658.
- Gruber, N. and J.L. Sarmiento (1997), Global patterns of marine nitrogen fixation and denitrification, *Global Biogeochem. Cycles*, 11, 235–266.
- Gu, D.F. and S.G.H. Philander (1997), Interdecadal climate fluctuations that depend on exchanges between the tropics and extratropics, *Science*, 275, 805-807.
- Hoering, T., and H.T. Ford (1960), The isotope effect in the fixation of nitrogen by Azotobacter, *J. Am. Chem. Soc.*, 82, 376– 378.
- Johnson, G.C., and D.W. Moore (1997), The Pacific subsurface countercurrents and an inertial model, *Journal of Physical Oceanography*, 27, 2448–2459.
- Johnson, G.C. and M.J. McPhaden (1999), Interior pycnocline flow from the subtropical to the equatorial Pacific Ocean, *Journal of Physical Oceanography*, 29, 3073–3098.
- Johnson, G.C., Sloyan, B.M., Kessler, W.S., and K.E. McTaggart (2002), Direct measurements of upper ocean current and water properties across the tropical Pacific during the 1990s, *Progress in Oceanography*, 52, 31–61.
- Kaiser J., M.K. Reuer, B. Barnett , and M.L. Bender (2005), Marine productivity estimates from continuous O₂ / Ar ratio measurements by membrane inlet mass spectrometry, *Geophysical Research Letters*, 32, L19605, doi:10.1029/2005GL023459.

- Karl, D. M., R. Letelier, D.V. Hebel, D.F. Bird, and C.D. Winn (1992), Trichodesmium blooms and new nitrogen in the north Pacific gyre, in Carpenter, E.J., Capone, D.G., and Rueter, J.G., editors, *Marine Pelagic Cyanobacteria: Trichodesmium and other Diazotrophs*, Dordrecht, Kluwer Academic, 219–237.
- Karstensen, J., L. Stramma, and M. Visbeck (2008), Oxygen minimum zones in the eastern tropical Atlantic and Pacific oceans, *Progress in Oceanography*, 77, 331-350.
- Kessler, W.S. (2006), The circulation of the eastern tropical Pacific: A review, *Progress in Oceanography*, 69, 181-217.
- Kessler, WS and L. Gourdeau (2007), The annual cycle of circulation of the southwest subtropical pacific, analyzed in an ocean GCM, *Journal of Physical Oceanography*, 37, 1610-1627.
- Knapp, A.N., Sigman, D.M., and F. Lipschultz (2005), N isotopic composition of dissolved organic nitrogen and nitrate at the Bermuda Atlantic Time-series Study site, *Global Biogeochemical Cycles*, 19, GB1018, doi:10.1029/2004GB002320.
- Knapp, A.N., P.J. DiFiore, C. Deutsch, D.M. Sigman, and F. Lipschultz (2008), Nitrate isotopic composition between Bermuda and Puerto Rico: Implication for N₂ fixation in the Atlantic Ocean, *Global Biogeochemical Cycles*, 22, GB3014, doi:10.1029/2007GB003107.
- Liu, K.K., and I.R. Kaplan (1989), The eastern tropical Pacific as a source of ¹⁵N-enriched nitrate in seawater off southern California, *Limnology and Oceanography*, 34, 820– 830.
- Liu, K.K. (1979), Geochemistry of inorganic nitrogen compounds in two marine environments: The Santa Barbara Basin and the ocean off Peru, Thesis USC.
- Lukas, R. (1986), The termination of the equatorial undercurrent in the eastern Pacific, *Progress in Oceanography*, 16, 63–90.
- Mahaffey, C., Michaels A.F., and D.G. Capone, (2005), The conundrum of marine N₂ fixation, *American Journal of Science*, 305, 546-595.
- Masotti, I., D. Ruiz-Pino, and A. Le Bouteiller (2007), Photosynthetic characteristics of Trichodesmium in the southwest Pacific Ocean: importance and significance, *Marine Ecology-Progress Series*, 338, 47-59.
- McCartney, M.S. (1982), The subtropical recirculation of mode waters. *Journal of Marine Research*, 40, 427-464.

Newsome, S.D., P.L. Koch, M.A. Etner, D. Aurioles-Gamboa (2006), Using carbon and nitrogen isotope values to investigate maternal strategies in northeast Pacific otariids, *Marine Mammal Science*, 22, 556–572.

Raimbault, P. and N. Garcia (2008), Evidence for efficient regenerated production and dinitrogen fixation in nitrogen-deficient waters of the South Pacific Ocean: impact on new and export production estimates, *Biogeosciences*, 5, 323–338.

Rowe, G.D., Firing, E., and G.C. Johnson (2000), Pacific equatorial subsurface countercurrent velocity, transport, and potential vorticity, *Journal of Physical Oceanography*, 30, 1172–1187.

Sarmiento J.L., N. Gruber, M.A. Brzezinski, and J.P. Dunne (2004), High-latitude control of thermocline nutrients and low latitude biological productivity, *Nature*, 427, 56-60.

Sigman, D.M., M.A. Altabet, R. Francois, D.C. McCorkle, and G. Fischer (1999), The $\delta^{15}\text{N}$ of nitrate in the Southern Ocean: Consumption of nitrate in surface waters, *Global Biogeochemical Cycles*, 13, 1149-1166.

Sigman, D.M., M.A. Altabet, D.C. McCorkle, R. Francois, and G. Fischer (2000), The $\delta^{15}\text{N}$ of nitrate in the Southern Ocean: Nitrogen cycling and circulation in the ocean interior, *Journal of Geophysical Research*, 105, 19599-19615.

Sigman, D.M., K.L. Casciotti, M. Andreani, C. Barford, M. Galanter, and J.K. Bohlke (2001), A bacterial method for the nitrogen isotopic analysis of nitrate in seawater and freshwater, *Analytical Chemistry*, 73, 4145-4153.

Sigman, D. M., J. Granger, P.J. DiFiore, M.M. Lehmann, R. Ho, G. Cane, and A. van Geen (2005), Coupled nitrogen and oxygen isotope measurements of nitrate along the eastern North Pacific margin, *Global Biogeochemical Cycles*, 19, GB4022, doi:10.1029/2005GB002458.

Sigman, D. M., P. J. DiFiore, M. P. Hain, C. Deutsch, and D. M. Karl (2009), Sinking organic matter spreads the nitrogen isotope signal of pelagic denitrification in the North Pacific, *Geophysical Research Letters*, 36, L08605, doi:10.1029.

Sloyan, B.M., G.C. Johnson, and W.S. Kessler (2003), The Pacific cold tongue: A pathway for interhemispheric exchange, *Journal of Physical Oceanography*, 33, 1027-1043.

Strutton, P.G., W. Evans, and F.P. Chavez (2008), Equatorial Pacific chemical and biological variability, 1997-2003, *Global Biogeochemical Cycles*, 22, GB2001, doi:10.1029/2007GB003045.

Toggweiler, J.R., K. Dixon, and W.S. Broecker (1991), The Peru upwelling and the ventilation of the South Pacific thermocline, *J. Geophys. Res.*, 96, 20467–20497.

Tsuchiya, M. (1981), The origin of the Pacific equatorial 13 degrees water, *Journal of Physical Oceanography*, 11, 794-812.

Tsuchiya, M., R. Lukas, R.A. Fine, E. Firing, and E. Lindstrom (1989), Source waters of the Pacific equatorial undercurrent, *Progress in Oceanography*, 23, 101–147.

Westberry, T.K., and D.A. Siegel (2006), Spatial and temporal distribution of *Trichodesmium* blooms in the world's oceans, *Global Biogeochemical Cycles*, 20, GB4016, doi:10.1029/2005GB002673.

Wyrtki, K. (1967), Circulation and water masses in the eastern equatorial Pacific Ocean, *International Journal of Oceanology and Limnology*, 1, 117–147.

Wyrtki, K. (1981), An estimate of equatorial upwelling in the Pacific. *Journal of Physical Oceanography*, 11, 1205–1214.

Vöss, M., J.W. Dippner, and J.P. Montoya (2001), Nitrogen isotope patterns in the oxygen-deficient waters of the eastern tropical North Pacific Ocean, *Deep Sea Res., Part I*, 48, 1905–1921.

Yoshikawa, C., Y. Yamanaka, T. Nakatsuka, (2005), An ecosystem model including nitrogen isotopes: Perspectives on a study of the marine nitrogen cycle, *Journal of Oceanography*, 5, 921-942.

II. Tropical Pacific nutrient dynamics of the past 1200kyr: an eastern equatorial Pacific record of surface nitrate uptake using sediment N isotopes

2.0 Introduction

On interannual timescales, the distribution of equatorial Pacific sea surface temperatures (SSTs) varies between the “La Nina” state (an extreme form of so-called “normal” conditions) with cool water in the east and warm in the west, and the “El Nino” state where this zonal SST gradient breaks down. Through feedbacks between the upper tropical Pacific Ocean and the atmosphere, these seemingly small changes in SSTs on interannual timescales are the primary driver of global climate variability in the present—the so-called El Nino-Southern Oscillation (ENSO) [*Ropelewski and Halpert, 1987*]. It is possible that the basic physical principles involved in this climate feedback system are relevant on the timescales associated with ice age cycling [*Cane and Clement, 2000*]. In fact, changes in the mean state of the tropical Pacific upper ocean that are analogous to these ENSO events have been directly implicated as a forcing of or reaction to major changes to continental icesheets on the orbital timescales of 41,000 and 100,000 years (100kyr) [*Cane and Clement, 2000; Philander and Fedorov, 2003*]. It has also been proposed that seasonal variations in local incoming solar radiation (insolation) are the primary determinant of mean conditions in the tropical Pacific—favoring either the modern “normal” or favoring a mean state resembling “El Nino” conditions on 23kyr (precessional) frequencies [*Clement et al., 1999*].

In exploring the link between the mean state of the tropical Pacific and the global climate system on these glacial to interglacial timescales, the results so far have

been inconsistent, with some studies showing a clear high latitude connection with the tropics [*CLIMAP*, 1976; *Medina-Elizade and Lea*, 2005; *Liu and Herbert*, 2004] and other studies finding local insolation changes (on 23kyr frequencies) to be most relevant [*Stott et al.*, 2002; *Koutavas et al.*, 2002; *Beaufort et al.*, 2001; *Perks et al.*, 2002]. There are a variety of limitations and contradictions between these and other sediment archives that have made it difficult to provide a reliable record of tropical Pacific conditions over glacial to interglacial cycles (see *Mix*, [2006] for a review).

Here I outline a relatively simple method of estimating Eastern Equatorial Pacific (EEP) thermocline depth—a key component of ENSO variability—through a unique application of the nitrogen isotopic composition of equatorial Pacific sediments. In particular, I demonstrate that by using an array of sediment cores, it is possible to isolate the signal imparted to sedimentary organic matter from the consumption of nitrate in EEP surface waters—a signal that is most likely driven predominantly by the depth of the EEP thermocline [*Turk et al.*, 2001; *Strutton et al.*, 2008]. This investigation of the equatorial Pacific’s role in climate cycling on orbital timescales is critical to understanding one of the fundamental mechanisms comprising the global climate system.

2.1 Background

Nitrogen (N)—a required nutrient for all life—is primarily found in the ocean as nitrate. Phytoplankton incorporate the N isotopic composition of nitrate ($\delta^{15}\text{N-NO}_3^-$), where $\delta^{15}\text{N}$ is measured versus atmospheric N_2 and equals

$$\left[\left(\frac{^{15}\text{N}/^{14}\text{N}}{\text{sample}} / \left(\frac{^{15}\text{N}/^{14}\text{N}}{\text{atmosphere}} \right) - 1 \right) \right]$$

into their biomass and some of this organic

material is deposited on the seafloor. Utilizing the simple guidelines that N_2 fixation decreases $\delta^{15}N-NO_3^-$ and water column denitrification (hereafter “denitrification”) increases $\delta^{15}N-NO_3^-$ (see references in Chapter 1), variability in sediment organic matter $\delta^{15}N$ (hereafter “sediment $\delta^{15}N$ ”) has been interpreted as representing changes in denitrification [*Altabet et al.*, 1995; *Ganeshram and Pederson*, 1998, *Ganeshram et al.*, 2000] and N_2 fixation [*Haug et al.*, 1998]. However, sediment $\delta^{15}N$ is also sensitive to nutrient utilization, because phytoplankton fractionate against NO_3^- with higher $\delta^{15}N-NO_3^-$. Specifically, when surface NO_3^- is not completely consumed, fractionation by phytoplankton occurs and exported $\delta^{15}N$ of PARTICULATE NITROGEN will be less than the $\delta^{15}N-NO_3^-$ delivered to the surface.

These competing effects on sediment $\delta^{15}N$ can be illustrated in the nutrient dynamics of the tropical Pacific—a region where an east-west tilt of the thermocline plays the dominant role in the distribution of surface ocean nutrients [*Turk et al.*, 2001]. The easterly trade winds force the upwelling of relatively cool, nutrient-rich water in the eastern equatorial Pacific (EEP) creating the “cold tongue” (Figure 2.1). This eastern shoaling of the thermocline / nutricline is balanced by very warm surface waters and thermocline depression in the western equatorial Pacific (WEP), which causes the relatively warm, nutrient-poor waters of the “warm pool”. Thus, the east-west thermocline tilt is closely connected to the east-west sea surface temperature (SST) and nutrient gradient. As might be expected, during El Nino (La Nina) events with a reduced (increased) thermocline tilt, productivity decreases (increases) in the

EEP; but because of shallower (deeper) thermocline in the WEP, productivity increases (decreases) in the WEP [Turk *et al.*, 2001; Strutton *et al.*, 2008].

This gradient in surface nutrients imparts a stamp on sedimentary $\delta^{15}\text{N}$. As discussed in Chapter 1 (and seen in Figure 2.2), the sub-thermocline $\delta^{15}\text{N-NO}_3^-$ is relatively homogenous (6.8-7.2‰) across the tropical Pacific, with a value $\sim 2\text{‰}$ higher than the deep ocean average—a result of mixing with denitrified waters in the eastern tropical Pacific. Because of the similarity in $\delta^{15}\text{N-NO}_3^-$ delivered to the surface ocean (hereafter “initial $\delta^{15}\text{N-NO}_3^-$ ”) between the EEP and WEP, the difference in sediment $\delta^{15}\text{N}$ in these regions should only be affected by the differential consumption of surface ocean NO_3^- . Complete NO_3^- consumption in the WEP implies that organic matter exported to the seafloor will have the same $\delta^{15}\text{N}$ as initial $\delta^{15}\text{N-NO}_3^-$ (in Figure 2.2); this equivalence is in fact observed for sediment trap organic particles in this region [Yoshikawa *et al.*, 2005]. Because of incomplete NO_3^- utilization, sediment $\delta^{15}\text{N}$ in the EEP will be several units lower than the initial $\delta^{15}\text{N-NO}_3^-$ (Figure 2.2). Therefore, sediment $\delta^{15}\text{N}$ in the WEP and EEP registers the initial $\delta^{15}\text{N-NO}_3^-$ (that is the product of strength of the eastern tropical Pacific denitrification), but this signal is also overprinted in EEP sediments (pushed to lower values) by changing surface NO_3^- consumption. In short, the WEP sediment $\delta^{15}\text{N}$ is a baseline for complete nitrate consumption for all sites with similar $\delta^{15}\text{N-NO}_3^-$ (all of the subsurface equatorial Pacific as described in Chapter 1) and the east-west gradient in sediment $\delta^{15}\text{N}$ is an estimate for nutrient consumption in the east. The degree to which tropical Pacific nutrients are delivered to surface waters is driven by changes in thermocline tilt.

Consequently, changes in the sedimentary East-West $\delta^{15}\text{N}$ gradient could monitor these aspects of upper equatorial Pacific Ocean over ice age cycles.

2.2 Materials and Methods

Samples were obtained from sediment cores in the eutrophic EEP (ODP Site 849: 0°N , 110°W 3839m and core site RC13-112: 1.2°S , 101°W , 3851m) and the oligotrophic WEP (ODP Site 806B: 0°N , 160°E 2521m) (Figure 2.1). A published sediment $\delta^{15}\text{N}$ record from oligotrophic California continental margin (“CA Margin” ODP 1012) [Liu *et al.*, 2005] is also considered (Figure 2.1). The equatorial Pacific sediment chronologies were constructed by matching foraminiferal oxygen isotope ratio measurements ($\delta^{18}\text{O}$, with similar construction as $\delta^{15}\text{N}$, but standardized to Pee Dee Belemnite) with the foraminiferal $\delta^{18}\text{O}$ stack of *Lisiecki and Raymo*, [2005] (Figure 2.3). Published foraminiferal $\delta^{18}\text{O}$ measurements were used for ODP core site 806B (*C. wuellerstorfi* from *Bickert et al.*, [1993]; *G. ruber* from *Medina-Elizade and Lea*, [2005]), but to span core gaps in this core, additional sample material from nearby core sites ODP 805C and RNDB 74P were used (based on the $\delta^{18}\text{O}$ records of *G. sacculifer* from *Berger et al.*, [1993]; *Perks et al.*, [2002]; and *Memorie Yasuda*, Unpublished Data). For ODP core site 849, the age model was based on $\delta^{18}\text{O}$ measurements on mixed benthic species by *Mix et al.*, [1995].

To determine the concentration and N isotopic ratio for whole sediment $\delta^{15}\text{N}$, samples were freeze-dried, homogenized using an agate mortar and pestle, encapsulated in tin, and combusted in a Costech Elemental Analyzer connected via a

Con-Flo III to a Thermo-Finnigan XP isotope ratio mass spectrometer. All samples were referenced to IAEA sediment standard PACS2 (courtesy of the Ganeshram laboratory, University of Edinburgh) as well as my own in-house reference materials constructed from deep-sea sediment from the east and western equatorial Pacific. These in-house references were provided from “flow-in” sediment cores in the EEP and WEP and they have very similar N concentrations, whole sediment $\delta^{15}\text{N}$, and non-organic components. This reference material was crucial to appropriately estimating any “matrix effects” during $\delta^{15}\text{N}$ analysis of these very low N samples (typically $\sim 0.01\%$).

2.3 Results

In this study, I closely compare measurements made in several sediment cores and therefore required an excellent age model synchronization between all sites. Working under the assumption that the benthic foraminifera at all deep Pacific sites are bathed in seawater with the same $\delta^{18}\text{O}$ value, all $\delta^{18}\text{O}$ values were converted to a common scale and each curve was matched via absolute $\delta^{18}\text{O}$ values. The published age model of *Liu et al.*, [2005] was not altered. As can be seen in Figure 2.3, this synchronization produces excellent results for the relatively slow sedimentation rate deep-sea sediment cores with only minor and infrequent inconsistencies. Using this age model construction, the absolute age model error is estimated to be on the order of $\pm 2\text{kyr}$.

As described in Chapter 1 and shown in Figure 2.2, the initial $\delta^{15}\text{N-NO}_3^-$ is approximately the same (ranging from $\sim 6.8\text{-}7.2\text{‰}$) throughout the tropical Pacific, but the zonal gradient in nitrate consumption produces a gradient in sediment $\delta^{15}\text{N}$. For example, incomplete nitrate consumption in the EEP (and the fractionation against higher $\delta^{15}\text{N-NO}_3^-$ in the mixed layer) results in the export of lower sediment $\delta^{15}\text{N}$ at this site. This is contrasted with the WEP surface waters, where nitrate is completely consumed and the $\delta^{15}\text{N}$ exported to the sediments is approximately equal to subsurface $\delta^{15}\text{N-NO}_3^-$. Therefore, assuming the homogeneous distribution of equatorial Pacific $\delta^{15}\text{N-NO}_3^-$ and complete consumption of nitrate in the WEP is retained over the late Pleistocene (as in the modern ocean) the WEP sediment $\delta^{15}\text{N}$ can be used as the baseline for complete nitrate consumption relative to other equatorial Pacific sediment $\delta^{15}\text{N}$ records. Therefore, the magnitude of the difference between the EEP and WEP sediment $\delta^{15}\text{N}$ should scale to the relative amount of nitrate consumption occurring in the EEP mixed layer. For example, higher photosynthetic uptake rates or decreased delivery of thermocline nutrients to EEP waters (e.g. by the deepening of the thermocline) will change the degree to which this NO_3^- is consumed, resulting in increased utilization of the available NO_3^- , and a higher $\delta^{15}\text{N}$ in the organic matter exported to sediments.

This technique of isolating the isotopic signature of changing nitrate consumption is demonstrated using relatively short sediment $\delta^{15}\text{N}$ records ($\sim 140\text{kyr}$) from the WEP (a small section of the entire ODP 806B record—Figure 2.4a) and EEP (from the RC13-112 piston core—Figure 2.4b). As would be expected from an area of

incomplete NO_3^- consumption, EEP sediment $\delta^{15}\text{N}$ is consistently several units lower than the same measurements made in WEP sediments. To estimate the isotopic imprint on EEP sediment $\delta^{15}\text{N}$ resulting from varying nitrate consumption, the difference between the WEP and EEP is calculated first by mathematically resampling at 1kyr resolution via linear interpolation using Analyseries 2.0.4 (a software package by Paillard *et al.*, [1996]) and then by taking the absolute difference between the resampled records—a calculation referred to here as “ $\Delta\delta^{15}\text{N}$ ” (Figure 2.4c). The grey lines around the sediment $\delta^{15}\text{N}$ (Figures 2.4a and 2.4b) represent a 2kyr lead and lag for each age model. In order to constrain the impact these possible age model errors have on $\Delta\delta^{15}\text{N}$, I calculated $\Delta\delta^{15}\text{N}$ values for the worst case scenario age model errors—2kyr lead in one core and 2kyr lag in the other (grey lines in Figure 2.4c). This experiment shows that while age model adjustments could modify (dampening or enhancing) the $\Delta\delta^{15}\text{N}$ variable, age model errors of this magnitude would not alter the basic character of the record. Furthermore, the largest changes to $\Delta\delta^{15}\text{N}$ (caused by possible age model errors) are associated with the transition from $\delta^{18}\text{O}$ maximum to $\delta^{18}\text{O}$ minimum (deglaciations), and it is more straightforward to synchronize the large $\delta^{18}\text{O}$ shifts between core sites.

While Figure 2.4 illustrated the variability of WEP and EEP sediment $\delta^{15}\text{N}$ over the past 140kyr, Figure 2.5 provides longer records for both the WEP and for another, longer EEP sediment $\delta^{15}\text{N}$ record (ODP 849) over the past 1200kyr. As is seen for the shorter $\delta^{15}\text{N}$ records of Figure 2.4, the absolute value of EEP sediment $\delta^{15}\text{N}$ is consistently lower than the WEP (Figure 2.4c), which is expected from a core

site that receives the same initial $\delta^{15}\text{N-NO}_3^-$, but without complete NO_3^- consumption in surface waters (see Figure 2.1). While both the WEP and EEP sediment $\delta^{15}\text{N}$ records show considerable variability, over long timescales ($>100\text{kyr}$) these records are nearly parallel with each other.

In addition to these sites, a sediment $\delta^{15}\text{N}$ record from *Liu et al.*, [2005] on the California Margin (CA Margin) is shown for comparison with the WEP sediment $\delta^{15}\text{N}$ (Figure 2.5b). The WEP and CA Margin records share a great deal of variability from ~ 200 to 1200kyr . Nitrate is completely consumed in surface waters above the CA Margin site and the source of NO_3^- in this region is elevated in $\delta^{15}\text{N-NO}_3^-$ through mixing with denitrified waters of the Eastern Tropical North Pacific (ETNP) [*Altabet et al.*, 1999; *Castro et al.*, 2001]. As discussed in Chapter 1, the initial $\delta^{15}\text{N-NO}_3^-$ in the WEP is strongly influenced by denitrification not only in the ETNP, but also in the Eastern Tropical South Pacific (ETSP). The deviation between the WEP and CA Margin records is thoroughly discussed in Chapter 3, but it is included in this comparison to illustrate that for much of the past 1200kyr , these records that share a common source of $\delta^{15}\text{N-NO}_3^-$ variability also share very similar sediment $\delta^{15}\text{N}$ variability.

The tactic for isolating the NO_3^- utilization signal from sediment $\delta^{15}\text{N}$ that was demonstrated in Figure 2.4 is similarly applied to the 1200kyr sediment $\delta^{15}\text{N}$ record in the EEP (ODP 849) (Figure 2.5d). This $\Delta\delta^{15}\text{N}$ variable is plotted on a reversed Y-axis so that upwards (downwards) represents increased (decreased) NO_3^- consumption. While there is a good deal of variability, the long-term trend shows a step towards

consistently higher $\Delta\delta^{15}\text{N}$ at $\sim 350\text{kyr}$, which through this interpretation indicates decreased NO_3^- consumption for EEP surface waters. Comparing this EEP NO_3^- utilization record with global icesheet volume (Figure 2.6a) [Lisiecki and Raymo, 2005] and a proxy record of SST in the EEP (Figure 2.6b), illustrates that these records have very little shared variability with $\Delta\delta^{15}\text{N}$. In particular, while icesheet volume and the EEP SST have large amplitude glacial to interglacial cyclicity (primarily at frequencies of $\sim 100\text{kyr}$), the $\Delta\delta^{15}\text{N}$ variable shows little shared variability at this frequency.

$\Delta\delta^{15}\text{N}$ can be compared with other possible measures of nutrient cycling in the eastern Pacific. The simplest sedimentary proxies for marine productivity are based on the relative abundance of sedimentary material that is only derived by surface water phytoplankton. Specifically, sedimentary opal in the EEP is composed of diatoms that dominate the primary productivity in the turbulent waters of upwelling regions [Tozzi *et al.*, 2004]. While the %Opal record is not from the same site as the $\Delta\delta^{15}\text{N}$ variable (and therefore isn't expected to be the most accurate comparison), some of the essential trends in %Opal also appear in the $\Delta\delta^{15}\text{N}$ record—higher %Opal coinciding with lower NO_3^- consumption—especially over precessional periods.

Taking a closer look at the $\Delta\delta^{15}\text{N}$ variable for the past 500kyr (Figure 2.7), there is a close resemblance to the modeled output of Clement *et al.* [1999]—a coupled atmosphere-ocean model of the tropical Pacific with forcing entirely from orbital scale changes in incoming solar radiation (insolation). The output of this model is the SST anomaly in a box from 5°N to 5°S , 150°W to 90°W (the “NINO3” region),

an area where positive SST anomalies are associated with El Niño events (decreased east-west SST gradient and thermocline tilt) in the modern ocean. This model output is dominated by precessional cyclicity (19-23kyr frequency) because (as outlined in *Clement et al.* [1996]) the ocean-atmosphere dynamics of the tropical Pacific are especially sensitive to rectification effects associated by precessional modulation of the seasonal cycle. It is especially important to note that variability in $\Delta\delta^{15}\text{N}$ and the *Clement et al.* model show a high degree of coherence with and the phase is consistent with the physics of the model. The shading in Figure 2.7 highlights the periods of higher NINO3 SSTs (and modeled changes in thermocline tilt), most of which are shared with periods of lower $\Delta\delta^{15}\text{N}$ (and therefore increased NO_3^- consumption).

A closer examination of the relationship between global icesheet variability (Figure 2.8a) and $\Delta\delta^{15}\text{N}$ (estimated EEP nitrate utilization) (Figure 2.8b) further illustrates the very different characteristics of these records. $\Delta\delta^{15}\text{N}$ is compared with measurements of atmospheric dust from the Vostok ice core from Antarctica (Figure 2.8c), because it has been hypothesized that airborne dust may supply iron—a limited micro-nutrient in the equatorial Pacific surface waters—to the EEP and directly impact the uptake of nitrate [*Martin*, 1990]. The variability of these two records, however, has very little in common.

These results can be summarized by simple spectral analysis, using the Arand Spectral software (available from *Philip Howell*, Brown University) (Figure 2.9). To provide a direct comparison with the cycling of icesheet volume, the same analysis was applied to both $\Delta\delta^{15}\text{N}$ and the deep-sea $\delta^{18}\text{O}$ record of *Lisiecki and Raymo*, [2005] (Figure 2.10). The analyses were divided into 3 time periods of the past 1200kyr: 0-

400kyr, 400-800kyr, and 800-1200kyr. As is obvious by eye from Figures 2.7 and 2.8, these results show that $\Delta\delta^{15}\text{N}$ variable has a large precessional component (19-23kyr) for all time scales and reduced or non-specific power at the strongest frequencies of icesheet variability—41kyr and 100kyr (Figure 2.10).

Finally, $\Delta\delta^{15}\text{N}$ (EEP nitrate consumption) can be compared with the east-west equatorial Pacific SST gradient calculated from paleotemperature proxies in the very same sedimentary sequences (Figure 2.11). This comparison is direct, because the age models for both gradient series are the same, and the SST values for each core were linearly interpolated to create a common 1kyr spacing between samples, just as for $\Delta\delta^{15}\text{N}$. While $\Delta\delta^{15}\text{N}$ is calculated by taking the difference of fundamentally the same measurement, the ΔSST is calculated from estimated SST values based on Mg/Ca in surface-dwelling foraminifera for the WEP [*Medina-Elizade and Lea, 2005*] and the alkenone unsaturation ratio for the EEP [*McClumont and Rosell-Mele, 2005*]. Note that a more complete SST reconstruction exists from ODP 846 record (as seen in Figure 2.6), but the synchronization of this record would create an additional source of uncertainty in the comparison. In general, the $\Delta\delta^{15}\text{N}$ and ΔSST shifts are coherent at the precessional periods (reduced $\Delta\delta^{15}\text{N}$, indicative of higher consumption, corresponds with higher SST in the east). However, the obvious difference between these two time series is that the ΔSST records show evidence for lower frequency change (at 41 kyr and 100 kyr periods), while the $\Delta\delta^{15}\text{N}$ does not.

2.4 Discussion

The principle argument of this study is that the history of EEP nitrate consumption can be determined by using an array of sediment $\delta^{15}\text{N}$ records and that these records monitor the depth of the EEP thermocline—a crucial component of the tropical Pacific ocean-atmosphere dynamical feedback that affects modern global climate. If this is an accurate interpretation, then the response of the $\Delta\delta^{15}\text{N}$ helps constrain this dynamical feedback over ice age cycles. The essential inference of $\Delta\delta^{15}\text{N}$ is that it is primarily a product of local insolation (precessional) forcing. The huge changes in high latitude climate associated with ice age cycling seemed to have had little to no influence on equatorial thermocline tilt.

However, the various dimensions of this conclusion must be explored in more detail. Firstly, the interpretation of $\Delta\delta^{15}\text{N}$ as a proxy of EEP thermocline depth can be considered. Support for this interpretation comes from productivity records, such as EEP diatom abundance, which (despite the problems associated with abundance proxies) shares many long-term characteristics with $\Delta\delta^{15}\text{N}$ (Figure 2.6). For example, the shift towards higher $\Delta\delta^{15}\text{N}$ at ~300kyr (increased EEP upwelling) is associated with the trend towards higher diatom abundance [Murray *et al.*, 1995] in the east and also a dramatic phytoplankton regime change in the WEP to “warm water taxa” favoring a deeper thermocline [Zhang *et al.*, 2007]. Along these same lines, sediment productivity proxies show an east to west see-saw on 23kyr timescales, interpreted as changes in the delivery of nutrients caused by the east-west alteration of thermocline depth [Beaufort *et al.*, 2001]. Furthermore, while not experimental evidence, the

characteristics of $\Delta\delta^{15}\text{N}$ are highly consistent with the *Clement et al.*, [1999] model output that is a purely physical response of equatorial Pacific ocean-atmosphere dynamics to insolation (Figure 2.7).

Nevertheless, there are potential biases that might complicate the application of $\Delta\delta^{15}\text{N}$ as strictly a proxy for EEP upwelling. For instance, the low $\delta^{15}\text{N-NO}_3^-$ (~5‰) found in the Southern Subsurface Counter Current, mixes towards the equator near 90°W (see Chapter 1 for full details). The influence on $\delta^{15}\text{N-NO}_3^-$ in surface waters above the RC13-112 site (~2°S, 90°W) is relatively small (perhaps 0.5‰ lower than average tropical Pacific subthermocline water), but this circulation feature might vary over ice ages and therefore provide an additional source of $\Delta\delta^{15}\text{N}$ variability. This possibility required the construction of a $\delta^{15}\text{N}$ record further west at 0°N, 110°W (ODP 849), where it would not be influenced by this lower $\delta^{15}\text{N-NO}_3^-$ water. Another potential non-upwelling source of variability in $\Delta\delta^{15}\text{N}$ might involve the removal of EEP nutrient limitation through iron addition during dry glacial periods (as proposed by *Martin*, [1990]). However, a quick comparison between the ice core dust records and the $\Delta\delta^{15}\text{N}$ record (Figure 2.8) suggests little or no connection.

While *Beaufort et al.*, [2001] found anti-phased behavior between EEP and WEP productivity on precessional timescales, another similar study found that productivity in both regions are completely in-phase [*Perks et al.*, 2002], a result that is completely inconsistent with thermocline driven productivity. However, measurements of equatorial Pacific sediment %N from this study (for the same sediment sites as *Perks*) should be at least as good a measure of surface ocean

productivity as *Perks et al.*, [2002] or *Beaufort et al.*, [2001] and these measurements are $\sim 90^\circ$ out of phase for the 23kyr frequency (please see Appendix B for more details). While these results are not completely anti-phased as seen in *Beaufort et al.*, [2001], this certainly does not support the *Perks et al.*, [2002] and therefore, the weight of evidence supports the interpretation of the $\Delta\delta^{15}\text{N}$ variable as primarily forced by changes in EEP upwelling.

A more problematic and difficult to constrain source of variability may be from changes in the “pre-formed” nitrate concentrations delivered to EEP surface waters—the concentration that is determined in source waters. Changes in pre-formed nutrient concentrations will have no effect on $\Delta\delta^{15}\text{N}$ if the NO_3^- uptake ratio (NO_3^- consumed/ NO_3^- source concentration) is unchanged. However, if the demand for NO_3^- in surface waters does not change, but pre-formed nutrient concentrations are modified, the effect on $\Delta\delta^{15}\text{N}$ might be indistinguishable from changes in EEP upwelling (see Appendix B for calculations and figures describing this effect). Previous studies have suggested that changes in sub-Antarctic mode water formation during deglaciation may provide a large increase in equatorial Pacific thermocline nutrients during the deglacial transition [*Spero and Lea*, 2002]. Based on the modern $\delta^{15}\text{N}\text{-NO}_3^-$ measurements and the discussion of tropical Pacific source waters in Chapter 1, it does not appear that the sub-Antarctic waters have this direct connection to tropical Pacific thermocline. But if this did occur during glacial periods, the likely results would be a decrease in NO_3^- utilization—higher $\Delta\delta^{15}\text{N}$ —during the glacial to interglacial transition. In fact, however, lower $\Delta\delta^{15}\text{N}$ (increased NO_3^- consumption) is

found for the past 5 glacial terminations (Figure 2.8). While it is possible that the hypothesized pulse of high nutrient water relieves nutrient stress and increases NO_3^- consumption, if this were an important feature of the $\Delta\delta^{15}\text{N}$ record, a strong 100kyr frequency should be and is not evident in the spectral analysis (Figure 2.9). As for changes in pre-formed nutrients during other time periods, if equatorial Pacific thermocline source waters are in the subtropics (as suggested in Chapter 1) or sub-Antarctic waters, variability from these regions would be expected to display typical higher latitude frequencies—either at 41kyr and / or 100kyr frequencies that are generally associated with higher latitude processes such as icesheet growth. However, the consistent dominance of precessional cyclicity (usually considered to be an indicator of tropical processes) in the $\Delta\delta^{15}\text{N}$ record strongly suggests that $\Delta\delta^{15}\text{N}$ forcing is grounded in the tropics (Figure 2.9).

As a proxy record of EEP upwelling, there is one fundamental insight provided by the $\Delta\delta^{15}\text{N}$ variable—glacial to interglacial changes in icesheet size (~100kyr timescale) have no effect on the upper ocean dynamics of the tropical Pacific (and by corollary, the tropical Pacific has no effect on icesheet dynamics on timescales longer than precessional periods). This is evident from the comparison of deep ocean $\delta^{18}\text{O}$ with $\Delta\delta^{15}\text{N}$ (Figures 2.6 and 2.8) and is confirmed by spectral analysis (Figure 2.9 and 2.10). Furthermore, while there are some low frequency changes to the $\Delta\delta^{15}\text{N}$ record, there appears to be no significant change associated with the dramatic switch from 41kyr to ~100kyr ice age cycling at ~950kyr (the so-called “Mid-Pleistocene Revolution”) [Shackleton and Opdyke, 1976; Pisias and Moore, 1981]. Clearly,

throughout the past 1200kyr the equatorial Pacific thermocline tilt is dominated by precessional cycling (19-23kyr frequency) (Figure 2.9). This primarily ~23kyr frequency to thermocline tilt is clear support for the ideas put forth by *Clement et al.*, [1999] that changes in solar insolation on orbital timescales can influence the mean state of the tropical Pacific (Figure 2.7).

However, this dominant 23kyr frequency of the equatorial Pacific thermocline tilt provides an interesting contrast with the implications of some proxy records of equatorial Pacific SST. Previous studies have generally found that temperatures in the east and west are strongly associated with the lower frequencies of 41kyr and 100ky, suggesting an influence by icesheet or atmospheric CO₂ dynamics [*Medina-Elizade and Lea, 2005; Liu and Herbert, 2004*]. There are obvious differences between $\Delta\delta^{15}\text{N}$ and SST proxy data from the EEP (Figure 2.6). Some difference might be expected, because while both the $\Delta\delta^{15}\text{N}$ variable and SST should be influenced by thermocline tilt, SST might also be affected by heating and cooling associated with glacial to interglacial changes to the radiative budget (greenhouse gases). However, a more precise comparison would be between $\Delta\delta^{15}\text{N}$ and the SST gradient between the WEP and EEP (Figure 2.11). While there is some agreement between the records, the calculated SST gradient and $\Delta\delta^{15}\text{N}$ are not well aligned for the entire time period shown here. Furthermore, at times (for instance at ~1200kyr) the SST gradient provides unlikely values of ~0°C difference between WEP and EEP surface waters. One of the strengths in using $\Delta\delta^{15}\text{N}$ to estimate thermocline tilt (as opposed to the SST gradient) is that the EEP and WEP measurements for $\Delta\delta^{15}\text{N}$ are made using the same

proxy, while SST is reconstructed by various methods (Mg/Ca ratios in the WEP, alkenone unsaturation in the EEP) with inherently different limitations and assumptions associated with each method (see *Mix*, [2006] for more discussion on this). The comparison with $\Delta\delta^{15}\text{N}$ might therefore provide more detailed insight to the processes responsible for the unreasonable ΔSST values (Figure 2.11). The results presented here suggest that there would be considerable value in expanding such multi-proxy comparisons across the equatorial Pacific on a variety of timescales.

2.5 Conclusions

Here I have introduced an array of sediment $\delta^{15}\text{N}$ records in the equatorial Pacific that provides unique insight to the tilt of the tropical Pacific thermocline over the past 1200kyr—a part of the upper ocean dynamics that drive global climate variability. In particular, these sediment $\delta^{15}\text{N}$ records were strategically located along a gradient in surface nutrients, which allowed the identification of not only the secular changes in $\delta^{15}\text{N}$ of nitrate, but also the variations in eastern equatorial Pacific (EEP) nitrate utilization and therefore EEP thermocline depth. Because thermocline depth in the EEP is an important aspect of the tropical Pacific upper ocean dynamics that produce global climate variability in the present, the $\Delta\delta^{15}\text{N}$ variable provides a history of this important component of the tropical climate system for the past 1200kyr. This estimate for EEP thermocline depth indicates that high latitude processes such as icesheet variability had little to no influence on the tropical climate system. Rather, the

tilt of the tropical Pacific thermocline is primarily influenced from changes in local seasonal insolation on 23kyr timescales (precession).

2.7 Figures

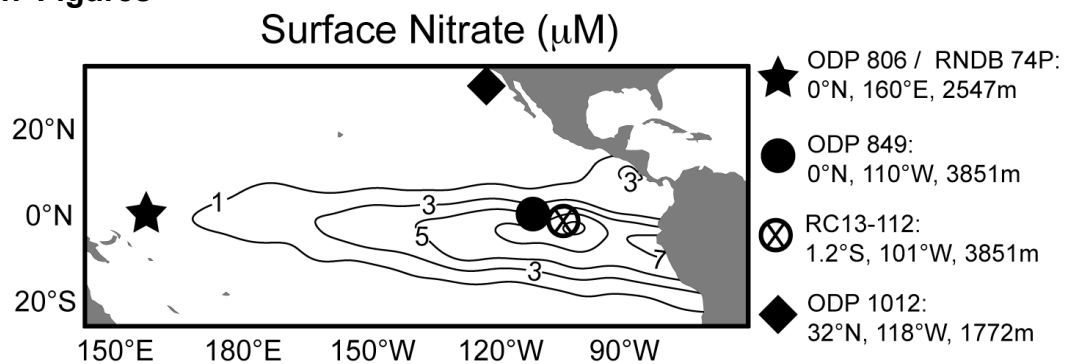


Figure 2.1: Climatological surface NO_3^- concentrations and locations for sediment core records discussed in this chapter (data from World Ocean Atlas 2005 [García et al., 2006]).

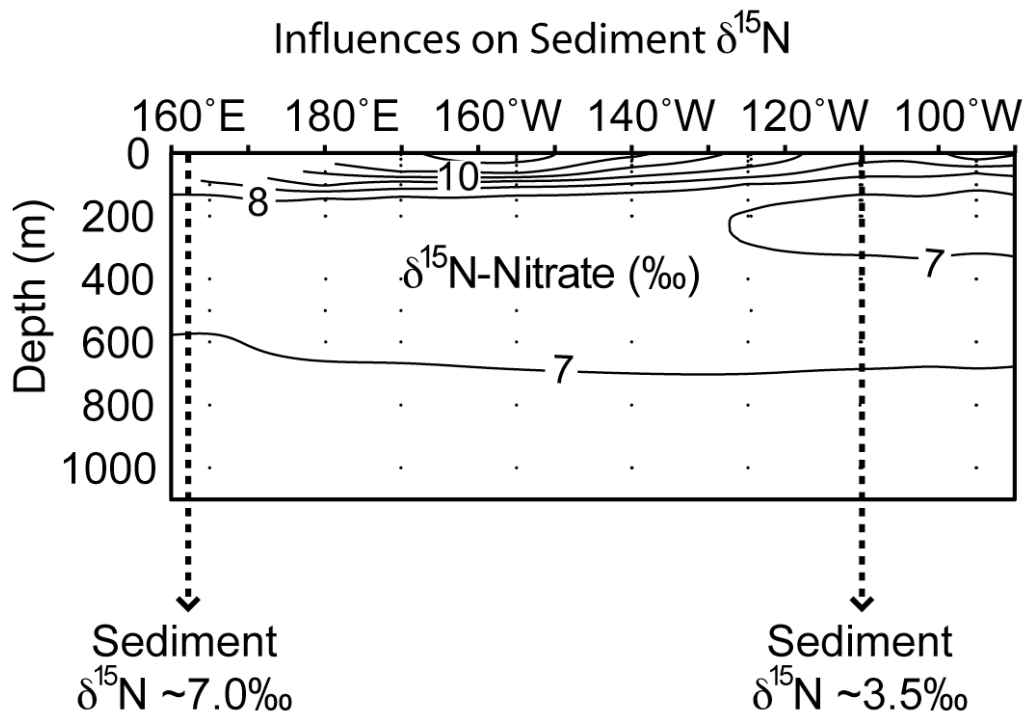


Figure 2.2: Measurements of $\delta^{15}\text{N-NO}_3^-$ along the equatorial Pacific (from Chapter 1), with expected $\delta^{15}\text{N-PARTICULATE NITROGEN}$ export to sediments for the eastern and western equatorial Pacific according to mean surface NO_3^- concentrations, an initial $\delta^{15}\text{N-NO}_3^-$ of 7‰ and the steady state fractionation equations of *Mariotti et al.* [1981] (See Appendix B for more information). Note that NO_3^- is completely consumed by phytoplankton in WEP surface waters and therefore there are no $\delta^{15}\text{N-NO}_3^-$ measurements. The $\delta^{15}\text{N-NO}_3^-$ delivered to the surface (“initial $\delta^{15}\text{N-NO}_3^-$ ”) in the east and west ranges from 6.8-7.2‰, a value that is primarily determined by mixing with denitrified waters in the eastern tropical Pacific (see Chapter 1). The increase in $\delta^{15}\text{N-NO}_3^-$ in the euphotic zone (the top ~100m) is from fractionation by phytoplankton during the uptake of NO_3^- . Because NO_3^- is completely consumed in the WEP, $\delta^{15}\text{N-PARTICULATE NITROGEN}$ exported to WEP sediments is equal to the initial $\delta^{15}\text{N-NO}_3^-$ delivered to the surface and therefore records the variability of initial $\delta^{15}\text{N-NO}_3^-$. However, because of incomplete NO_3^- consumption (and fractionation during nitrate uptake), $\delta^{15}\text{N-PARTICULATE NITROGEN}$ exported to EEP sediments is less than the initial $\delta^{15}\text{N-NO}_3^-$ delivered to the surface. Therefore, EEP sediment $\delta^{15}\text{N}$ is simultaneously recording changes in initial $\delta^{15}\text{N-NO}_3^-$ and changes in surface ocean NO_3^- utilization.

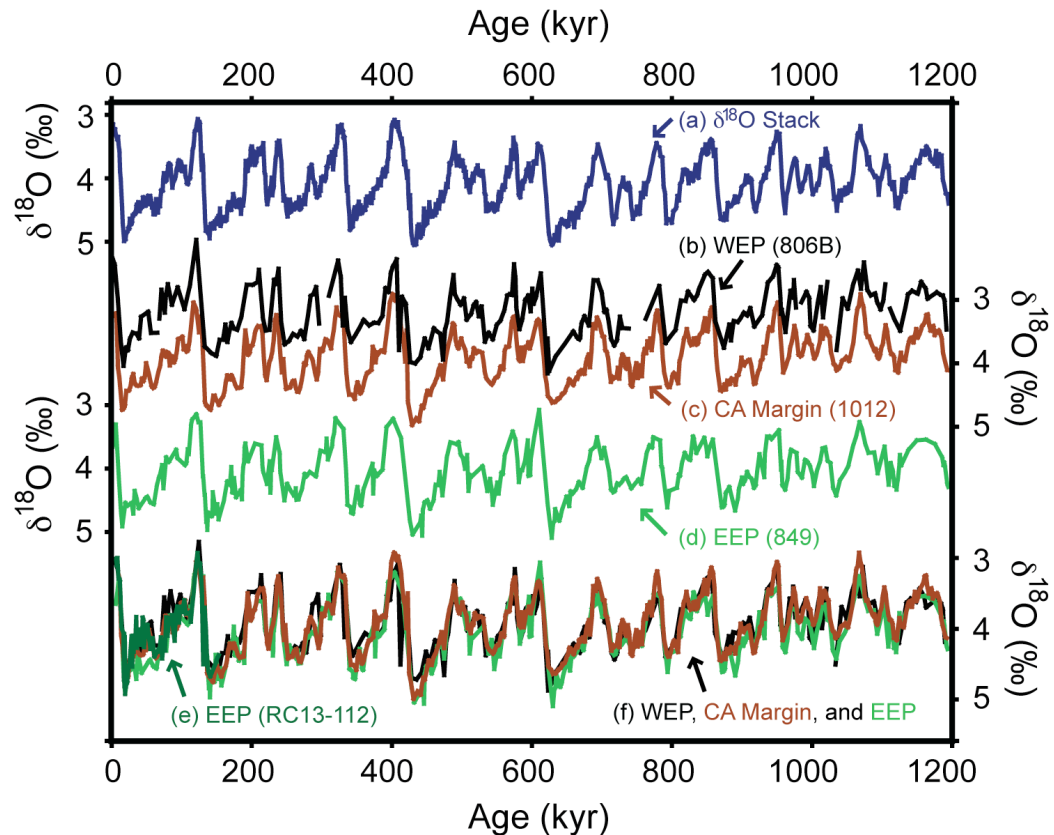


Figure 2.3: Sediment age model synchronization is based on matching foraminiferal $\delta^{18}\text{O}$ with the global $\delta^{18}\text{O}$ stack of (a) *Lisiecki and Raymo*, [2005] with similar measurements made in the (b) Western Equatorial Pacific (WEP) ODP site 806B (from *Bickert et al.*, [1993]), the (c) California Margin (CA Margin) ODP site 1012 (from of *Liu et al.*, [2005]), the (d) Eastern Equatorial Pacific (EEP) ODP site 849 (from *Mix et al.*, [1995]), and (e) EEP site RC13-112 (this study). We adjusted each sediment core $\delta^{18}\text{O}$ values to illustrate the clear overlap (f) between all age models discussed here.

Calculating $\Delta\delta^{15}\text{N}$: Isolating the NO_3^- Utilization Signal

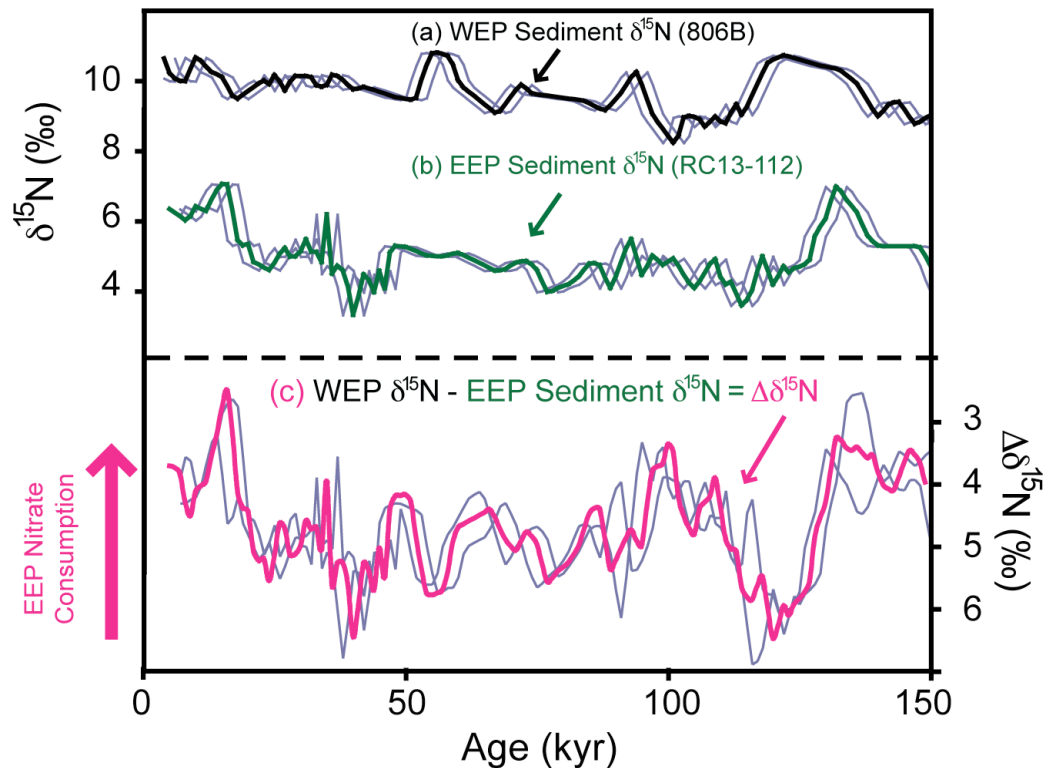


Figure 2.4: This figure provides 150kyr long records of (a) WEP sediment $\delta^{15}\text{N}$ (ODP 806B) and (b) EEP sediment $\delta^{15}\text{N}$ (RC13-112), along with (c) the calculated difference between (a) and (b) (“ $\Delta\delta^{15}\text{N}$ ”). As described in Figure 2.2, depending on the core location, sediment $\delta^{15}\text{N}$ in the equatorial Pacific may be recording one or more signals. The (a) WEP provides a record of changes to the initial $\delta^{15}\text{N}\text{-NO}_3^-$ (caused by eastern tropical Pacific denitrification), but the (b) EEP $\delta^{15}\text{N}$ record is influenced by changes in initial $\delta^{15}\text{N}\text{-NO}_3^-$ and changes in NO_3^- consumption. Therefore, the difference between WEP and EEP sediment $\delta^{15}\text{N}$ gives the (c) estimate for NO_3^- consumption. The grey lines around (a) and (b) are a 2kyr lead and lag for each age model. The grey lines around (c) show the effects of a 2kyr lead in one sediment record with a simultaneous 2kyr lag in the other, providing an age model offset of 4kyr. These results show that while age model adjustments could possibly dampen or enhance the $\Delta\delta^{15}\text{N}$ output, they would not alter the basic characteristics of the $\Delta\delta^{15}\text{N}$ record.

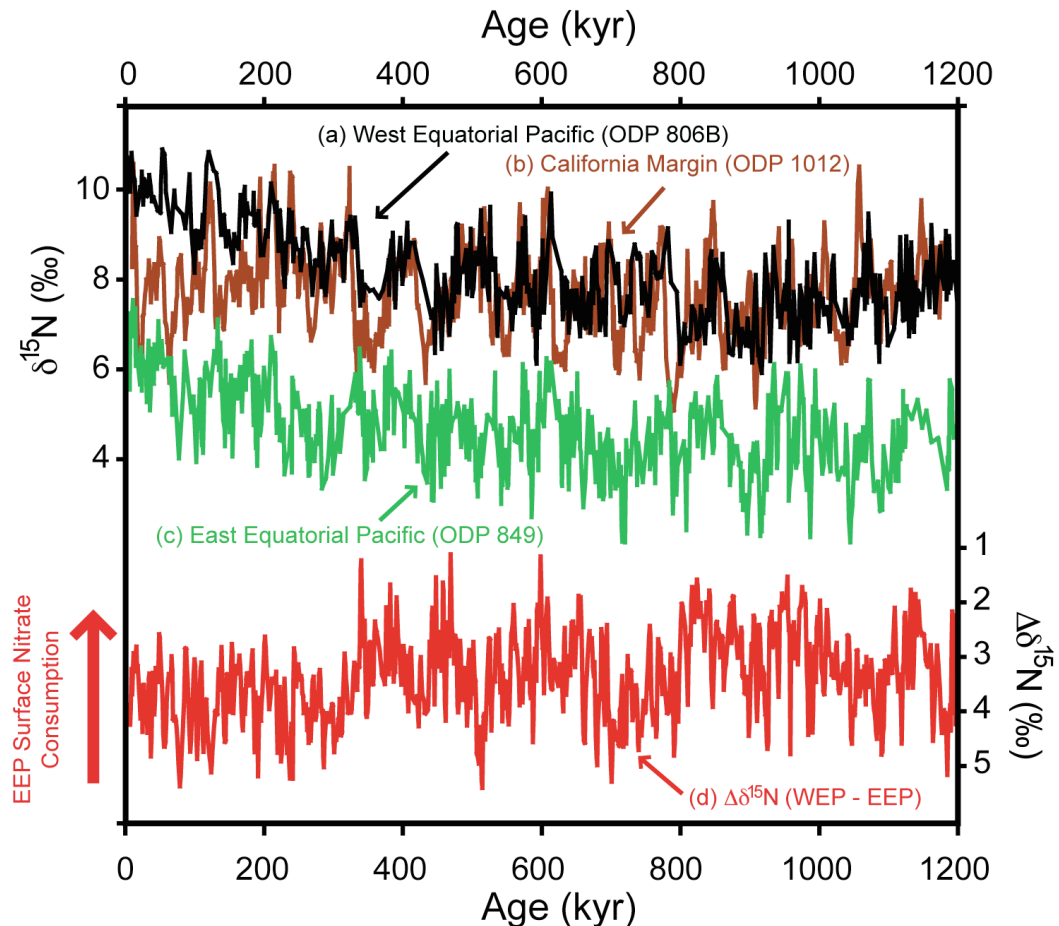


Figure 2.5: Sediment $\delta^{15}\text{N}$ for (a) the Western Equatorial Pacific (ODP 806B), (b) California Margin (ODP 1012) [Liu et al., 2005], and (c) Eastern Equatorial Pacific (ODP 849) for the past 1200kyr. While Figure 2.4 demonstrated the technique of disentangling the N isotopic signals in EEP sediment $\delta^{15}\text{N}$ over the past 150kyr, (d) is the difference between the WEP (a) and (c) another EEP core site (ODP 849). Because this core site is slightly to the west of the EEP site in Figure 2.4, there are some differences in the records (due to differences in surface nitrate consumption). This $\Delta\delta^{15}\text{N}$ variable is plotted with a reversed scale, so that increased relative NO_3^- consumption by phytoplankton is upwards.

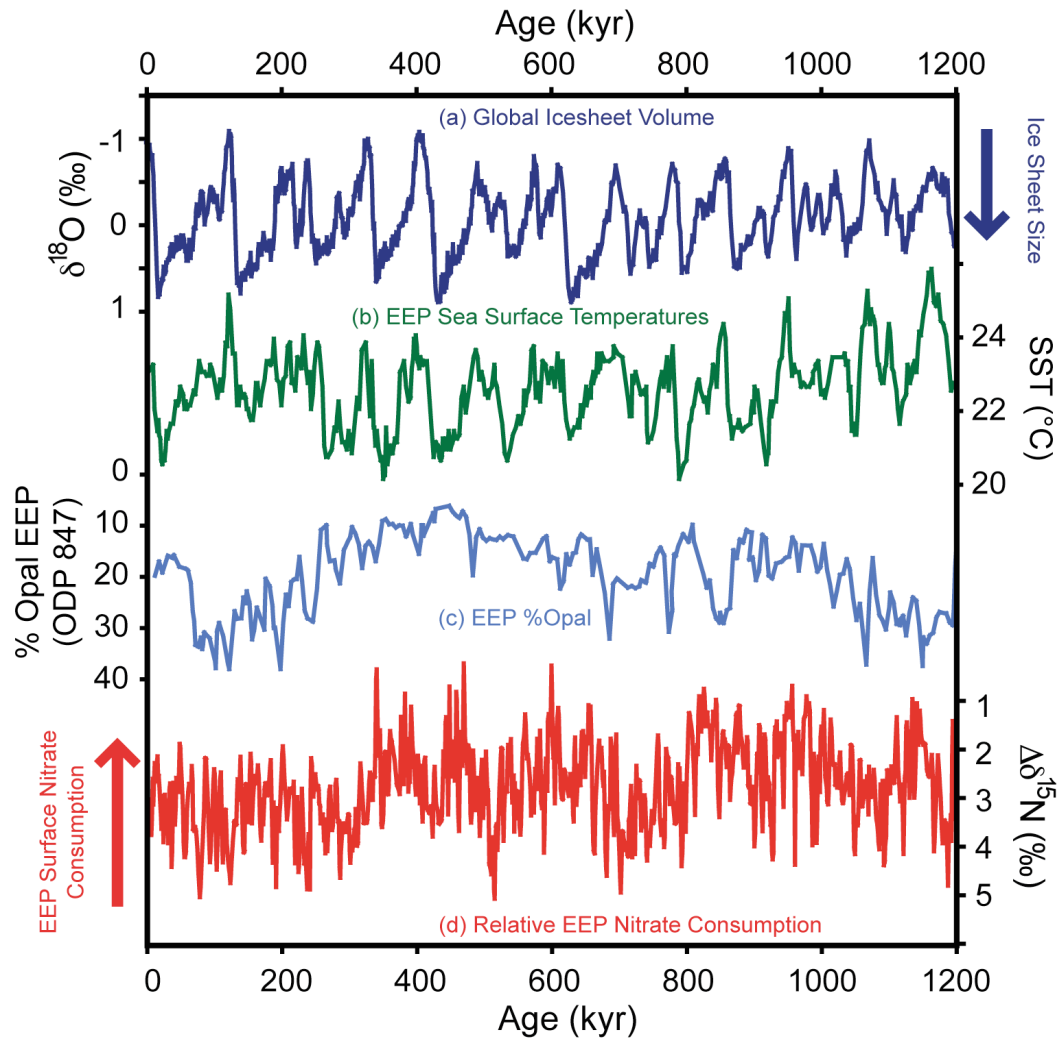


Figure 2.6: The (a) $\delta^{18}\text{O}$ of benthic foraminifera record (normalized) approximates the size of continental ice sheets [Lisiecki and Raymo, 2005]. The estimate of sea surface temperature (SST) in the EEP (b) is from the ODP site 846 at 3°S , 90°W [Liu and Herbert, 2004]. Percent sedimentary opal (c) is from the EEP site ODP 847 [Murray et al., 1995]. The (d) absolute difference between the WEP (ODP 806B) and EEP (ODP 849) sediment $\delta^{15}\text{N}$ is as seen in Figure 2.5.

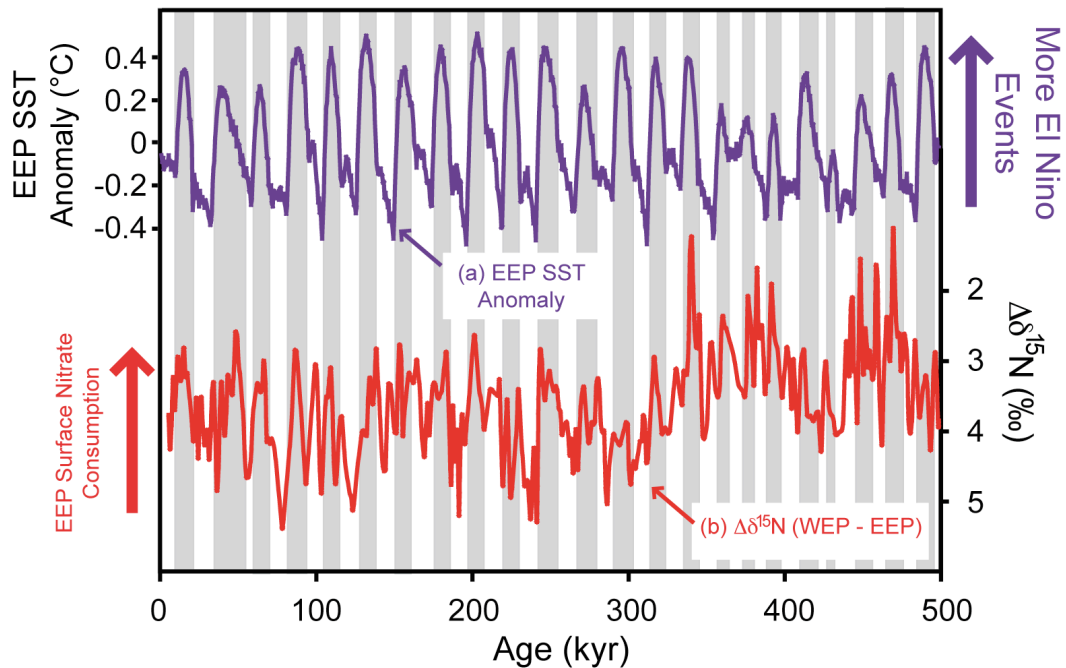


Figure 2.7: Comparison between the (a) modeled estimates for SST anomalies in the EEP (the so-called “NINO3” region: 5°N to 5°S, 150°W to 90°W) [Clement *et al.*, 1999] and (b) the estimated degree of EEP NO₃⁻ consumption (see Figures 2.5 and 2.6). Generally speaking, positive anomalies in the NINO3 region are associated with periods of reduced EEP upwelling (warm anomalies in the EEP) while negative SST anomalies are associated increased thermocline tilt and increased EEP upwelling. Shading indicates periods of anomalously high SST for the EEP, which are generally associated with increased NO₃⁻ consumption in the EEP.

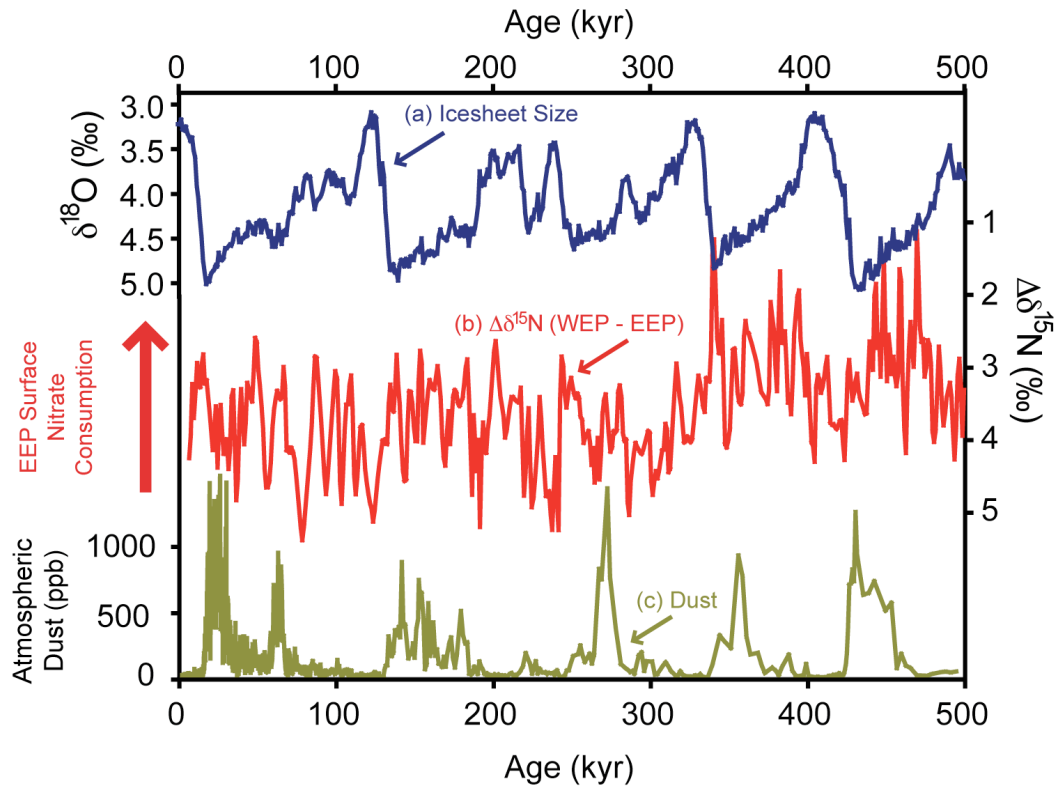


Figure 2.8: Comparison between (a) icesheet variability (from *Lisiecki and Raymo*, [2005]), (b) our $\Delta\delta^{15}\text{N}$ variable and (c) the atmospheric dust concentrations for the past 700kyr (from *Petit et al.*, [1990]).

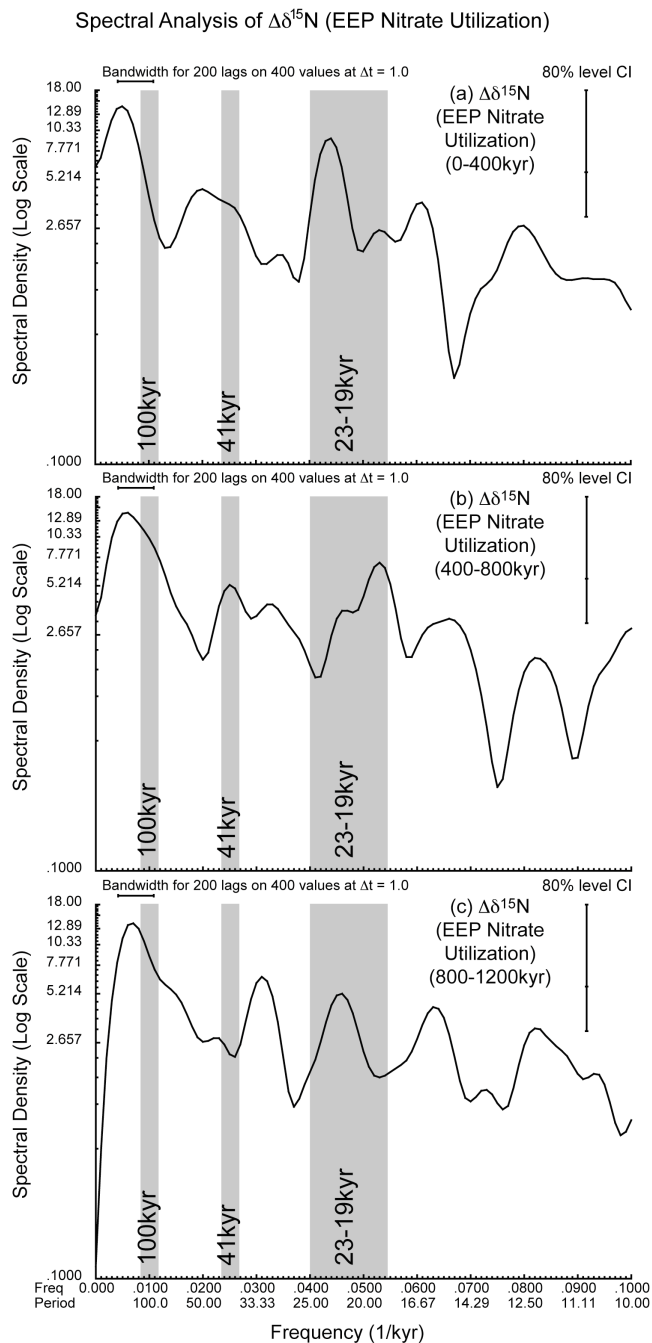


Figure 2.9: Blackman-Tukey spectral analysis for $\Delta\delta^{15}\text{N}$ (as seen in Figures 2.5 and 2.6: EEP nitrate utilization) over three time periods: (a) 0-400kyr, (b) 400-800kyr and (c) 800-1200kyr. The primary orbital frequencies influencing climate (19-23kyr, 41kyr, and 100kyr) are shaded and “CI” stands for Confidence Interval. The 19-23kyr frequency has the most power of the primary planetary frequencies through all time periods.

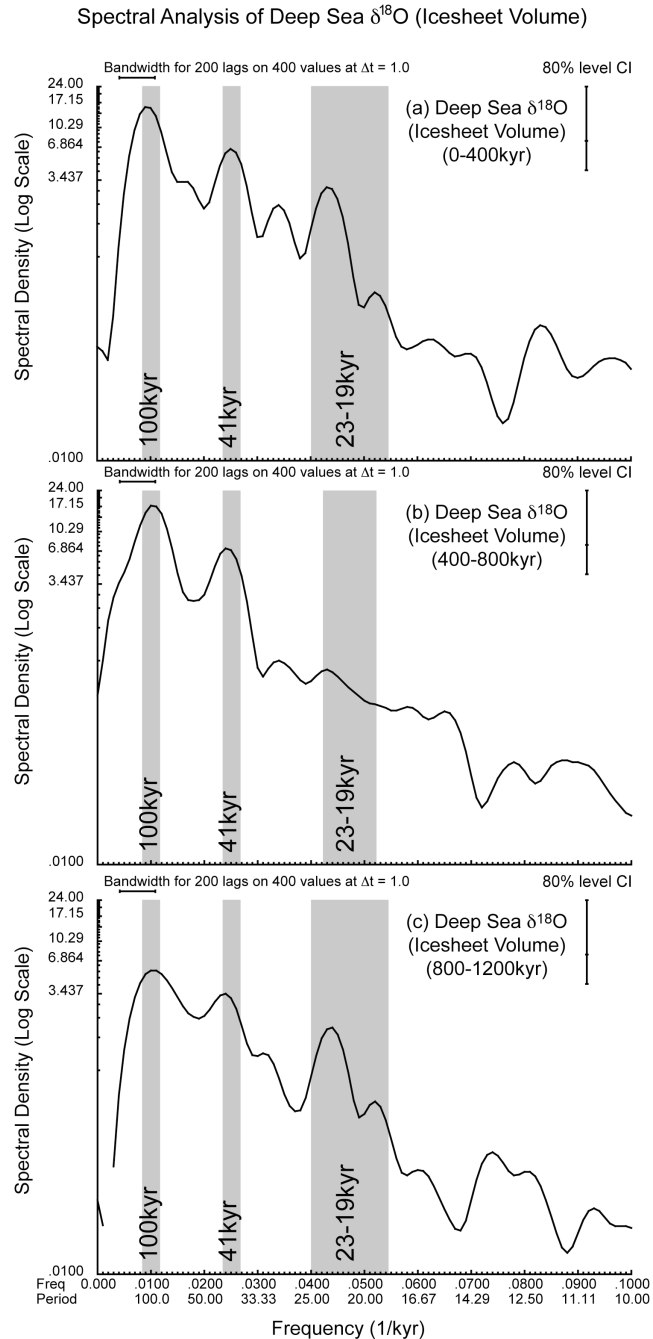


Figure 2.10: Blackman-Tukey spectral analysis for benthic foraminifera $\delta^{18}\text{O}$ (deep sea $\delta^{18}\text{O}$ as a proxy for icesheet volume, as seen in Figure 2.6) over three time periods: (a) 0-400kyr, (b) 400-800kyr and (c) 800-1200kyr. As originally discussed [Shackleton and Opdyke, 1976; Pisias and Moore, 1981], the 100kyr frequency in icesheet volume is not evident prior to ~900kyr, which most likely describes the increase of the 100kyr frequency between the 800-1200kyr and 400-800kyr intervals.

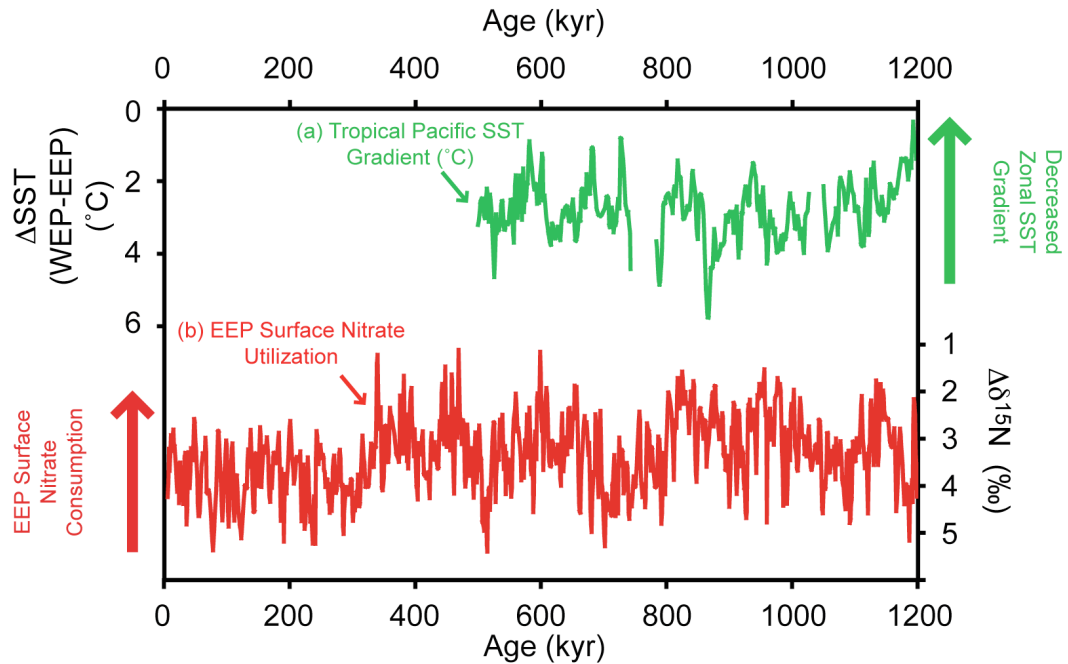


Figure 2.11: Comparison between (a) equatorial Pacific zonal SST gradient, calculated using data from ODP 806B in the WEP [Medina-Elizade and Lea, 2005] and ODP 849 in the EEP [McClymont and Rosell-Mele, 2005]. Our $\Delta\delta^{15}\text{N}$ variable (b) is included for comparison and was calculated from the very same sediment cores as (a).

2.6 References

- Beaufort, L., T. de Garidel-Thoron, A. C. Mix, N. G. Pisias (2001), ENSO-like Forcing on Oceanic Primary Production During the Late Pleistocene, *293, Science*.
- Cane, M.A. and A.C. Clement (2000), A Role for the Tropical Pacific Coupled Ocean-Atmosphere System on Milankovitch and Millennial Timescales. Part II: Global Impacts, *In: P.U. Clark and R.S. Webb (Editors), Mechanisms of Millennial-Scale Global Climate Change, 29, American Geophysical Union, 373.*
- Clement, A.C., R. Seager, M.A. Cane, and S.E. Zebiak (1996), An Ocean Dynamical Thermostat, *Journal of Climate, 9, 2190-2196.*
- Clement, A.C., R. Seager, and M.A. Cane (1999), Orbital controls on the El Niño/Southern Oscillation and the tropical climate, *Paleoceanography, 14, 441-456.*
- CLIMAP Project Members (1976), The Surface of the Ice-Age Earth, *Science, 19, 1131-1137.*
- Koutavas, A., J. Lynch-Stieglitz, T.M. Marchitto Jr., and J.P. Sachs (2002), El Niño-like pattern in ice age tropical Pacific sea surface temperature, *Science, 297, 226-230.*
- Liu, Z. and T.D. Herbert (2004), High-latitude influence on the eastern equatorial Pacific climate in the early Pleistocene epoch, *Nature, 427, 720-723.*
- Mariotti, A., C. Germon, P. Hubert, P. Kaiser, R. Letolle, A. Tardieux, and P. Tardieux (1981), Experimental determination of nitrogen kinetic isotope fractionation: some principles; illustration for the denitrification and nitrification processes, *Plant and Soil, 62, 413-430.*
- Martin, J.H. (1990), Glacial-interglacial CO₂ change: the iron hypothesis, *Paleoceanography, 5, 1-13.*
- McClymont, E.L. and A. Rosell-Mele (2005), Links between the onset of modern Walker circulation and the mid-Pleistocene climate transition, *Geology, 33, 389-392*
- Mix, A.C, N.G. Pisias, W. Rugh, J. Wilson, A.E. Morey, T. Hagelberg, (1995): Benthic foraminifer stable isotope record from Site 849 (0-5 Ma): local and global climate changes, *In: Pisias, N.G. et al., (eds.), Proceedings of the Ocean Drilling Program, Scientific Results, College Station, TX, 138, 371-412.*
- Mix, A.C. (2006), Running hot and cold in the eastern equatorial Pacific, *Quaternary Science Reviews, 25, 1147-1149.*

Murray, D.W., J.W. Farrell, and V. McKenna (1995), Biogenic sedimentation at site 847, eastern equatorial Pacific Ocean during the past 3 M.Y., In: Pisias, N.G. *et al.*, (eds.), *Proceedings of the Ocean Drilling Program, Scientific Results*, College Station, TX, 138, 429-459.

Paillard, D., L. Labeyrie, and P. Yiou (1996), Macintosh program performs time-series analysis, *Eos*, 77, 379.

Petit, J.R., L. Mounier, J. Jouzel, Y. Korotkevitch, V. Kotlyakov, and C. Lorius (1990), Paleoclimatological implications of the Vostok core dust record, *Nature*, 343, 56-58.

Philander, S. G. and A. V. Fedorov (2003) Role of tropics in changing the response to Milankovich forcing some three million years ago, *Paleoceanography*, 18, 1045, doi:10.1029/2002PA000837

Pisias, N.G., and T.C. Moore Jr. (1981), The evolution of the Pleistocene climate: a time series approach, *Earth and Planetary Science Letters*, 52, 450–458.

Ropelewski, C.F. and M.S. Halpert (1987), Global and Regional Scale Precipitation Patterns Associated with the El Nino/Southern Oscillation, *Monthly Weather Review*, 111, 1606-1626.

Shackleton, N.J., Opdyke, N.D., 1976. Oxygen-isotope and paleomagnetic stratigraphy of Pacific core V28-239: Late Pliocene to latest Pleistocene, *Geological Society of America Memoir*, 145, 449–464.

Spero, H. J. and D. W. Lea (2002), The Cause of Carbon Isotope Minimum Events on Glacial Terminations, *Science*, 296, 522-525.

Stott, L. K. Cannariato, R. Thunell, G. H. Haug, A. Koutavas and S. Lund (2004), Decline of surface temperature and salinity in the western tropical Pacific Ocean in the Holocene epoch, *Nature*, 431, 56-59.

Strutton, P. G., W. Evans, and F. P. Chavez (2008), Equatorial Pacific chemical and biological variability, 1997–2003, *Global Biogeochemical Cycles*, 22, GB2001, doi:10.1029/2007GB003045.

Tozzi, S., O. Schofield, and P. Falkowski (2004), Historical climate change and ocean turbulence as selective agents for two key phytoplankton functional groups *Marine Ecology Progress Series*, 274, 123–132.

Turk, D., M. J. McPhaden, A. J. Busalacchi, M. R. Lewis (2001), Remotely sensed biological production in the equatorial Pacific, *Science*, 293, 471-474.

III. The composition and evolution of deep-sea sediment nitrogen

3.0 Introduction

The N isotopic composition of sedimentary organic matter (hereafter “sediment $\delta^{15}\text{N}$ ” or “whole sediment $\delta^{15}\text{N}$ ” when other sedimentary fractions are discussed) has often been used to infer past surface ocean nutrient dynamics because raining organic particles must be sensitive to the principal N isotopic composition of the NO_3^- source (initial $\delta^{15}\text{N}\text{-NO}_3^-$) and the relative amount of NO_3^- consumption [after *Altabet and Francois*, 1994]. However, an important assumption in sedimentary studies is that the primary (surface ocean) isotopic signature is retained upon burial and unaffected by the microbial alteration of organic matter after deposition on the seafloor (“early diagenesis” or more simply “diagenesis”) [*Holmes et al.*, 1999; *Altabet*, 1996; *Freudenthal et al.*, 2001; *Gaye-Haake et al.*, 2005; *Lehmann et al.*, 2002]. All sediments undergo some decomposition after reaching the seafloor, with large changes to the organic-rich sediments on the continental margins [*Jahnke et al.*, 1990] and lesser alteration found in deep-sea sediment (>2000m) organic matter because of its association with biominerals [*King*, 1977; *Ingalls et al.*, 2003], or clay [*Muller*, 1977]. Thus, the quantitative application of sediment $\delta^{15}\text{N}$ from deep-sea sediment sites could be called into question by the appearance of apparently anomalous sedimentary $\delta^{15}\text{N}$ values. For example, several deep-sea sediment $\delta^{15}\text{N}$ records show a upcore trend towards higher values over long (>200kyr) timescales (see *Altabet*, [2001] and *Galbraith et al.*, [2008] for examples), and in many locations, there is also an offset between predicted and actual deep-sea coretop sediment $\delta^{15}\text{N}$ of ~2-3‰ [*Altabet and Francois*, 1994; *Altabet*, 1996; *Gaye-Haake et al.*, 2005; and

more]. Identifying the origin of apparent post-depositional shift in deep-sea sediment $\delta^{15}\text{N}$ is important, because it would be the key to interpretation of records throughout the ocean basins, regardless of sedimentation environment. Furthermore, while some alternatives to using deep-sea bulk sediment $\delta^{15}\text{N}$ have been developed, such as examining the $\delta^{15}\text{N}$ within diatom frustule [*Crosta and Shemesh, 2002; Shemesh et al., 1993; Sigman et al., 1999; Robinson et al., 2005*] and within foraminifera tests [*Altabet and Curry, 1989; Ren et al., 2009*], these methods require laborious preparatory steps, making the construction of long time-series (such as my $\delta^{15}\text{N}$ records discussed in Chapter 2) much less tractable.

Here I consider the features of two deep-sea sediment $\delta^{15}\text{N}$ records from the equatorial Pacific that at first glance might be construed as resulting from sedimentary diagenesis. I investigate the N isotopic composition of different sedimentary components at these sites, along with various whole sediment and diatom-bound $\delta^{15}\text{N}$ measurements from other previously published studies. This analysis leads to the conclusion that diagenesis is not the explanation for apparent enrichment of sediment $\delta^{15}\text{N}$ at the equatorial Pacific sites—a conclusion that, in turn, prompts exploration of other potential explanations for sedimentary $\delta^{15}\text{N}$ trends worldwide.

3.1 Materials and Methods

In order to address these fundamental questions about the composition and possible alteration of deep-sea sedimentary N, I use several drill and piston cores from the Eastern and Western Equatorial Pacific (EEP and WEP respectively) along with a

previously published record from the California Margin (CA Margin from *Liu et al.*, [2005]) (Figure 3.1). These core sites range from shallow continental margin, high sedimentation rate, and high organic matter sediments of the CA Margin to the relatively deep, low sedimentation rate, low organic matter sediments in the equatorial Pacific. The modern annual mean surface NO_3^- concentrations for the tropical and subtropical north Pacific is also shown in Figure 3.1. In the eastern equatorial Pacific, there is a broad pool of surface NO_3^- that steadily diminishes towards the west. This region is known as the “cold tongue” because trade winds force a shoaling of the thermocline, delivering cool, nutrient-rich waters to eastern surface waters. Several sediment records can be found both under the relatively high NO_3^- pool in the east (RC13-112 / ODP 849—“EEP” sites) and under the nitrate-free western equatorial Pacific (RNDB 74P / ODP 806—“WEP” sites). The California Margin (ODP 1012—“CA Margin” site) is also located under nitrate-free surface waters.

As discussed in Chapter 2, sediment age was determined by matching foraminiferal $\delta^{18}\text{O}$ measurements with the benthic foraminifera $\delta^{18}\text{O}$ stack of *Lisiecki and Raymo*, [2005] (Figure 3.2). Published foraminiferal $\delta^{18}\text{O}$ measurements were used for ODP core site 806B (*C. wuellerstorfi* from *Bickert et al.*, [1993]; *G. ruber* from *Medina-Elizade and Lea*, [2005]), but to span core gaps, samples from nearby ODP 805C (*G. sacculifer* from *Berger et al.*, [1993]) and RNDB 74P (*G. sacculifer* from *Perks et al.*, [2002] and *Memorie Yasuda, Unpublished Data*) were used by matching the foraminiferal $\delta^{18}\text{O}$ in all cores. For ODP core site 849 I used the $\delta^{18}\text{O}$ measurements on mixed benthic species by *Mix et al.*, [1995]. The age model for sediment core RC13-112 is based on the $\delta^{18}\text{O}$ of benthic foraminifera *Uvigerina*

species, measured on a MAT 252 isotope ratio mass spectrometer at Scripps Institution of Oceanography. Minimum age model errors are on the order of a few kyr for all sediment cores.

To determine the concentration and N isotopic ratio for whole sediment $\delta^{15}\text{N}$, samples were dried, homogenized using an agate mortar and pestle, encapsulated in a tin capsule, and combusted in a Costech Elemental Analyzer connected via a Con-Flo III to a Thermo-Finnigan XP isotope ratio mass spectrometer. All samples were referenced to IAEA sediment standard PACS-2 (courtesy of the Ganeshram laboratory, University of Edinburgh) as well as my own in-house reference materials constructed from deep-sea sediment from the east and western equatorial Pacific. These in-house references were provided from “flow-in” sediment cores in the eastern and western equatorial Pacific, with very uniform N concentrations, whole sediment $\delta^{15}\text{N}$, and non-organic components. This reference material was crucial to appropriately estimating any “matrix effects” during $\delta^{15}\text{N}$ analysis of these very low N samples (typically $\sim 0.01\%$). The measurements of WEP and EEP sediment $\delta^{15}\text{N}$ (in Figure 3.3) have an analytical precision of $\pm 0.3\%$ (based on reproducibility of in-house standards from the EEP and WEP).

Select samples from the RNDB 74P in the WEP (nearly identical core site as ODP 806B) were also measured for whole sediment $\delta^{15}\text{N}$. Splits of this sample were then separated into “coarse” ($>63\mu\text{m}$) and “fine” ($<63\mu\text{m}$) fractions and measured for $\delta^{15}\text{N}$. Additionally, sediment samples from the EEP (RC13-112) were measured for whole sediment $\delta^{15}\text{N}$ with splits of these samples being measured for “diatom-bound

$\delta^{15}\text{N}$ ” via the methods of *Robinson et al.*, [2004]. In short, samples were decalcified (using 10% HCl) and through a series of treatments, the opal-fraction of the sediment was isolated. Smear slides of these samples confirm that they are primarily composed of diatoms. This fraction was then dissolved and the isotopic composition of the remaining N was measured via the “denitrifier method” of *Sigman et al.*, [2001] at Princeton University.

All necessary sediment core site information can be found in Table 3.1.

3.2 Results

The WEP and EEP sites share common source water characteristics (as outlined in Chapter 1) because the $\delta^{15}\text{N-NO}_3^-$ delivered to surface waters (initial $\delta^{15}\text{N-NO}_3^-$) throughout the tropical Pacific is strongly influenced by mixing with the eastern tropical north and south Pacific (ETNP and ETSP respectively). While the $\delta^{15}\text{N-NO}_3^-$ delivered to each site is very similar, the expression of $\delta^{15}\text{N}$ in the organic matter exported from the surface is different for EEP sediment because of isotopic fractionation against nitrate with ^{15}N (resulting in lower $\delta^{15}\text{N}$ organic matter exported to the sediments—see Chapter 2 for more discussion on this). Of particular interest in this study are the long-term trends that appear to be almost equally shared between the cores, especially the trend towards higher values that appears—from these records—to extend as far back as 800kyr. This long-term trend towards higher sediment $\delta^{15}\text{N}$ is also present in a variety of deep-sea sediment $\delta^{15}\text{N}$ records from the Pacific and Atlantic (Figure 3.4). While the records in Figure 3.4 have trends that increase upcore

almost throughout the entire length of the records, the Northwest Sub-Arctic Pacific and Gulf of Alaska records have increasing trends that appear to begin somewhat later. Worth noting in the discussion of the possible causes for this apparent enrichment trend is that all of these sediment $\delta^{15}\text{N}$ records are under eutrophic waters, where surface NO_3^- concentrations are never completely consumed in the modern day; this aspect adds a complication in establishing an expected $\delta^{15}\text{N}$ value for any given time.

When the WEP sediment $\delta^{15}\text{N}$ is viewed singly (as in Figure 3.3) it appears to have much of the same characteristics as other deep-sea sediment $\delta^{15}\text{N}$ records (Figure 3.4), such as the close similarity in the upcore trend towards higher $\delta^{15}\text{N}$. However, in comparing this deep-sea sediment $\delta^{15}\text{N}$ record with a much different site on the continental shelf off the west coast of the United States (Figure 3.5)—the CA Margin site has an order of magnitude more organic matter and a much higher sedimentation rate [Liu *et al.*, 2005]—the $\delta^{15}\text{N}$ records nearly overlap before $\sim 200\text{kyr}$; both records show highest values during interglacial periods and lowest values during glacial periods (please note that these records share the same Y-axis in Figure 3.5). The differences between the WEP and CA Margin sediment $\delta^{15}\text{N}$ records are illustrated by simple subtraction, $\Delta\delta^{15}\text{N}$, in Figure 3.5c (discussed in Chapter 2)—each record was resampled to create a common timescale of 1kyr using a piecewise linear interpolation between points (using Analyseries by Paillard *et al.*, [1996]), and the difference was calculated. The differences between the WEP and CA Margin for the majority of these 1200kyr records are primarily during glacial periods, when the CA Margin has somewhat lower $\delta^{15}\text{N}$ values—sediment $\delta^{15}\text{N}$ for all interglacial periods up until the

most recent are the same or very close to the same values for both sites. The only shared characteristic of these distant sedimentary sites—they are over 9000km apart—is that the ETNP plays a role in determining initial $\delta^{15}\text{N-NO}_3^-$ for both sites. In particular, source waters to the CA Margin site (the California Undercurrent) are primarily derived from waters that have mixed significantly with the denitrified waters of the ETNP [Castro *et al.*, 2001; Altabet *et al.*, 1999], but the $\delta^{15}\text{N-NO}_3^-$ of WEP source water is established through mixing with both the ETNP and ETSP waters (Chapter 1). As a result, the CA margin site record could be viewed as a baseline for assessing higher than expected values found in the WEP sediment. Furthermore, the similarity between the long-term $\delta^{15}\text{N}$ trend in the WEP (exhibited by increasing $\Delta\delta^{15}\text{N}$) and all other deep-sea sediment $\delta^{15}\text{N}$ records (Figure 3.4) suggests that whatever process is driving this trend towards higher $\delta^{15}\text{N}$ in the WEP is also responsible for similar increasing trends for the other deep-sea sediment sites.

For a more detailed analysis of WEP sediments, I separately determined the $\delta^{15}\text{N}$ and %N (percent contribution to whole sediment N) of the coarse (>63 μm) and fine (<63 μm) fractions in core RNDB 74P (Figure 3.6). This sediment component analysis was undertaken because the coarse fraction is almost entirely foraminifera, with coccolithophores, diatoms, radiolaria, clay, and organic matter comprising the fine fraction. Calculated (as opposed to measured) values for fine fraction contribution to whole sediment N and $\delta^{15}\text{N}$ were used because of the apparent loss of water soluble N during sample preparation. This calculation was based on an isotopic mass balance

assuming that the $\delta^{15}\text{N}$ and N concentration of the coarse and fine fractions equal the whole sediment $\delta^{15}\text{N}$ and N concentration:

To calculate fine fraction N concentration:

$$\text{Equation 1: } ([\text{N}]_{\text{whole}}) = ([\text{N}]_{\text{coarse}}) + ([\text{N}]_{\text{fine}})$$

To calculate fine fraction $\delta^{15}\text{N}$:

$$\text{Equation 2: } (\delta^{15}\text{N}_{\text{whole}})([\text{N}]_{\text{whole}}) = (\delta^{15}\text{N}_{\text{coarse}})([\text{N}]_{\text{coarse}}) + (\delta^{15}\text{N}_{\text{fine}})([\text{N}]_{\text{fine}})$$

The size fraction measurements were made for two time periods spanning high and low $\Delta\delta^{15}\text{N}$ (shaded regions in Figure 3.6a) in order to determine the connection between sedimentary composition and whole sediment $\delta^{15}\text{N}$. The earliest time period (from 402 to 340kyr) was chosen because it spans the first large deviation between the whole sediment $\delta^{15}\text{N}$ of 806B and 1012. This time period has minimum $\Delta\delta^{15}\text{N}$ ($\sim 0\%$) at the beginning and end, but an almost 4‰ peak in $\Delta\delta^{15}\text{N}$ in the middle. The later, most recent, time period is from 5 to 30kyr and covers a time period where WEP sediment $\delta^{15}\text{N}$ is consistently higher than the CA Margin record.

The percent N contributed from the coarse fraction varies from less than 10% in the earliest samples (~ 380 to 400kyr) to almost 30% around 12kyr (Figure 3.6b). Furthermore, the N isotopic composition of coarse and fine fractions increases in parallel by 2‰ between the early and later sections, roughly matching the increase in whole sediment $\delta^{15}\text{N}$ (Figure 3.6c). The $\delta^{15}\text{N}$ of the coarse fraction was nearly always the highest of all the sedimentary components. However, because the coarse fraction was never a dominant source of %N, the whole sediment $\delta^{15}\text{N}$ was nearly identical to the fine fraction $\delta^{15}\text{N}$ throughout both time periods.

Nevertheless, the consistently high $\delta^{15}\text{N}$ values of the coarse fraction suggest that significant shifts in sediment composition might influence the long-term trends in whole sediment $\delta^{15}\text{N}$. Therefore, the long-term WEP sedimentary compositional trends deserve further scrutiny. Figure 3.7 displays a variety of these measures, many within the same core as the WEP sediment $\delta^{15}\text{N}$ record for ODP 806B. Measurements of (a) % CaCO_3 in the WEP are remarkably stable throughout the 1200kyr shown here [Janecek *et al.*, 1993; Schwarz *et al.*, 1996]. By contrast, the EEP shows much larger bulk compositional variations, almost entirely accounted for by increased opal in these sediments [Murray *et al.*, 1995]. The coarse fraction (c) from the WEP (ODP 806B) for the past 1200kyr shows that there has been considerable variability over the course of this record [Memorie Yasuda, unpublished data]. This record can be compared to a fragmentation index from the same core (ODP 806B) [Memorie Yasuda, unpublished data]—the ratio of broken and whole planktonic foraminifera tests (d), normally interpreted as an indicator of CaCO_3 dissolution. While peak values for the fragmentation index match with many of the minima in the coarse fraction (c), there appears to be a trend towards greater coarse fraction from about 400kyr that is not reproduced in the Fragmentation Index. The $\Delta\delta^{15}\text{N}$ variable (e) is included for comparison. Though there are some discrepancies, all the long-term trends in sediment composition go in a direction that might encourage higher bulk sediment $\delta^{15}\text{N}$.

Another perspective on this issue comes from measurements of diatom-bound $\delta^{15}\text{N}$ from the EEP sediment core RC13-112. Figure 3.7 displays an example of these measurements, along with whole sediment $\delta^{15}\text{N}$ from splits of the same sample and a

three-point smoothing of the diatom-bound $\delta^{15}\text{N}$. Coretop $\delta^{15}\text{N}$ values for each measurement are nearly identical and while whole sediment and diatom-bound $\delta^{15}\text{N}$ are not identical throughout the record, the offset is relatively minor. This is especially important considering that these samples are during a very large increase in whole sediment $\delta^{15}\text{N}$ (age at the bottom of this record is $\sim 25\text{kyr}$). This congruence between whole sediment and diatom bound $\delta^{15}\text{N}$ is typical of other sites as well (Figure 3.7); the published diatom-bound $\delta^{15}\text{N}$ of the Gulf of Alaska ODP Site 887 overlaps the whole sediment $\delta^{15}\text{N}$ from the same core [Galbraith *et al.*, 2008]. The age of the sediments at the bottom of this record (800cm) is $\sim 104\text{kyr}$. Thus there are numerous examples of diatom-bound $\delta^{15}\text{N}$ measurements that match the high values of whole deep-sea sediment $\delta^{15}\text{N}$ records (Figures 3.3, 3.4 and 3.5), even those that show an increasing trend.

Finally, the relationship between the expected (based on $\delta^{15}\text{N-NO}_3^-$ below the euphotic zone—the initial value delivered to surface waters) and actual coretop sediment $\delta^{15}\text{N}$ can be seen in Figure 3.9. All sites in this figure are high sedimentation rate cores from continental margin sites and coretop sediment $\delta^{15}\text{N}$ are within or just below the 1:1 line. The few locations that are below the 1:1 line are all from regions that might be characterized by incomplete NO_3^- consumption in surface waters.

3.3 Discussion

Recently deposited sediment undoubtedly undergoes some degree of decomposition, but the effect of this diagenesis on sedimentary $\delta^{15}\text{N}$ is still a matter of

debate. Typically, the long-term trend towards higher values found in the equatorial Pacific sediment $\delta^{15}\text{N}$ records (Figure 3.3) and found in other deep-sea sediment sites (Figure 3.4) would be strongly suggestive of fractionation during the decomposition of organic N. However, the comparison between WEP and CA Margin sediment $\delta^{15}\text{N}$ records—showing a high degree of overlap for almost 1 million years (Figure 3.5) despite large differences in location and sedimentary composition—helps to constrain the interpretation of sedimentary $\delta^{15}\text{N}$ variability, because the CA Margin record can serve as a quantitative baseline for the WEP record. Because the processes affecting the WEP core site are likely to be active in other deep-sea sediment sites, the constraints placed on these equatorial Pacific cores are also likely to apply to many other deep-sea sites.

In determining possible explanations for the long term trend towards higher WEP sediment $\delta^{15}\text{N}$ (when compared to the CA Margin, this is primarily during glacial periods), a biologically-based process of diagenetic enrichment appears to be a much less viable explanation than a process that selectively preserves or periodically contributes higher than expected $\delta^{15}\text{N}$. Measuring the N and $\delta^{15}\text{N}$ composition of the coarse ($>63\mu\text{m}$) and fine ($<63\mu\text{m}$) fraction of sediment provides a simple and effective way of isolating zooplankton fossils from the organic detritus and phytoplankton fossils. Generally speaking, if sediment $\delta^{15}\text{N}$ were accurately recording surface ocean $\delta^{15}\text{N-NO}_3^-$, it would be expected that whole sediment $\delta^{15}\text{N}$ would be closest to the phytoplankton $\delta^{15}\text{N}$ in the fine fraction. Direct comparisons of the coarse and fine fraction WEP sediments (Figure 3.6) show that the coarse fraction is nearly always

enriched relative to whole sediment $\delta^{15}\text{N}$ and that the contribution from the coarse fraction to whole sediment N is somewhat higher during the more recent period (5-30kyr) when $\Delta\delta^{15}\text{N}$ is high. However, despite the increased coarse fraction influence, the largest difference between fine fraction and whole sediment $\delta^{15}\text{N}$ is +0.5‰ during a ~4‰ peak in $\Delta\delta^{15}\text{N}$ (Figure 3.6c). This suggests that changes in sediment composition can slightly skew the whole sediment $\delta^{15}\text{N}$ towards higher values, but an enrichment of 0.5‰ cannot explain the ~4‰ higher than expected values (above the CA Margin baseline) for WEP sediment $\delta^{15}\text{N}$.

If the fraction containing foraminifera cannot significantly affect whole sediment $\delta^{15}\text{N}$, perhaps the fine fraction itself is biased from selective preservation. It is possible that the $\delta^{15}\text{N}$ associated with fine fraction CaCO_3 fossils—primarily the remains of coccolithophorids—is affected by carbonate dissolution, which is generally weakest during glacial periods and strongest in mid- to later interglacial periods [Farrell and Prell, 1991]. However, the glacial vs. interglacial contrast for sediment $\delta^{15}\text{N}$, with the same or very similar values during interglacial periods, but higher than expected values during glacial periods (Figure 3.5) argues against this possibility. Could there be changes in the sediment fossil assemblage—the species composition—that could account for the increase in whole sediment $\delta^{15}\text{N}$? There is considerable variability in the abundance of individual foraminifera species in WEP sediments [Zhang *et al.*, 2007], but the previous discussion has shown the influence of foraminifera on whole sediment $\delta^{15}\text{N}$ is negligible relative to the observed $\Delta\delta^{15}\text{N}$. Diatom abundance is uniformly low for WEP sediments [Lange *et al.*, 1993] and is

more than likely to be less significant than foraminifera with regards to shifting whole sediment $\delta^{15}\text{N}$. The assemblage of coccolithophorids fossils have dramatically changed from a global peak in abundance during MIS 11 [Barker *et al.*, 2006] to much lower levels throughout the equatorial Pacific and after $\sim 300\text{kyr}$ there was a switch to a species composition favoring “warm water taxa” in the WEP [Chiyonobu *et al.*, 2006]. While this association between increasing $\Delta\delta^{15}\text{N}$ and a shift in the fundamental composition of a major phytoplankton group is worth considering, there is, as yet, no evidence that any coccolithophore taxa incorporate a $\delta^{15}\text{N}$ signature higher than ambient $\delta^{15}\text{N-NO}_3^-$. Furthermore, the decrease in the total coccolithophore abundance and a reduced influence on whole sediment $\delta^{15}\text{N}$ suggests that a change in this group’s species composition is even less likely to drive whole sediment $\delta^{15}\text{N}$.

It could be argued that both the fine and coarse sediment fractions are skewed towards higher values because organic matter enriched in $\delta^{15}\text{N}$ —perhaps because of diagenetic processes—has adhered to the various biogenic fossils (carbonate tests and coccoliths, opal frustules and skeletons). But measurements on mixed WEP foraminifera samples with all external organic matter removed are very similar to whole and fine fraction $\delta^{15}\text{N}$ in coretop sediments: 10.8‰ for cleaned foraminifera [Haojia Ren, Unpublished Data] versus $\sim 10\text{‰}$ in whole sediment $\delta^{15}\text{N}$ and 11.4‰ for the coarse fraction (Figure 3.6). Furthermore, the strongest argument against enriched organic matter in deep-sea sediments comes from my diatom-bound $\delta^{15}\text{N}$ measurements from the EEP, which has an almost identical trend towards higher $\delta^{15}\text{N}$ values. These measurements for the most recent $\sim 25\text{kyr}$ are identical to whole

sediment $\delta^{15}\text{N}$ in the coretop and not substantially different throughout the record (Figure 3.7). The high similarity between diatom-bound and whole sediment $\delta^{15}\text{N}$ is also observed for two deep-sea sediment sites in the sub-Arctic North Pacific (Figure 3.7 and *Galbraith et al.*, [2008]). While these diatom-bound $\delta^{15}\text{N}$ records show considerable variability around the whole sediment $\delta^{15}\text{N}$ values, this variability should be expected for seasonally blooming phytoplankton that are living in surface waters with differing degrees of NO_3^- consumption throughout the year. In fact, one benefit of whole sediment $\delta^{15}\text{N}$ is that it is an integrated measurement of surface ocean export and should show less bias to any particular season.

The fundamental insight provided by these data is that during a time period of supposed diagenetic enrichment in deep-sea whole sediment $\delta^{15}\text{N}$ (the last ~30kyr in Figure 9 a-c and the last 100kyr in Figure d-e) there is essentially no difference between whole sediment N and the protected N inside diatom frustules. As concluded by *Galbraith et al.*, [2008], the strong similarity between diatom-bound and whole sediment $\delta^{15}\text{N}$ strongly implies that surface ocean processes, not diagenesis or other sedimentary processes, are the primary source of sediment $\delta^{15}\text{N}$ variability in these deep-sea sediments.

If diagenetic fractionation or selective preservation / export in sediments is not responsible for higher than expected deep-sea sediment $\delta^{15}\text{N}$, what can explain the trend toward higher $\delta^{15}\text{N}$? The timing of the divergence between the WEP and CA Margin sediment $\delta^{15}\text{N}$ records may provide some clues. The most likely explanation for this divergence lies in the different sources of $\delta^{15}\text{N}$ - NO_3^- to each site. The ETNP

influences $\delta^{15}\text{N-NO}_3^-$ delivered to both sites, but the ETSP also influences $\delta^{15}\text{N-NO}_3^-$ delivered to the WEP site (see Chapter 1 for more details). Acknowledging this dual influence, the most simple and direct explanation for the apparently higher than expected WEP sediment $\delta^{15}\text{N}$ is that denitrification in the ETSP is periodically stronger than the ETNP, especially during glacial periods.

There is no a priori reason for denitrification strength in these two regions to be correlated over long timescales. For example, during glacial periods, denitrification strength in the ETNP—it has been suggested—is regulated by changes in the size of the North American Icesheet [*Ganeshram and Pedersen, 1998*], which is not likely to be a strong influence on denitrification in the ETSP. There is also a striking difference in the geochemistry of the regions—the depths where denitrification occur in the ETSP peak at ~250-300m, but in the ETNP the denitrification peak is at ~400m with a much broader depth range (see discussion in Chapter 1 and *Deutsch et al., [2001]*). The relatively thin depth profile for ETSP denitrification is in part determined by the extent of oxygen poor waters, which are shallow enough to be sensitive to fluctuations in tropical Pacific thermocline depth [*Morales et al., 1999*]. In the modern ocean, shallower thermocline depths in the equatorial Pacific and ETSP (usually occurring during La Nina events) lead to an increased volume of oxygen poor waters. While the presence of oxygen poor waters does not determine the strength of denitrification, oxygen poor waters are prerequisite for denitrification, and shallower thermocline produces an increase in photosynthetic production (which increases oxygen demand). Assuming this sensitivity between thermocline tilt and the volume of oxygen poor waters in the ETSP [*Morales et al., 1999*] existed for the past 1000kyr, my hypothesis

for increased ETSP denitrification would call for a long-term increase in thermocline tilt. While there may be questions about the efficacy of Sea Surface Temperature (SST) proxies, they unequivocally show a long-term shoaling of the eastern tropical Pacific thermocline over the past ~3 million years [*Medina-Elizade and Lea, 2005; Dekens et al., 2007*]. My own results from Chapter 2 also indicate a generally shallower EEP thermocline for the late-Pleistocene, especially since about 300 to 400kyr. These findings set in place the necessary environment for increasing ETSP denitrification throughout the mid to late-Pleistocene.

This is not to say that ETSP denitrification doesn't decrease during glacial periods—the comparison between WEP and CA Margin sediment $\delta^{15}\text{N}$ clearly shows very similar values for all interglacial periods with only slight offsets for the last two interglacial periods (Figure 3.5). The unequal nature of denitrification in the ETNP and ETSP during glacial periods (higher in the ETSP) may be explained by greater declines in ETNP denitrification from the presence of the Laurentide icesheet (as is explicitly detailed by *Ganeshram and Pederson, [1998]*). This higher $\delta^{15}\text{N-NO}_3^-$ (from the ETNP and ETSP) during glacial periods can only be expected to mix as far as it is observed in the modern day—throughout the tropics with signs of mixing in the subtropics (Chapter 1). The CA Margin is then only recording $\delta^{15}\text{N-NO}_3^-$ variability from ETNP denitrification, which happens to be somewhat lower than the $\delta^{15}\text{N-NO}_3^-$ produced from ETSP denitrification.

While this explanation is completely consistent with the equatorial Pacific and the CA Margin sediment $\delta^{15}\text{N}$ records, how is this consistent with the other deep-sea

sediment $\delta^{15}\text{N}$ records (Figure 3.4)? It is not expected that changes in $\delta^{15}\text{N-NO}_3^-$ from ETSP denitrification would influence the sub-Arctic Pacific, which in the modern day has $\delta^{15}\text{N-NO}_3^-$ values that are nearly 2‰ less than the tropical Pacific (after *Galbraith et al.*, [2008]). However, this region (and the others seen in Figure 3.4) do not have complete NO_3^- consumption and small changes in the pre-formed NO_3^- concentrations would have large impacts on the relative NO_3^- utilization—if there is no change in NO_3^- uptake, but reduced supply, this results in more complete consumption and higher $\delta^{15}\text{N}$ exported to the sediments. I propose that a mid- to late-Pleistocene strengthening of ETSP denitrification (the ultimate NO_3^- sink) results in a slight decline in pre-formed NO_3^- , which increases NO_3^- consumption and therefore sediment $\delta^{15}\text{N}$ for deep-sea sediment sites outside of the equatorial Pacific (see Figure 3.10 for a synthesized view of this). In short, a higher rate of denitrification in the ETSP during glacial periods is the simplest explanation for these deep-sea sediment measurements that is also completely consistent with the various deep-sea sediment $\delta^{15}\text{N}$ records presented here.

I have provided a consistent explanation for the long-term increase in deep-sea sediment $\delta^{15}\text{N}$, but this explanation would not necessarily account for the ~3‰ offset between expected and observed $\delta^{15}\text{N}$ in some deep-sea coretop sediments (Figure 3.5) [*Altabet and Francois*, 1994; *Altabet*, 2001; *Gaye-Haake et al.*, 2005]. This offset is not seen for continental margin sites (Figure 3.9), suggesting that it is not a universal aspect of sedimentary $\delta^{15}\text{N}$. However, if diagenesis were responsible for this offset, some considerable differences would be expected between whole-sediment and

diatom-bound $\delta^{15}\text{N}$, because the diatom bound organic material is presumably resistant to diagenetic changes [Robinson *et al.*, 2004; Brunelle *et al.*, 2007; this study]. Thus far, there is no systematic evidence that demonstrates such a difference.

Diagenetic fractionation of organic matter $\delta^{15}\text{N}$ is also not consistent with PN exported surface waters, that show (using shallow and deep sediment traps) no change or, in some cases, a slight decrease in $\delta^{15}\text{N}$ of falling particulate N despite large decreases (from remineralization) in N content [Altabet, 1989; Altabet *et al.*, 1991; Saino and Hattori, 1987; Thunell *et al.*, 2004; Voss, 2001; Gaye-Haake *et al.*, 2005].

If there were an inherent microbial preference for compounds containing ^{14}N versus ^{15}N —as has been suggested [Holmes *et al.*, 1999; Altabet, 1996; Freudenthal *et al.*, 2001; Gaye-Haake *et al.*, 2005; and more]—these paired sediment trap studies should unequivocally show an increase in $\delta^{15}\text{N}$ with the decomposition of organic matter.

Furthermore, the N isotopic composition of this organic detritus on the seafloor (as an unconsolidated material known as “fluff”) is isotopically indistinguishable from sediment traps [Altabet, 2001]. It is only in the coretop sediment (the uppermost consolidated material) where organic material is found to have $\delta^{15}\text{N} \sim 2.5\text{-}3\text{‰}$ higher than sediment trap or predicted surface water export $\delta^{15}\text{N}$ [Altabet, 1996]. Finally, diagenetic fractionation would be expected to produce lower $\delta^{15}\text{N}$ in the products of remineralization, such as NH_4^+ . Yet in many different sedimentary environments, pore-water $\delta^{15}\text{N}\text{-NH}_4^+$ is either the same as, or slightly higher than whole sediment $\delta^{15}\text{N}$ [Sweeney and Kaplan, 1980; Velinsky *et al.*, 1991; Altabet, 1996; Prokopenko *et*

al., 2006a; 2006b]. All of this evidence argues against significant nitrogen isotopic enrichment upon microbial degradation of organic matter.

Instead, I suggest that observations of anomalously high $\delta^{15}\text{N}$ in core top sediments are more likely to be a product of mixing with older (early Holocene) sediments. For example, radiocarbon dated deep-sea coretop sediments along a depth gradient in the WEP are fairly old—from ~3000 to more than 4000 years old for the 2500m to >4000m water depth range (summarized by *Berger and Killingley*, [1982] and further discussed by *Broecker et al.*, [1999]). The implication here is that the primary factor determining the offset between expected and actual coretop sediment $\delta^{15}\text{N}$ is the sedimentation rate at the core site. Slower sedimentation rates in the deep-sea allow for extensive bioturbation of recently deposited sediments with older sediments (a process that is only enhanced by dissolution of sedimentary material). This explanation assumes that there was higher-than-modern $\delta^{15}\text{N}$ for sediments deposited during the mid to late Holocene—and this is, in fact, is a common feature in all sediment records, including diatom-bound $\delta^{15}\text{N}$ [*Crosta and Shemesh*, 2002; *Robinson et al.*, 2004; *Brunelle et al.*, 2007]. Therefore, I argue that the apparent offset in deep-sea sediment $\delta^{15}\text{N}$ is only an artifact of the slow sedimentation rates at the sites. This conclusion in turn implies that diagenetic overprinting of the primary $\delta^{15}\text{N}$ signature of organic particles raining from the surface ocean is not a significant problem that needs to be circumvented.

3.4 Conclusions

The primary objective of this study was to shed light on the apparent enrichment of deep-sea sedimentary nitrogen isotopes, an enrichment that is conventionally thought to be caused during the decomposition of organic matter. Using size fraction measurements and component specific measurements (including diatom-bound organic matter) in equatorial Pacific deep-sea sediment records, I assess in detail the supposed diagenetic trend of increasing $\delta^{15}\text{N}$ and conclude that no sedimentary transformations explain the increasing trend. The implications for WEP sediment are that the variability in WEP sediment $\delta^{15}\text{N}$ is driven strictly by changes in $\delta^{15}\text{N}\text{-NO}_3^-$ delivered to surface waters above this site—a value that is established (in the modern ocean) by mixing with denitrified waters of the ETNP and ETSP. Because variability in $\delta^{15}\text{N}\text{-NO}_3^-$ from the ETNP is well constrained, the observed increase in WEP sediment $\delta^{15}\text{N}$ must be the result of higher denitrification in the ETSP. This apparent increase in ETSP denitrification—and the likely decrease in NO_3^- concentrations—may help to explain the increasing values of other deep-sea sediment $\delta^{15}\text{N}$ records. Surface NO_3^- is not completely consumed at these sites; thus, with lower initial NO_3^- concentrations, the absolute amount of NO_3^- utilization increases and would be recorded as a sediment $\delta^{15}\text{N}$ increase (see Figure 3.10 for a synthesized view of this process). The anomalously high deep-sea coretop sediment $\delta^{15}\text{N}$ can be explained by the mixing (via dissolution and bioturbation) of younger organic matter with older material with higher $\delta^{15}\text{N}$. This exact process has been used to describe anomalously old (based on radiocarbon dating) deep-sea coretop sediments. Finally,

these results validate the use of deep-sea sediment $\delta^{15}\text{N}$ as a proxy for surface ocean N processes, thereby allowing new investigations about the important and little understood cycling of fixed nitrogen in the ocean.

3.5 Figures and Tables

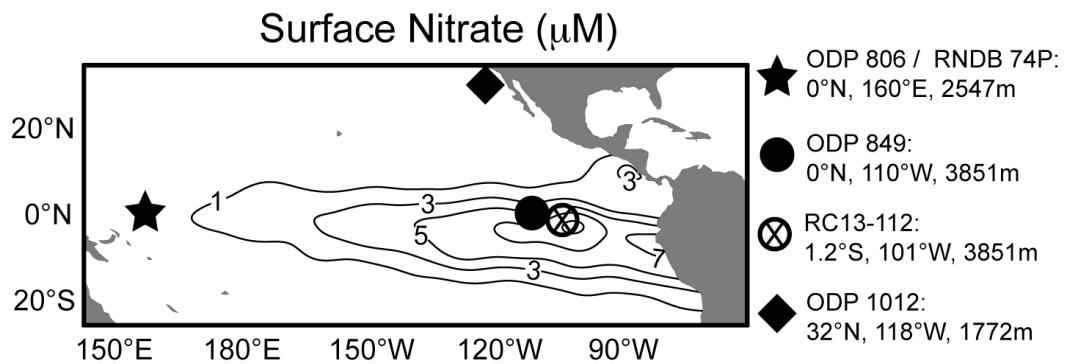


Figure 3.1: Climatological surface NO_3^- concentrations and locations for sediment core records discussed in this chapter (data from World Ocean Atlas 2005 [Garcia et al., 2006]).

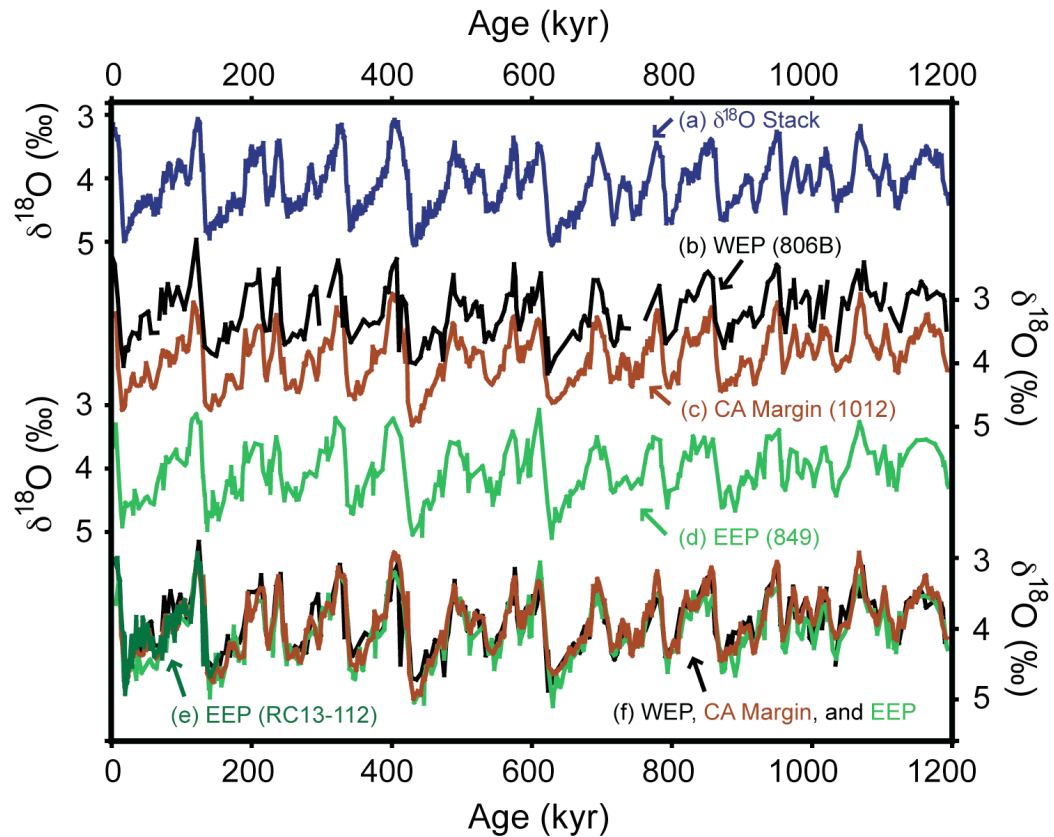


Figure 3.2: Sediment age model synchronization is based on matching foraminiferal $\delta^{18}\text{O}$ with the global $\delta^{18}\text{O}$ stack of (a) *Lisiecki and Raymo*, [2005] with similar measurements made in the (b) Western Equatorial Pacific (WEP) ODP site 806B (from *Bickert et al.*, [1993]), the (c) California Margin (CA Margin) ODP site 1012 (from of *Liu et al.*, [2005]), the (d) Eastern Equatorial Pacific (EEP) ODP site 849 (from *Mix et al.*, [1995]), and (e) EEP site RC13-112 (this study). We adjusted each sediment core $\delta^{18}\text{O}$ values to illustrate the clear overlap (f) between all age models discussed here.

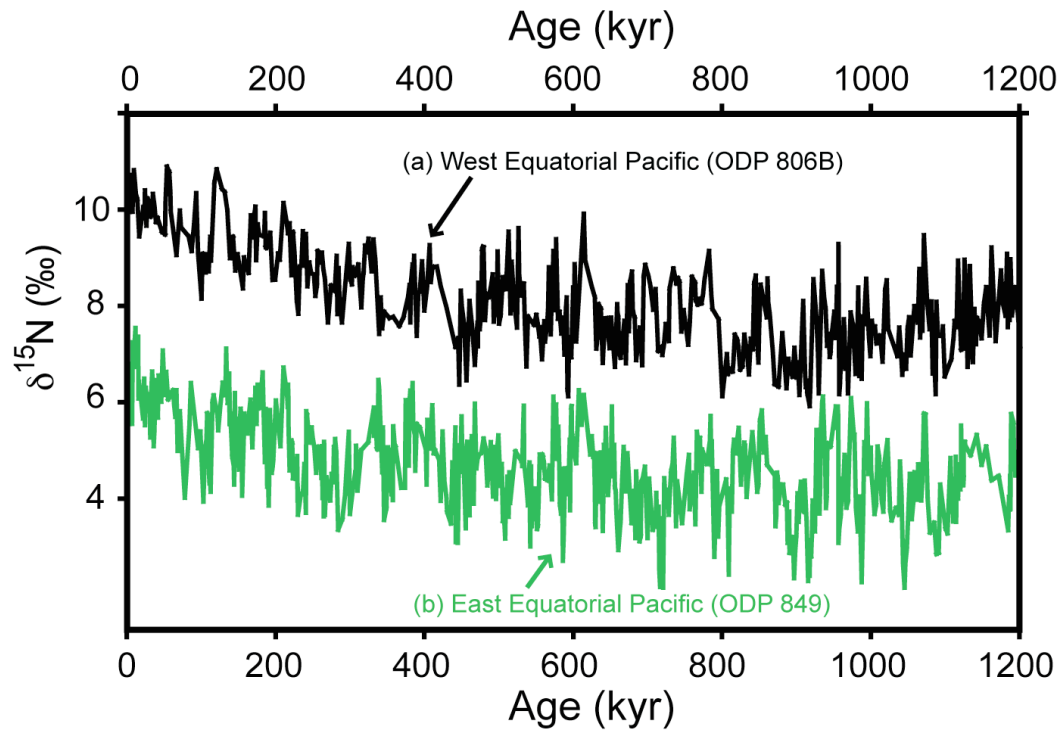


Figure 3.3: Sediment $\delta^{15}\text{N}$ records versus time for the (a) Western Equatorial Pacific and the (b) Eastern Equatorial Pacific (ODP 849). While these records are offset (from incomplete NO_3^- consumption in the EEP—see Chapter 2), there are distinct similarities in the long-term trends for each site, with the most obvious being a trend towards higher values in the past several 100kyr.

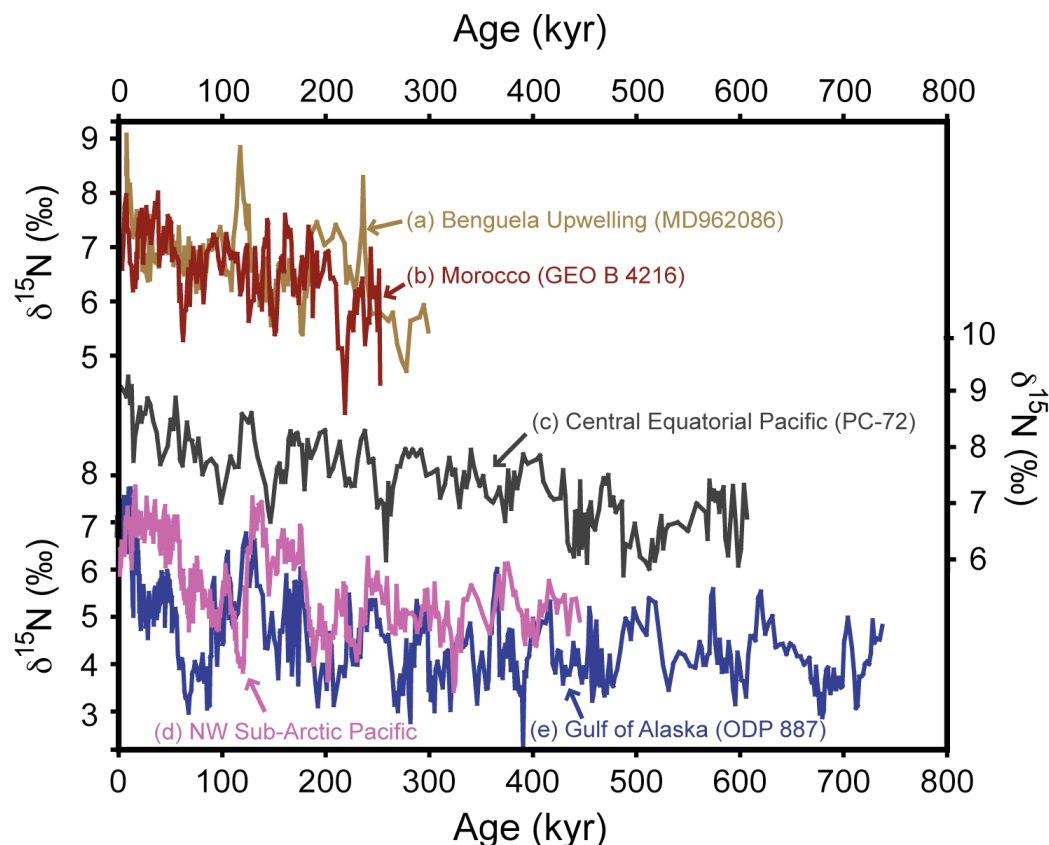


Figure 3.4 (a-d): Published sediment $\delta^{15}\text{N}$ records from deep-sea sediment cores (with original age models). The top three all show a similar trend of increasing $\delta^{15}\text{N}$ towards the present, but the (d) Northwest Sub-Arctic Pacific and the (e) Gulf of Alaska core presents an increasing trend towards the present only after $\sim 200\text{-}300\text{kyr}$. While these records are suitable as a demonstration of the apparently increasing $\delta^{15}\text{N}$ towards the present, it should be noted that changes in $\delta^{15}\text{N}\text{-NO}_3^-$ delivered to surface waters, or changes in NO_3^- consumption (all sites lie below surface waters with available NO_3^-) may impart an additional source of $\delta^{15}\text{N}$ variability. Sediment core site details can be found in Table 3.1.

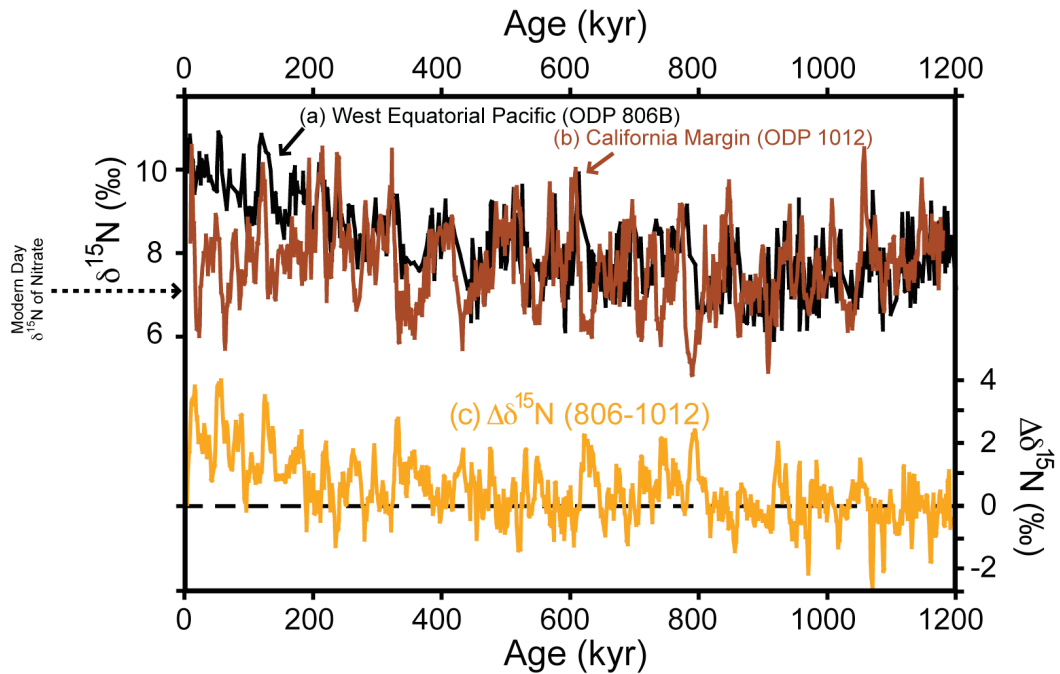


Figure 3.5: Sediment $\delta^{15}\text{N}$ records from the (a) Western Equatorial Pacific (ODP 806) and (b) California Margin (ODP 1012) for the past 1200kyr. While the CA Margin site has more than double the sedimentation rate and more than 10 times the organic matter contents of the Western Equatorial Pacific sediment, the sediment $\delta^{15}\text{N}$ records pre-300kyr show very similar magnitude and variability. The difference between the sediment $\delta^{15}\text{N}$ records of (a) and (b) can be seen in Figure 3.5c—referred to here as “ $\Delta\delta^{15}\text{N}$ ”. We have indicated at the 0kyr age, where our modern day $\delta^{15}\text{N}$ of nitrate measurements (see Chapter 1) indicate what the most recent sedimentary material should be.

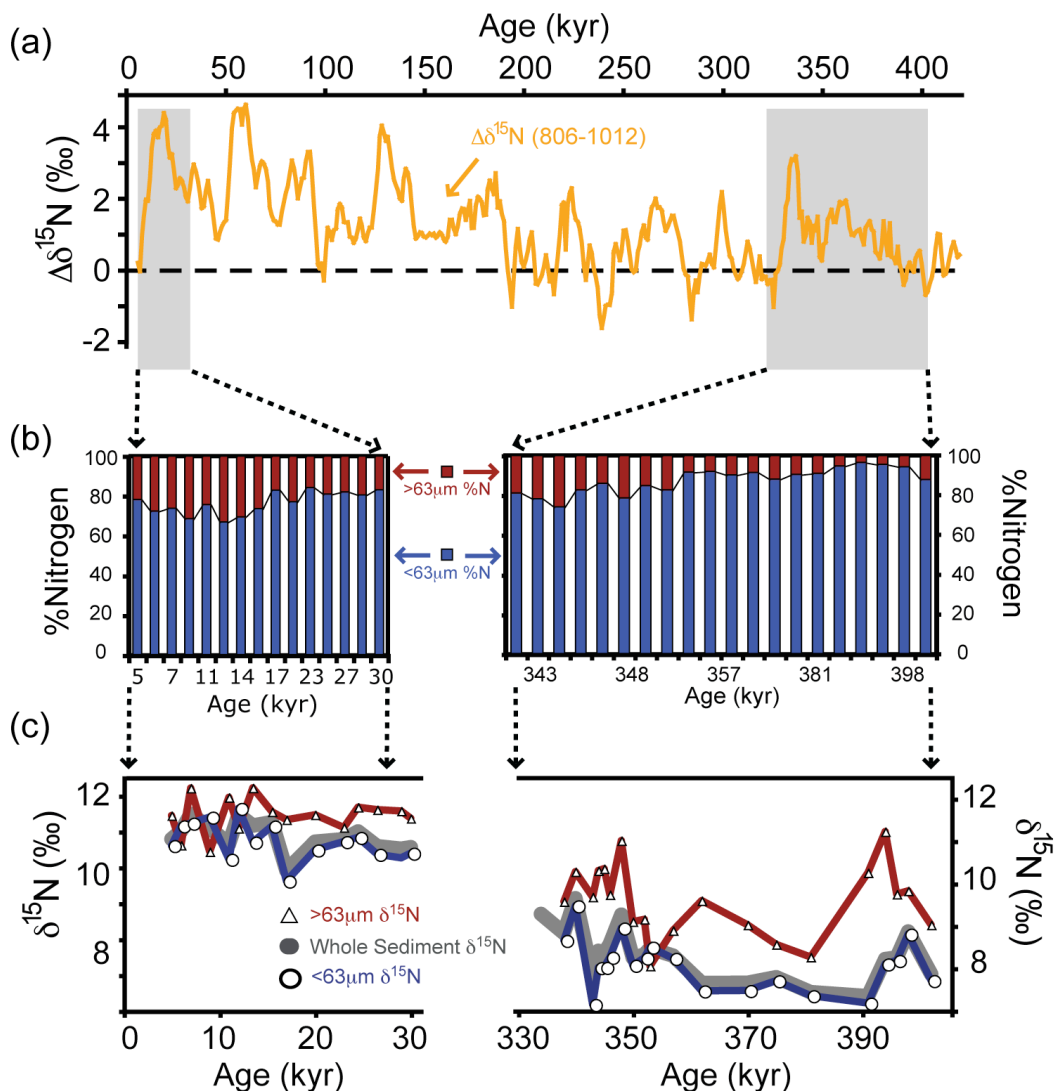


Figure 3.6: The contribution to WEP sediment N and $\delta^{15}\text{N}$ from coarse (>63μm) and fine (<63μm) fractions. Figure 3.6a is as seen in Figure 3.5c. Figure 3.6b shows the percent contribution to total N for each sedimentary fraction, across two time periods of varying $\Delta\delta^{15}\text{N}$. The coarse fraction contribution to whole sediment N increased from less than 10% in the beginning of the 340-400kyr period to ~20% at 340kyr and this higher contribution is seen throughout the more recent time period. The $\delta^{15}\text{N}$ for this time period shows clear differences between the different sedimentary fractions, but with the whole sediment $\delta^{15}\text{N}$ lying much closer to the fine fraction $\delta^{15}\text{N}$.

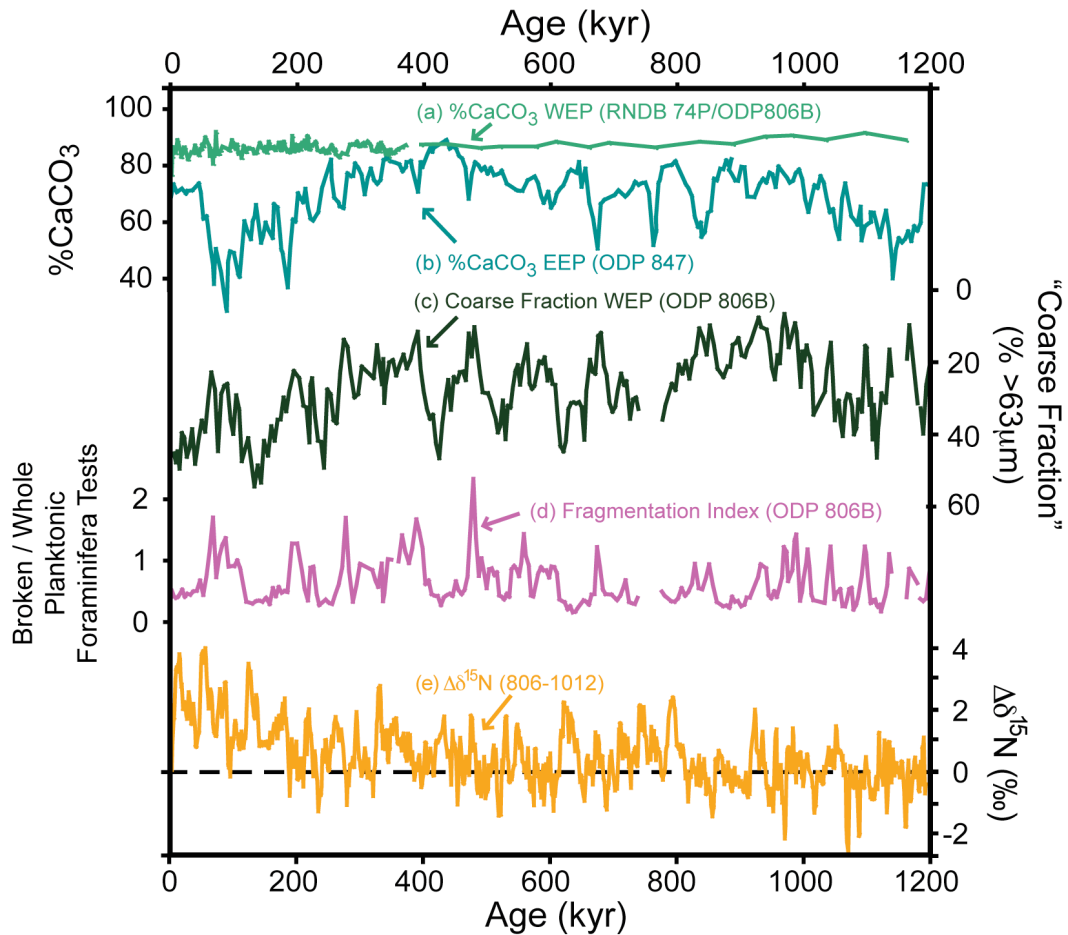


Figure 3.7: This figure displays several indicators of sedimentary composition for the eastern and western equatorial Pacific (EEP and WEP) sites. Figure 3.7a and 3.7b show the CaCO₃ composition through the past 1200kyr for the WEP and EEP respectively. Of note is the relatively constant CaCO₃ composition of the WEP for the past 1200kyr in comparison with large changes in EEP CaCO₃ [Schwarz *et al.*, 1996; Janecek, 1993; Murray *et al.*, 1995]. Figure 3.7c shows that the WEP CaCO₃ contents contain a varying amount of material greater than the 63µm fraction of dried sediment, which is primarily foraminifera [Berger *et al.*, 1993]. Figure 3.7d is the ratio of fragmented and whole planktonic foraminifera tests in ODP 806B [Memorie Yasuda, Unpublished Data]. Figure 3.7e is the same $\Delta\delta^{15}\text{N}$ as seen in Figure 3.5c.

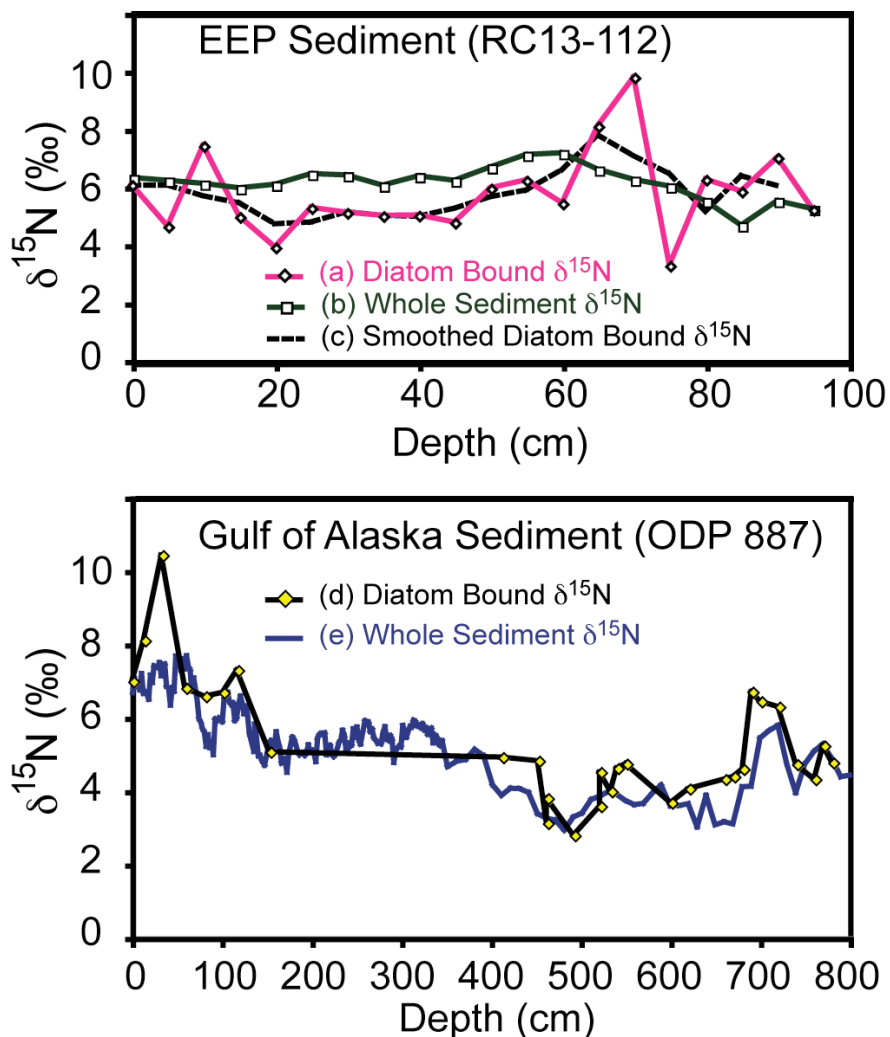


Figure 3.8: (a-e) Comparison of whole sediment $\delta^{15}\text{N}$ with diatom-bound $\delta^{15}\text{N}$ in (a and b) for the EEP (RC13-112) [This Study]. Figure 3.7c is the 3-point smoothing of Figure 3.8a. Figure 3.8d and 3.8e is the diatom-bound and whole sediment $\delta^{15}\text{N}$ values for the sub-Arctic Pacific core site ODP 887 [Galbraith et al., 2008].

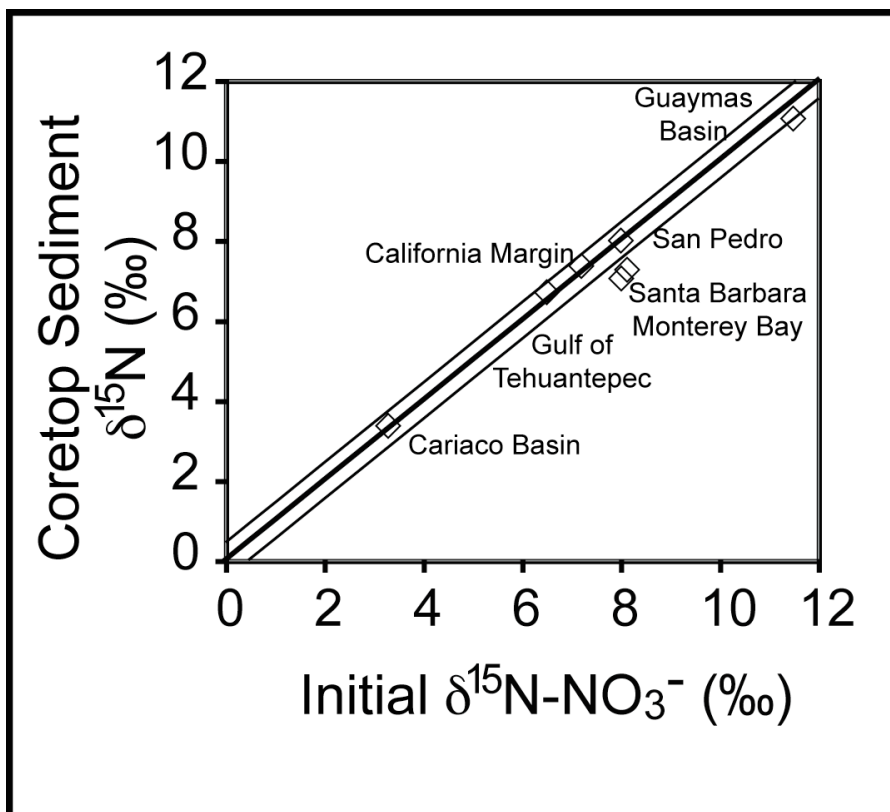


Figure 3.9: Coretop sediment $\delta^{15}\text{N}$ versus the initial $\delta^{15}\text{N-NO}_3^-$ delivered to surface waters from studies in the Cariaco Basin [Thunell *et al.*, 2004a], Gulf of Tehuantepec [Thunell and Kepple, 2004b], California (CA) Margin [Maria Prokopenko *unpublished data*; Hendy *et al.*, 2004], Monterey Bay [Altabet *et al.*, 1999], Santa Barbara Basin [Maria Prokopenko *unpublished data*; Emmer and Thunell, 2000], San Pedro Basin [Maria Prokopenko *unpublished data*; Altabet *et al.*, 1999], and Guaymas Basin (Gulf of California) [Pride *et al.*, 1999]. As discussed by Altabet and Francois [1994], where NO_3^- is completely consumed, sub-euphotic zone $\delta^{15}\text{N-NO}_3^-$ (before enrichment during consumption) should equal the exported $\delta^{15}\text{N}$ of particulate N and coretop sediment $\delta^{15}\text{N}$ —sub-euphotic zone $\delta^{15}\text{N-NO}_3^-$ and coretop sediment $\delta^{15}\text{N}$ should fall along the 1:1 line. An envelope for $\pm 0.5\text{‰}$ error in measuring $\delta^{15}\text{N-NO}_3^-$ and sediment $\delta^{15}\text{N}$ can be seen above and below the 1:1 line. Measurements from nearly all sites fall within the error bars, with the Santa Barbara Basin and Monterey Bay falling below the 1:1 most likely from fractionation during incomplete surface water NO_3^- consumption.

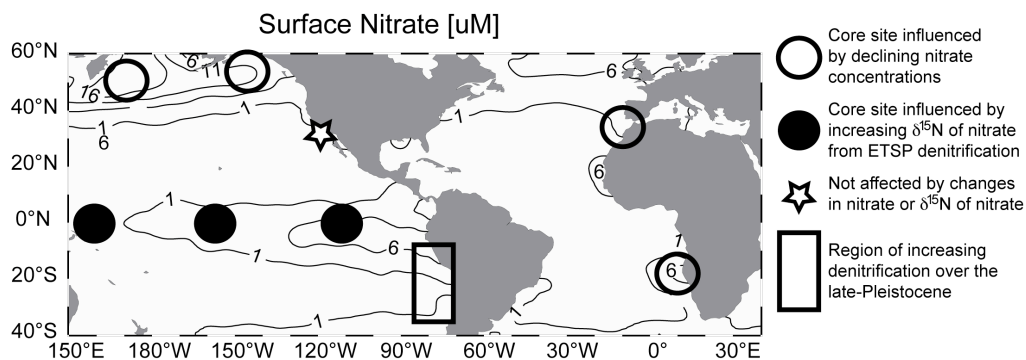


Figure 3.10: Map view of climatological mean surface nitrate concentrations (from World Ocean Atlas 2005 [Garcia et al., 2006]), all deep-sea sediment sites discussed in this study and descriptions of the processes that explain the long-term trend towards higher $\delta^{15}\text{N}$. It is suggested in the text that increased denitrification in the Eastern Tropical South Pacific influences all of these sites either by enriching initial $\delta^{15}\text{N}\text{-NO}_3^-$ (sites with filled black symbols) or by decreasing pre-formed NO_3^- concentrations (unfilled symbols). Of note, the Moroccan Margin sediment $\delta^{15}\text{N}$ record is in an area of upwelling, nutrient-rich waters close to the coast and the nitrate concentrations are not visible at the scale of this map. All necessary core site information can be found in Table 3.1.

Table 3.1: Reference information for cores discussed in this study

Location	Core Name	Lat (°N)	Lon (°E)	Seafloor Depth (m)	Reference
Western Equatorial Pacific	ODP 806	0	159	2520	This Study
Western Equatorial Pacific	RNDB 74P	0	159	2520	This Study
Eastern Equatorial Pacific	ODP 849	0	-110	3851	This Study
Eastern Equatorial Pacific	RC13-112	-1.2	-101.4	3299	This Study
California Margin	ODP 1012	32	-118	1772	<i>Liu et al., [2005]</i>
Moroccan Margin	GEOB4216	30.63	12.4	2324	<i>Freudenthal et al., [2002]</i>
Benguela Upwelling	MD962086	-26	12	3606	<i>Pichevin et al., [2005]</i>
Central Equatorial Pacific	PC-72	0	-139.4	4298	<i>Altabet, [2001]</i>
Northwest Sub-Arctic Pacific	MD2416	51.27	167.2	2317	<i>Galbraith et al., [2008]</i>
Gulf of Alaska	ODP 887	54.7	211.55	3847	<i>Galbraith et al., [2008]</i>

3.6 References

- Altabet, M.A (1989), A time-series study of the vertical structure of nitrogen and particle dynamics in the Sargasso Sea, *Limnology and Oceanography*, 34, 1185-1201.
- Altabet, M.A, and W.B. Curry (1989), Testing models of past ocean chemistry using foraminiferal $\delta^{15}\text{N}$, *Global Biogeochemical Cycles*, 3,107-119.
- Altabet, M.A, W.G. Deuser, S. Honjo and C. Stienen (1991), Seasonal and depthrelated changes in the source of sinking particles in the N. Atlantic, *Nature*, 354, 136-139.
- Altabet, M.A. and R. Francois (1994), Sedimentary nitrogen isotopic ratio as a recorder for surface ocean nitrate utilization, *Global Biogeochemical Cycles*, 8, 103-116.
- Altabet, M. (1996), Nitrogen and carbon isotopic tracers of the source and transformation of particles in the deep sea, In: Ittekkot, V., Schäfer, P., Honjo, S., Depetris, P.J. (Eds.), Particle Flux in the Ocean. SCOPE, 57, Wiley & Sons, Chichester, 155– 184.
- Altabet, M.A., C. Pilskaln, R. Thunell, C. Pride, D. Sigman, F. Chavez, and R. Francois (1999), The nitrogen isotope biogeochemistry of sinking particles from the margin of the Eastern North Pacific, *Deep Sea Research, Part I*, 46, 655– 679.
- Altabet, M.A. (2001), Nitrogen isotopic evidence for micronutrient control of fractional NO_3^- utilization in the equatorial Pacific, *Limnology and Oceanography*, 46, 368–380.
- Barker, S., D. Archer, L. Booth, H. Elderfield, J. Henderiks, and R. E. M. Rickaby (2006), Globally increased pelagic carbonate production during the Mid-Brunhes dissolution interval and the CO_2 paradox of MIS 11, *Quaternary Science Reviews*, 25, 3278–3293.
- Berger, W. H., and J.S. Killingley (1982), Box cores from the equatorial Pacific: ^{14}C sedimentation rates and benthic mixing, *Marine Geology*, 45, 93-125.
- Berger, W.H., T. Bickert, H. Schmidt, G. Wefer, (1993), Quaternary oxygen isotope record of pelagic foraminifers: Site 806, Ontong Java Plateau, In: *Proceedings of the Ocean Drilling Program, Scientific Results*, 130, W. H. Berger et al., Eds. Ocean Drilling Program, College Station, TX, 711-744.
- Bickert, T., W.H. Berger, S. Burke, H. Schmidt, and G. Wefer (1993), Late Quaternary stable isotope record of benthic foraminifers: Sites 805 and 806, Ontong Java Plateau, In: *Proceedings of the Ocean Drilling Program, Scientific Results*, 130, W. H. Berger et al., Eds. Ocean Drilling Program, College Station, TX, 411-420.

Broecker, W. S., E. Clark, D. C. McCorkle, T-H. Peng, I.Hajdas, and G. Bonani, (1999), Evidence for a reduction in the carbonate ion content of the deep sea during the course of the Holocene, *Paleoceanography*, 14, 744-752.

Brunelle, B., D.M. Sigman, M.S. Cook, L.D. Keigwin, G.H. Haug, B. Plessen, G. Schettler, and S.L. Jaccard, (2007), Evidence from diatom-bound nitrogen isotopes for subarctic Pacific stratification during the last ice age and a link to North Pacific denitrification changes, *Paleoceanography*, 22, PA1215.

Castro, C.G., F.P. Chavez, and C.A. Collins (2001), Role of the California Undercurrent in the export of denitrified waters from the eastern tropical North Pacific, *Global Biogeochemical Cycles*, 15, 819-830.

Chiyonobu, S., T. Sato, R. Narikiyo, and M. Yamasaki (2006), Floral changes in calcareous nannofossils and their paleoceanographic significance in the equatorial Pacific Ocean during the last 500000 years, *Island Arc*, 15, 476–482.

Crosta, X., and A. Shemesh (2002), Reconciling down core anticorrelation of diatom carbon and nitrogen isotopic ratios from the Southern Ocean, *Paleoceanography*, 17, 1010, doi:10.1029/2000PA000565.

Dekens, P.S., A.C. Ravelo, and M.D. McCarthy (2007), Warm upwelling regions in the Pliocene warm period, *Paleoceanography*, 22, PA3211, doi:10.1029/2006PA001394.

Deutsch, C., N. Gruber, R.M. Key, J.L. Sarmiento, and A. Ganaschaud (2001), Denitrification and N₂ fixation in the Pacific Ocean, *Global Biogeochemical Cycles*, 18, GB4012, doi:10.1029/2003GB002189.

Farrell, J.W. and W.L. Prell (1991), Pacific CaCO₃ preservation and $\delta^{18}\text{O}$ since 4 Ma: Paleoceanic and paleoclimatic implications, *Paleoceanography*, 6, 485-498.

Freudenthal, T., T. Wagner, F. Wenzhffer, M. Zabel, G. Wefer (2001), Early diagenesis of organic matter from sediments of the eastern and subtropical Atlantic: evidence from stable nitrogen isotopes and carbon isotopes, *Geochimica et Cosmochimica Acta*, 65, 1795-1808.

Galbraith, E.D. (2006), Interaction between climate and the marine nitrogen cycle on glacial-interglacial timescales, Ph D. Thesis, University of British Columbia.

Galbraith, E.D., M. Kienast, S.L. Jaccard, T.F. Pedersen, B.G. Brunelle, D.M. Sigman, and T. Kiefer (2008), Consistent relationship between global climate and surface nitrate utilization in the western subarctic Pacific throughout the last 500 ka, *Paleoceanography*, 23, PA2212, doi:10.1029/2007PA001518

- Ganeshram, R.S., and T.F. Pedersen (1998), Glacial-interglacial variability in upwelling and bioproductivity off NW Mexico: Implications for Quaternary palaeoclimate, *Paleoceanography*, *13*, 634– 645.
- Gaye-Haake, B., N. Lahajnar, K. Emeis, D. Ungerb, T. Rixen, A. Suthhof, V. Ramaswamy, H. Schulz, A.L. Paropkari, M.V.S. Guptha, V. Ittekkot (2005), Stable nitrogen isotopic ratios of sinking particles and sediments from the northern Indian Ocean, *Marine Chemistry*, *96*, 243– 255.
- Garcia, H.E., R.A. Locarnini, T.P. Boyer, and J.I. Antonov, (2006), World Ocean Atlas 2005, Volume 4: Nutrients (phosphate, nitrate, silicate). S. Levitus, Ed. NOAA Atlas NESDIS 64, U.S. Government Printing Office, Washington, D.C., 396 pp.
- Hendy, I.L., Pedersen, T.F., Kennett, J.P., Tada, R., (2004), Intermittent existence of a southern Californian upwelling cell during submillennial climate change of the last 60 kyr. *Paleoceanography*, *19*, doi:10.1029/2003PA000965.
- Holmes M.E., Eichner C., Struck U., and Wefer G. (1999), Reconstruction of surface ocean nitrate utilization using stable nitrogen isotopes in sinking particles and sediments. In: *Use of proxies in paleoceanography: examples from the South Atlantic*, G. Fischer and G. Wefer, Eds., Springer, 447–468.
- Ingalls, A. E., C. Lee, S. G. Wakeham, and J. I. Hedges (2003), The role of biominerals in the sinking flux and preservation of amino acids in the Southern Ocean along 170°W, *Deep Sea Research, Part II*, *50*, 713– 738.
- Jahnke, R. A., C. E. Reimerst, and D. B. Craven (1990), Intensification of recycling of organic matter at the sea floor near ocean margins, *Nature*, *348*, 50-54.
- Janecek, T. R. (1993) Data Report: High-resolution carbonate and bulk grain-size data for sites 803-806 (0-2Ma), In: *Proceedings of the Ocean Drilling Program, Scientific Results*, W. H. Berger et al., Eds. Ocean Drilling Program, College Station, TX, *130*, 761-773.
- King, K, Jr. (1977), Amino acid survey of recent calcareous and siliceous deep-sea microfossils, *Micropaleontology*, *23*,180-193.
- Lange, C. B. and W. H. Berger (1993), Diatom productivity and preservation in the western equatorial Pacific: The Quaternary record, In: *Proceedings of the Ocean Drilling Program, Scientific Results*, W. H. Berger et al., Eds. Ocean Drilling Program, College Station, TX, *130*, 509-523.
- Lehmann, M.F., Bernasconi, S.M., Barbieri, A., McKenzie, J.A., (2002), Preservation of organic matter and alteration of its carbon and nitrogen isotope composition during

- simulated and in situ early sedimentary diagenesis. *Geochimica et Cosmochimica Acta*, 66, 3573– 3584.
- Liu, Z., M.A. Altabet, and T. D. Herbert (2005), Glacial-interglacial modulation of eastern tropical North Pacific denitrification over the last 1.8-Myr, *Geophysical Research Letters*, 32, L23607, doi:10.1029/2005GL024439.
- Lisiecki, L.E., and M.E. Raymo (2005), A Plio-Pleistocene stack of 57 globally distributed benthic $d^{18}\text{O}$ records, *Paleoceanography*, 20, PA1003, doi:10.1029/2004PA001071.
- Medina-Elizade, M., and D.W. Lea (2005), The Mid-Pleistocene Transition in the Tropical Pacific, *Science*, 310, 1009-1012.
- Mix, A.C, N.G. Pisias, W. Rugh, J. Wilson, A.E. Morey, T. Hagelberg, (1995): Benthic foraminifer stable isotope record from Site 849 (0-5 Ma): local and global climate changes, In: Pisias, N.G. *et al.*, (eds.), *Proceedings of the Ocean Drilling Program, Scientific Results*, College Station, TX, 138, 371-412.
- Morales, C.E., S.E. Hormaza, and J.L. Blanco (1999), Interannual variability in the mesoscale distribution of the depth of the upper boundary of the oxygen minimum layer off northern Chile (18°–24°S): Implications for the pelagic system and biogeochemical cycling, *Journal of Marine Research*, 57, 909–932.
- Muller, P.J. and E. Suess (1977), Interaction of organic compounds with calcium carbonate - III. Amino acid composition of sorbed layers, *Geochimica et Cosmochimica Acta*, 42, 941-949.
- Murray, D.W, J.W. Farrell, and V. McKenna (1995), Biogenic sedimentation at site 847, eastern equatorial Pacific Ocean during the past 3 M.Y., In: Pisias, N.G. *et al.*, (eds.), *Proceedings of the Ocean Drilling Program, Scientific Results*, College Station, TX, 138, 429-459.
- Paillard, D., L. Labeyrie, and P. Yiou (1996), Macintosh program performs time-series analysis, *Eos*, 77, 379.
- Perks, H.M., C.D. Charles, and R.F. Keeling (2002), Precessionally forced productivity variations across the equatorial Pacific, *Paleoceanography*, 17, 1037, 10.1029/2000PA000603.
- Pichevin, L., P. Martinez, P. Bertrand, R. Schneider, and J. Giraudeau (2005), Nitrogen cycling on the Namibian shelf and slope over the last two climatic cycles: Local and global forcings, *Paleoceanography*, 20, PA2006, doi:10.1029/2004PA001001.

- Pride, C., R. Thunell, D. Sigman, L. Keigwin, M. Altabet, and E. Tappa, (1999), Nitrogen isotopic variations in the Gulf of California since the last deglaciation: Response to global climatic change, *Paleoceanography*, *14*, 397-409.
- Prokopenko, M.G., D.E. Hammond, and L. Stott (2006a), Lack of isotopic fractionation of d15N of organic matter during long-term diagenesis in marine sediments, ODP Leg 202, Sites 1234 and 1235, In: Tiedemann, R., Mix, A.C., Richter, C., and Ruddiman, W.F. (Eds.), *Proceedings of the Ocean Drilling Program, Scientific Results*, 202.
- Prokopenko, M.G., D.E. Hammond, A. Spivack, and L. Stott (2006b), Impact of long-term diagenesis on d15N of organic matter in marine sediments: Sites 1227 and 1230, In: Tiedemann, R., Mix, A.C., Richter, C., and Ruddiman, W.F. (Eds.), *Proceedings of the Ocean Drilling Program, Scientific Results*, 202.
- Robinson, R.S., B.G. Brunelle, and D.M. Sigman (2004), Revisiting nutrient utilization in the glacial Antarctic: Evidence from a new method for diatom-bound N isotopic analysis, *Paleoceanography*, *19*, PA3001, doi:10.1029/2003PA000996.
- Robinson, R.S., D.M. Sigman, P.J. DiFiore, M.M. Rohde, T.A. Mashiotto, and D.W. Lea (2005), Diatom-bound 15N/14N: New support for enhanced nutrient consumption in the ice age subantarctic, *Paleoceanography*, *20*, PA3003, doi:10.1029/2004PA001114.
- Ren, H., D.M. Sigman, A.N. Meckler, B. Plessen, R.S. Robinson, Y. Rosenthal, G.H. Haug (2009), Foraminiferal Isotope Evidence of Reduced Nitrogen Fixation in the Ice Age Atlantic Ocean, *Science*, *323*, 244-248.
- Saino, T. and A. Hattori, (1987) Geographical variation of the water column distribution of suspended particulate organic nitrogen and its 15N natural abundance in the Pacific and its marginal seas, *Deep-Sea Research, Part A*, *34*, 807–827.
- Schwarz, B., A. Mangini, M. Segl (1996), Geochemistry of a piston core from Ontong Java Plateau (western equatorial Pacific): evidence for sediment redistribution and changes in paleoproductivity, *Geol Rundsch*, *85*, 536-545.
- A. Shemesh, S.A. Macko, C.D. Charles, G.H. Rau (1993), Isotopic Evidence for Reduced Productivity in the Glacial Southern Ocean, *Science*, *262*, 407-410.
- Sigman, D.M., M.A. Altabet, R. Francois, D.C. McCorkle, and J. Gaillard (1999), The isotopic composition of diatom-bound nitrogen in Southern Ocean sediments, *Paleoceanography*, *14*, 118–134.

Sigman, D.M., K.L. Casciotti, M. Andreani, C. Barford, M. Galanter, and J.K. Bohlke (2001), A bacterial method for the nitrogen isotopic analysis of nitrate in seawater and freshwater, *Analytical Chemistry*, 73, 4145–4153.

Sweeney, R.E. and I.R Kaplan (1980), Natural abundances of I-N as a source indicator for near-shore marine sedimentary and dissolved nitrogen, *Marine Chemistry*, 9, 81-94.

Thunell, R.C., Sigman, D. M., Muller-Karger, F., Astor, Y., Vareka, R., (2004a), Nitrogen isotopic dynamics of the Cariaco Basin, Venezuela. *Global Biogeochemical Cycles*, 18, GB3001.

Thunell, R.C., Kepple, A.B., (2004b), Glacial–Holocene d15N record from the Gulf of Tehuantepec, Mexico: implications for denitrification in the eastern equatorial Pacific and changes in atmospheric N2O. *Global Biogeochemical Cycles*, 18, GB1001.

Velinsky, D.J., DJ. Burdige and M.L. Fogel (1991), Nitrogen diagenesis in anoxic marine sediments: Isotope effects, Annual Report No., Carnegie Inst., 154-162.

Vöss, M., J.W. Dippner, and J.P. Montoya (2001), Nitrogen isotope patterns in the oxygen-deficient waters of the eastern tropical North Pacific Ocean, *Deep Sea Research, Part I*, 48, 1905–1921.

Zhang , J., P. Wang , Q. Li, X. Cheng, H. Jin, S. Zhang (2007) Western equatorial Pacific productivity and carbonate dissolution over the last 550 kyr: Foraminiferal and nannofossil evidence from ODP Hole 807A, *Marine Micropaleontology*, 64, 121–140.

Appendix A

Supplementary Text, Figures, and Tables for:

I. Subsurface tropical Pacific nitrogen isotope measurements of nitrate: a tracer for denitrification, N₂ fixation, and subsurface circulation

Supplementary Text A1:

In chapter 1, I investigate the source of anomalously low $\delta^{15}\text{N-NO}_3^-$ in the Southern Subsurface Counter Current (SSCC). One possible explanation is that that local N₂ fixation (in surface waters above the SSCC) is producing organic matter with $\delta^{15}\text{N}$ of \sim -2 to 0‰ (see references in Chapter 1), which could then be remineralized at depth and influence the $\delta^{15}\text{N-NO}_3^-$. However, this process would also increase the concentration of nitrate. The possible range of $[\text{NO}_3^-]$ added to this water mass can be calculated using an isotope mass balance:

$$(1) \delta^{15}\text{N-NO}_3^-_{\text{final}} * [\text{NO}_3^-]_{\text{final}} = \delta^{15}\text{N-NO}_3^-_{\text{initial}} * [\text{NO}_3^-]_{\text{initial}} + \delta^{15}\text{N-NO}_3^-_{\text{fixed}} * [\text{NO}_3^-]_{\text{fixed}}$$

$$(2) [\text{NO}_3^-]_{\text{initial}} = [\text{NO}_3^-]_{\text{final}} - [\text{NO}_3^-]_{\text{fixed}}$$

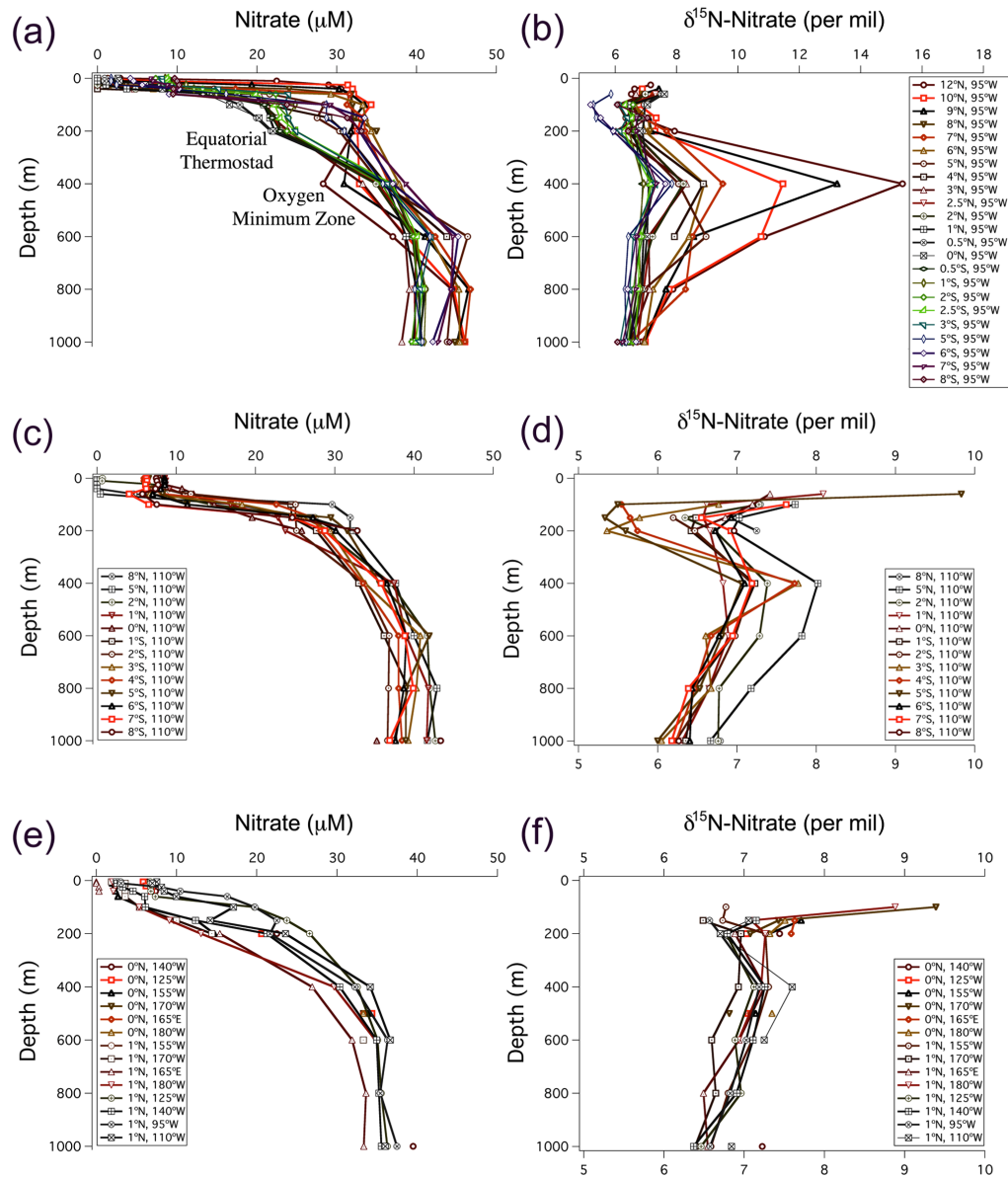
Where:

-- $\delta^{15}\text{N-NO}_3^-_{\text{final}}$ is 5.3‰

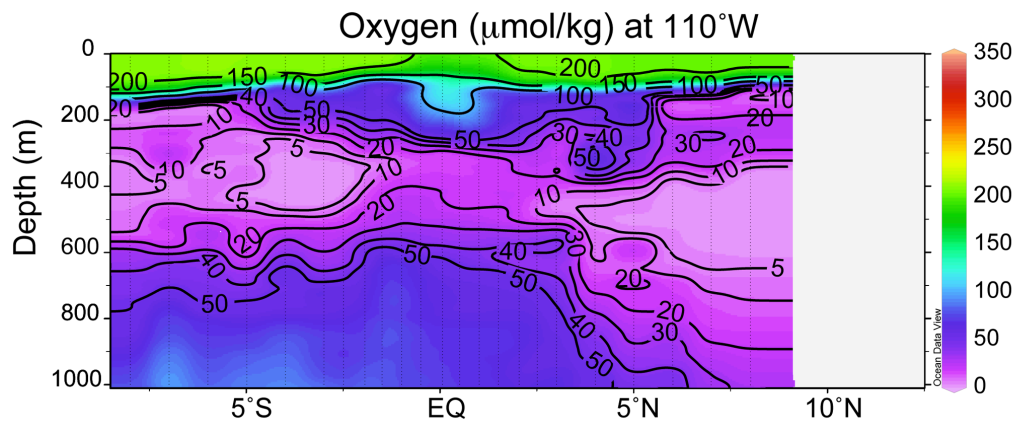
-- $[\text{NO}_3^-]_{\text{final}} = 30\mu\text{M}$, $\delta^{15}\text{N-NO}_3^-_{\text{initial}}$ is conservatively estimated from 6 to 7‰

-- $\delta^{15}\text{N-NO}_3^-_{\text{fixed}}$ is -2 and 0‰ (based on the work of *Carpenter et al.*, [1997]; *Delwiche et al.*, [1979]; *Hoering and Ford*, [1960]).

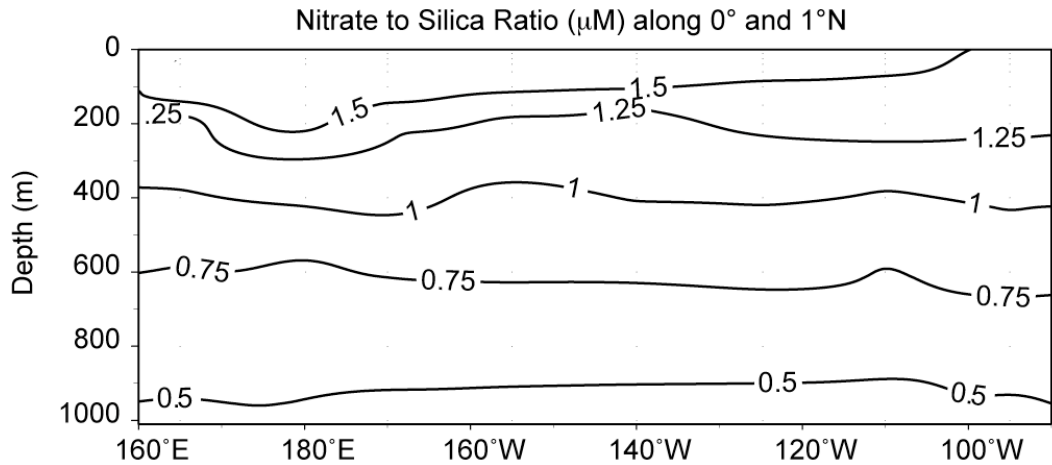
Equation (2) is used to solve for $[\text{NO}_3^-]_{\text{fixed}}$ in equation (1). These values equal an addition of $[\text{NO}_3^-]$ from 4.2 to 7.3 μM from N₂ fixation.



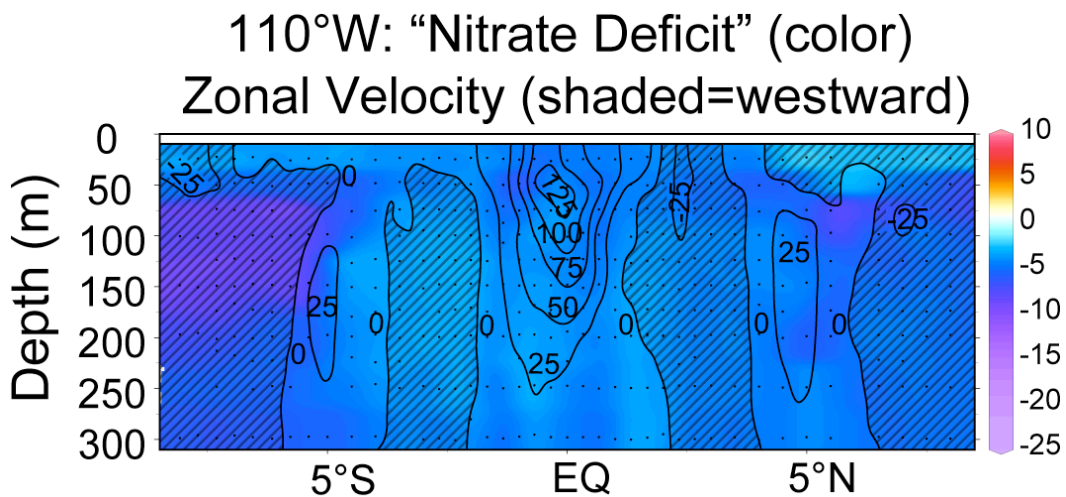
Appendix Figure A1: Concentrations of NO_3^- and $\delta^{15}\text{N}\text{-NO}_3^-$ for samples at all sampling sites (see Figure 1.4 for site locations).



Appendix Figure A2: Dissolved oxygen ($\mu\text{mol/kg}$) measurements for hydrocast stations on the 110°W transect (see Figure 1.4 for station locations) for October/November 2003 on the RV *Ronald H. Brown*.



Appendix Figure A3: Nitrate to silicic acid ratio versus depth along the 0° and 1°N in the tropical Pacific.



Appendix Figure A4: World Ocean Circulation Experiment (www.ewoce.org) distribution of N^* ($[NO_3^-] - ([phosphate] \cdot 16)$) and zonal velocity (contours) for waters along 110°W. Shaded contours are eastward-bound currents. The Southern Subsurface Counter Current is located at 5°S.

Appendix Table A1: Hydrocast station information for all seawater samples. All samples were taken at the leisure of NOAA's Tropical Atmosphere Ocean (TAO) program on board the RVs *Ka'imimoana* and *Ronald H. Brown*.

Date of Sampling	Latitude (°N)	Longitude (°E)	Deepest Sample (meters)
Oct./Nov. 2003	12.01	-94.83	1000m
Oct./Nov. 2003	10.02	-94.90	1000m
Oct./Nov. 2003	9.00	-94.92	1000m
Oct./Nov. 2003	8.09	-94.95	3013m
Oct./Nov. 2003	7.00	-94.97	1000m
Oct./Nov. 2003	6.00	-94.95	1000m
Oct./Nov. 2003	4.94	-95.06	1000m
Oct./Nov. 2003	4.00	-95.00	1000m
Oct./Nov. 2003	3.00	-94.97	1000m
Oct./Nov. 2003	2.50	-95.00	1000m
Oct./Nov. 2003	2.00	-95.00	1000m
Oct./Nov. 2003	1.00	-95.04	1000m
Oct./Nov. 2003	0.50	-95.05	1000m
Oct./Nov. 2003	0.08	-95.06	3000m
Oct./Nov. 2003	-0.50	-95.12	1000m
Oct./Nov. 2003	-1.00	-95.18	1000m
Oct./Nov. 2003	-1.99	-95.19	1000m
Oct./Nov. 2003	-2.50	-95.08	1000m
Oct./Nov. 2003	-3.01	-95.08	1000m
Oct./Nov. 2003	-5.06	-95.09	1000m
Oct./Nov. 2003	-5.06	-95.09	1000m
Oct./Nov. 2003	-6.00	-95.20	1000m
Oct./Nov. 2003	-7.00	-95.23	1000m
Oct./Nov. 2003	-8.00	-95.26	3803m
Oct./Nov. 2003	-8.00	-110.06	3203m
Oct./Nov. 2003	-7.00	-110.05	1000m
Oct./Nov. 2003	-6.00	-110.03	1000m
Oct./Nov. 2003	-4.99	-110.01	1000m
Oct./Nov. 2003	-4.00	-110.00	1000m
Oct./Nov. 2003	-3.00	-109.99	1000m
Oct./Nov. 2003	-1.95	-109.94	1000m
Oct./Nov. 2003	-1.00	-109.97	1000m
Oct./Nov. 2003	0.06	-109.93	3503m
Oct./Nov. 2003	1.00	-110.16	1000m
Oct./Nov. 2003	2.00	-110.00	1000m
Oct./Nov. 2003	5.00	-110.07	1000m
Oct./Nov. 2003	8.01	-110.10	4002m
September 2004	-0.17	-124.35	4000m
September 2004	0.04	-139.88	1500m
November 2004	0.04	-154.99	1500m

(Table A1 Continued from page 105)

November 2004	0.01	-170.01	5014m
November 2004	-0.01	165.05	4100m
December 2004	0.05	-179.91	3322m
June 2005	1.01	-154.97	1000m
July 2005	1.01	-170.01	1000m
July 2005	1.00	165.02	1000m
August 2005	1.00	-179.84	1000m
September 2005	1.01	-124.78	1000m
September 2005	1.00	-139.96	1000m
November 2005	1.00	-95.00	1000m
November 2005	1.00	-110.01	1000m

References for Appendix A

Carpenter, E., H. Harvey, B. Fry, and D. Capone (1997), Biogeochemical tracers of the marine cyanobacterium *Trichodesmium*, *Deep Sea Research, Part I*, 44, 27–38.

Delwiche, C.C., P.J. Zinke, C.M. Johnson, and R.A. Virginia (1979), Nitrogen isotope distribution as a presumptive indicator of nitrogen fixation, *Botanical Gazette*, 140, 65–69.

Hoering, T., and H.T. Ford (1960), The isotope effect in the fixation of nitrogen by *Azotobacter*, *Journal of the American Chemistry Society*, 82, 376–378.

Appendix B

Supplementary Text and Figures for:

II. Tropical Pacific nutrient dynamics of the past 1200kyr: an eastern equatorial Pacific record of surface nitrate uptake using sediment N isotopes

Supplementary Text B1:

The values for Figure 2.2 and Figure B1 were calculated using formulas for NO_3^- uptake based on (1) Rayleigh and (2) Steady State Fractionation [Mariotti *et al.*, 1981]:

(1) Rayleigh Fractionation:

$$\delta^{15}\text{N-PN}(\text{exported to sediment}) = \delta^{15}\text{N-NO}_3^- \text{ initial} + (\epsilon) * (f/1-f) * [\ln(f)]$$

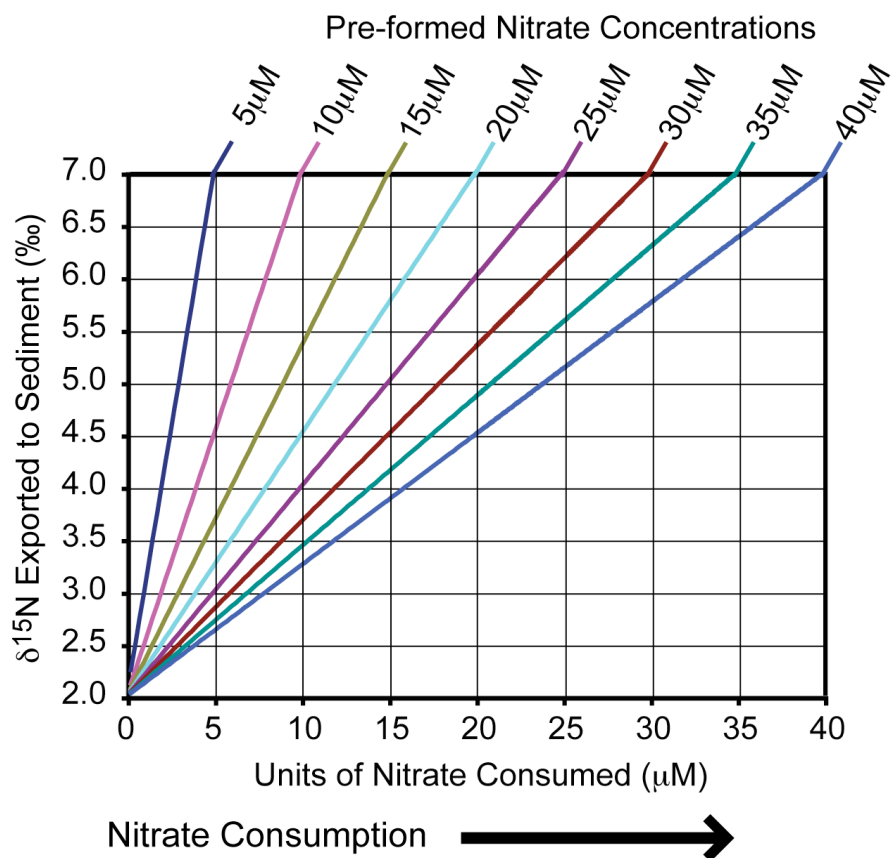
(2) Steady State Fractionation:

$$\delta^{15}\text{N-PN}(\text{exported to sediment}) = \delta^{15}\text{N-NO}_3^- \text{ initial} - (\epsilon) * (f)$$

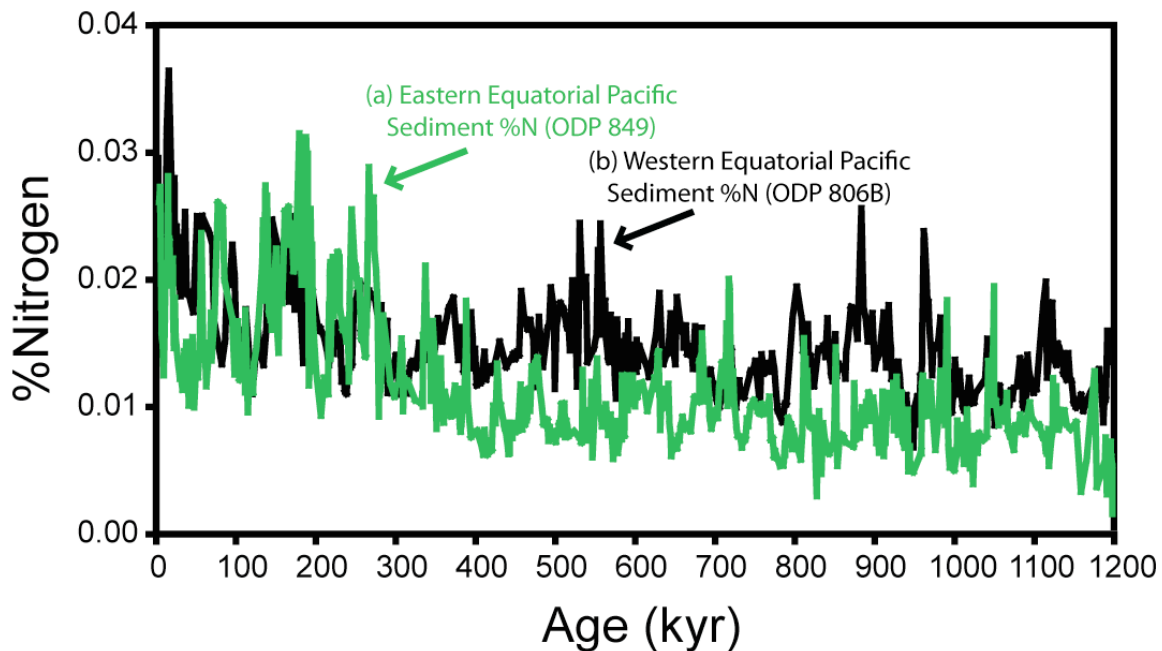
Where ϵ is assumed to be a constant 5‰ and “f” is the fraction of NO_3^- remaining.

To calculate the exported $\delta^{15}\text{N}$ at 110°W, I use $\delta^{15}\text{N-NO}_3^- \text{ initial} = 7\text{‰}$, starting nitrate concentration of 14 μM , and final nitrate concentration of 8 μM . Unsure as to the most likely type of fractionation (Rayleigh versus Steady State), we use an intermediate exported $\delta^{15}\text{N}$ of 3.5‰.

Calculating the change in $\delta^{15}\text{N}$ exported to the sediment for a hypothetical surface ocean location where $15\mu\text{M}$ of NO_3^- are consumed despite changes in pre-formed NO_3^- concentration, increasing pre-formed NO_3^- concentrations from $20\mu\text{M}$ to $25\mu\text{M}$ will result in a decrease of $\delta^{15}\text{N-PN}$ from 5.8‰ to 5.0‰ . See Appendix Figure B1 for a more thorough illustration of the effects on changing nitrate concentration on exported $\delta^{15}\text{N}$.

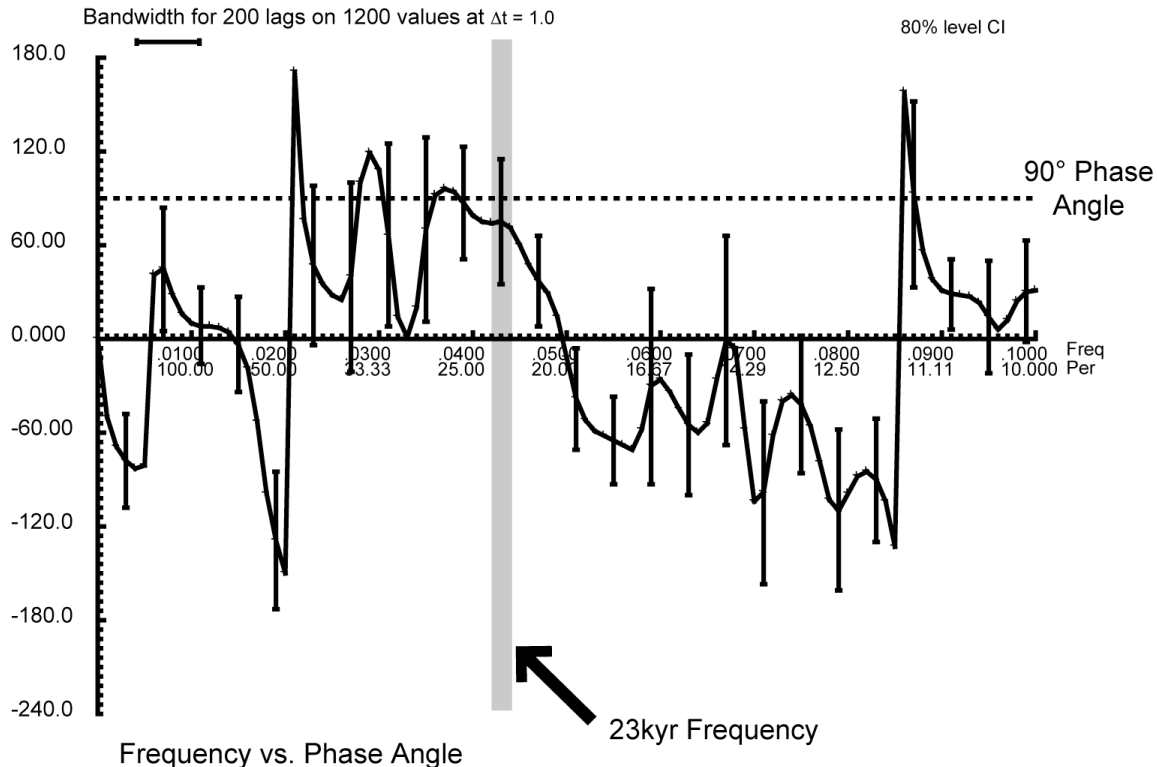


Appendix Figure B1: Calculations of $\delta^{15}\text{N}$ exported to sediments ($\delta^{15}\text{N}$ -PN) versus the amount of NO_3^- consumed (relative to pre-formed NO_3^- concentrations) for a variety of pre-formed NO_3^- concentrations. The purpose of this figure is to illustrate how changes in pre-formed NO_3^- concentrations delivered to surface waters can affect the $\delta^{15}\text{N}$ -PN exported to sediments.



Appendix Figure B2: Sediment %N measurements for (a) EEP sediment core ODP 849 (Green) and (b) WEP sediment core ODP 806B (Black) versus age.

Equatorial Pacific Percent N Phasing (West Versus East)



Appendix Figure B3: Frequency versus Phase Angle for EEP and WEP sediment core %N (seen in Appendix Figure B2). The primary goal of this figure is to highlight the nearly 90° out of phase behavior of these %N records at the 23kyr frequency. Phase angle calculations were made using the Arand Crospec program (available from Philip Howell and Brown University).

References for Appendix B

Mariotti, A., C. Germon, P. Hubert, P. Kaiser, R. Letolle, A. Tardieux, and P. Tardieux (1981), Experimental determination of nitrogen kinetic isotope fractionation: some principles; illustration for the denitrification and nitrification processes, *Plant and Soil*, 62, 413-430.